2010

Development and application of techniques for the acquisition of ultra-wideline solid-state NMR spectra

Alan W. MacGregor
University of Windsor

Development and Application of Techniques for the Acquisition of Ultra-Wideline Solid-State NMR Spectra

by
Alan W. MacGregor

A Thesis
Submitted to the Faculty of Graduate Studies and Research
through Chemistry and Biochemistry
in Partial Fulfillment of the Requirements for the
Degree of Master of Science at the
University of Windsor

Windsor, Ontario, Canada
2010

Your file Votre référence
ISBN: 978-0-494-62748-8
Our file Notre référence
ISBN: 978-0-494-62748-8

Declaration of Co-Authorship / Previous Publication

I. Co-Authorship Declaration

I acknowledge that Chapter 2 of this thesis has been submitted for publication. I also acknowledge that my supervisor, Dr. Robert W. Schurko, has provided guidance throughout the whole of this work and has edited this thesis.

The lead (II) thiolates discussed in Chapter 3 were synthesized and provided by the research group of Dr. Glen Briand (Mt. Allison), and the group 13 guanidinate compounds discussed in Chapter 4 were prepared and provided by the research group of Dr. Séan T. Barry (Carleton). Victor Terskikh at the National Ultra-high Field NMR facility for Solids is acknowledged for providing the data acquired at 21.1 T in Chapter 4.

Senior members our lab group trained me in the use of our NMR spectrometer, and supervised my usage of it. The main contributors in this regard were Dr. Luke A. O'Dell for the work discussed in Chapter 2, and Mr. Aaron J. Rossini for the work discussed in Chapters 3 and 4. Dr. Joel A. Tang also provided supervision for the work discussed in Chapter 4.

I am aware of the University of Windsor Senate Policy on Authorship and I certify that I have properly acknowledged the contribution of other researchers to my thesis, and have obtained written permission from each of the co-author(s) to include the above material(s) in my thesis. I certify that, with the above qualification, this thesis, and the research to which it refers, is the product of my own work.

II. Declaration of Previous Publication

This thesis includes 1 original paper that has been previously published/submitted for publication in peer reviewed journals, as follows:

Chapter 2: *MacGregor, A.W.; O'Dell, L.A.; Schurko, R.W. New Acquisition Methods for the Acquisition of Broad Solid-state NMR Spectra of Spin-1/2 Nuclides. Phys. Chem. Chem. Phys., Submitted for publication, April 2010.*

I certify that I have obtained a written permission from the copyright owner(s) to include the above published material(s) in my thesis. I certify that the above material describes work completed during my registration as graduate student at the University of Windsor.

I declare that, to the best of my knowledge, my thesis does not infringe upon anyone's copyright nor violate any proprietary rights and that any ideas, techniques, quotations, or any other material from the work of other people included in my thesis, published or otherwise, are fully acknowledged in accordance with the standard referencing practices. Furthermore, to the extent that I have included copyrighted material that surpasses the bounds of fair dealing within the meaning of the Canada Copyright Act, I certify that I have obtained a written permission from the copyright owner(s) to include such material(s) in my thesis.

I declare that this is a true copy of my thesis, including any final revisions, as approved by my thesis committee and the Graduate Studies office, and that this thesis has

not been submitted for a higher degree to any other University or Institution.

Abstract

Wideline and ultra-wideline (UW) (*i.e.*, > 250 kHz broad) solid-state NMR (SSNMR) spectra are acquired for a wide variety of nuclei (*i.e.*, ^{119}Sn, ^{195}Pt, ^{199}Hg, ^{207}Pb, ^{27}Al, ^{71}Ga) using multiple acquisition techniques. The WURST-CPMG pulse sequence is shown to acquire such patterns efficiently and without the need for piecewise acquisition. Preliminary investigations into the use of optimal control theory (OCT) are also carried out, and show promise for future studies. Additionally, a series of Pb(II) thiolate species, which exhibit unique Pb bonding environments, are characterized with ^{207}Pb SSNMR. Density Functional Theory (DFT) calculations are performed to determine chemical shielding (CS) tensor orientations within the molecular frame, which are then correlated to the experimental spectra. Finally, several group 13 guanidinates (guan = MeN-C(N^{i}Pr$_2$)-NMe) are studied via ^{27}Al and ^{71}Ga SSNMR at 9.4 T and 21.1 T, and experimental data is complemented with *ab initio* calculations, and the CS and electric field gradient tensor parameters are found to have a great dependence on metal coordination number and the nature of the metal-ligand bond.

Acknowledgements

First and foremost, I must thank my supervisor Dr. Rob Schurko for accepting me into his research group, and for continually providing guidance along the way. Studying solid-state NMR is not an easy undertaking, but Rob did his best to help me out from my first day at the office, and for that I am grateful.

Thanks also to Dr. T. B. Carmichael and Dr. C Ezeife. for being on my M.Sc. thesis committee, and agreeing to read through this work. Dr. P. J. Dutton is thanked for chairing my defense.

I also must acknowledge all the members of the Schurko group: Dr. Kris Harris, Aaron Rossini, Hiyam Hamaed, Bryan Lucier, Alex Reidel, Chris Mireault and Tatjana Milovic, as well as former members Dr. Luke O'Dell, Dr. Joel Tang and Marcel Hildebrand; thanks for all of your help, and for making the office an enjoyable place to be.

Since I have arrived in Windsor, I have had the opportunity to meet lots of new friends and foster relationships that I hope will last a long time. Thanks for all of the great times, you know who you are. To Ben Cooper and Chris Guignion; thanks for being a great roommate and generous landlord, respectively, and for putting up with me over the past 2 years.

Finally, thanks to my parents, Byron and Helen, for your constant emotional (and sometimes financial) support, and to my siblings, Andrew and Krista, for the late night chats and constant encouragement.

Contents

List of Tables

List Of Figures

List of Abbreviations

ADF	Amsterdam Density Functional
B3LYP	Becke's three parameter hybrid functional using the correlation functional of Lee, Yang and Parr
CP	cross-polarization
CPMG	Carr-Purcell Meiboom-Gill
CS	chemical shielding
CSA	chemical shielding anisotropy
CT	central transition
DFT	density functional theory
DMPE	dimethylphosphinoethane
DPPE	diphenylphosphinoethane
EFG	electric field gradient
Et	ethyl group, $CH_2CH_3^-$
FID	free induction decay
FT	Fourier transform
guan	guanidinate group = $(Me_2N\text{-}C(N^iPr)_2)$
^{i}Pr	isopropyl group, $-CH_2(CH_3)_2$
MAS	magic angle spinning
Me	methyl group, CH_3^-
NMR	nuclear magnetic resonance
NS	nuclear shielding
OCT	optimal control theory
o.d.	Outer diameter
ppm	parts per million

QCPMG	quadrupolar Carr-Purcell Meiboom-Gill
rf	radiofrequency
RHF	restricted Hartree-Fock
S/N	signal to noise
SSNMR	solid state nuclear magnetic resonance
TMEDA	tetramethylethylenediamine, $C_6H_{16}N_2$
WURST	wideband uniform-rate smooth truncation pulse sequence
ZORA	zeroth order regular approximation

List of Symbols

α, β, γ	Euler angles
α, β	nuclear spin state labels
γ	gyromagnetic ratio
$\delta_{11}, \delta_{22}, \delta_{33}$	principal components of the chemical shift tensor
δ_{iso}	isotropic chemical shift
η_Q	asymmetry of the electric field gradient tensor
κ	skew of the chemical shielding tensor
$\sigma_{11}, \sigma_{22}, \sigma_{33}$	principal components of the chemical shielding tensor
θ	angle describing the orientation of spin magnetization from the external magnetic field
τ_p	length of applied pulse
$\tau_1, \tau_2, \tau_3, \tau_4$	inter-pulse delays
$\boldsymbol{\mu}$	nuclear spin magnetic moment
ω_0	Larmor frequency (rad s^{-1})
ω_1	nutation frequency (rad s^{-1})
ω_Q	quadrupolar frequency ($rads^{-1}$)
υ_0	Larmor frequency (Hz)
υ_1	nutation frequency (Hz)
υ_{rf}	frequency of a radiofrequency pulse (Hz)
υ_Q	quadrupolar frequency (Hz)
Ω	span of the chemical shielding tensor
B_0	external magnetic field strength
B_1	applied magnetic field strength
C_Q	quadrupolar coupling constant

h	Planck's constant
$\hbar$	plack's constant, divided by 2π
$\mathcal{H}_Q$	Quadrupolar Hamiltonian
I	nuclear spin
$\mathbf{M}$	vector describing net magnetization
Q	quadrupole moment
T_1	spin-lattice relaxation time constant
T_2	transverse relaxation time constant
V_{11}, V_{22}, V_{33}	principal components of the electric field gradient tensor

Chapter 1

Introduction

1.1 NMR Spectroscopy

Nuclear magnetic resonance was first reported simultaneously by the research groups of Bloch and Purcell in 1946.[1,2] In the decades that have passed since then, NMR has become an indispensable tool for the characterization of structure and dynamics at the molecular level in virtually every area of chemical research. The advent of large, superconducting magnets, and advancements in hardware and software, have made it possible to conduct experiments which would have been considered virtually impossible in the past. The field of solid-state nuclear magnetic resonance (SSNMR) has greatly benefited from these advancements and has become an area of intense research over the past several decades.[3-8] SSNMR has been employed to study a wide variety of molecules and materials, including proteins,[9] polymers,[10] inorganic materials[11,12] and clays and minerals.[13] In this section, the interactions that give rise to SSNMR spectra are examined, along with a variety of techniques employed in their acquisition.

1.2 NMR Interactions

In this section, we discuss the physical interactions which give rise to the NMR phenomenon, and the informative fine structure observed in NMR spectra, as well as the manner in which these interactions are manifested in NMR spectra. In no way is this

section meant to be considered a complete treatment of these interactions; rather, the reader is presented with a rudimentary background of the basis for NMR. More comprehensive descriptions of the interactions which govern NMR are elegantly described elsewhere.[14-18]

1.2.1 General Considerations

The nuclear spin, I, is an intrinsic property of the nucleus and gives rise to spin angular momentum, described by a vector **I**, and a nuclear magnetic moment, $\boldsymbol{\mu}$, which are related through an inherent nuclear property called the gyromagnetic ratio:[18]

$$\boldsymbol{\mu} = \gamma \mathbf{I} \tag{1}$$

The spin can interact with a static magnetic field, $\mathbf{B}_0$, or an oscillating magnetic field induced by a radiofrequency (rf) pulse, $\mathbf{B}_1$. In the presence of a magnetic field, $\boldsymbol{\mu}$ will begin to precess about the axis of the field, $\mathbf{B}_0$, which is conventionally taken to be along the z-axis.

Spin is quantized such that the z-component of **I**, $I_z = m\hbar$, where $m = I, I - 1, \ldots, -I$, and represents the spin state of a given spin. The energy of interaction between $\boldsymbol{\mu}$ and $\mathbf{B}_0$ is given as:

$$E = -\boldsymbol{\mu} \cdot \mathbf{B}_0 = -\mu_z B_0 = -m\hbar\gamma B_0 \tag{2}$$

The rate of precession, ω_0, is known as the Larmor frequency and is dependent upon the magnitude of $\mathbf{B}_0$ and the gyromagnetic ratio:[18]

$$\omega_0 = -\gamma B_0 \quad (3)$$

Note, that Levitt's convention for the sign of the gyromagnetic ratio is applied here,[19] and that:

$$\omega_0 = 2\pi\nu_0 \quad (4)$$

1.2.2 The Zeeman Interaction

The Zeeman interaction is the fundamental interaction that gives rise to the NMR phenomenon. Outside of a magnetic field, the spin states of a nucleus are degenerate. This degeneracy is removed when a magnetic field is introduced, resulting in $2(I + 1/2)$ quantized spin states, which differ in energy by $\Delta E = \hbar\omega_0$.[18] The simplest case to consider is that of a nucleus with $I = 1/2$, which has two possible spin states, $m_I = +1/2$ and $m_I = -1/2$, or α and β, respectively.[20] An individual spin can be visualized as a magnetic moment which precesses about the external magnetic field, $\mathbf{B}_0$ (z-axis) at the Larmor frequency. The quantization of spin along $\mathbf{B}_0$ dictates that there are a limited number of possible states for precession; in the case of the spin-1/2 nucleus, there are two possibilities: α and β. Note that for a nucleus with a positive gyromagnetic ratio, the α spin state is lower in energy than the β spin state.

In treating the NMR experiment classically, a large number of spins (i.e., an ensemble) is normally considered. The spin states are populated according to the Boltzmann distribution:

$$\frac{N_\beta}{N_\alpha} = e^{-\frac{\hbar\omega_0}{kT}} \quad (5)$$

where N_α and N_β represent the populations of the α and β spin states, k is the Boltzmann constant and T is the temperature (in K). The Boltzmann distribution dictates that there are more spins in the lower energy α state; therefore, the net magnetization of the ensemble is a vector, **M**, that is parallel to $\mathbf{B}_0$. The population difference between the α and β states can be increased by increasing $\mathbf{B}_0$ or lowering the temperature. Both of these actions result in increased sensitivity, as the NMR signal can be shown to be proportional to:

$$S(t) = \frac{N\gamma^3\hbar^2 B_0^2}{4kT} e^{i\omega_0 t}$$

where N describes the natural abundance of the isotope under study, or the number of spins present.

1.2.3 Response to radiofrequency pulses

In an NMR experiment, the sample is placed in a coil (normally on a probe head) which is inserted into the large external magnetic field. When an oscillating (AC) current is passed through the coil, an oscillating magnetic field, $\mathbf{B}_1$, is produced along the axis of the coil, which is directed perpendicular to $\mathbf{B}_0$ (note, that this is the case for a solenoid coil; for solution NMR, a Helmholz coil is utilized). In the lab frame, the individual

magnetic moments precess about $\mathbf{B}_0$ at the Larmor frequency, ω_0. If $\mathbf{B}_1$ is applied such that it oscillates at a transmitter frequency of ω_{rf}, and $\omega_{rf} \approx \omega_0$ then it is possible to "tip" the net magnetization away from $\mathbf{B}_0$. The reason for this is best considered using the rotating frame, which is a frame rotating at ω_{rf} (ω_{rf} is the transmitter frequency in this case). If $\omega_{rf} = \omega_0$, ω_{rf} is said to be "on resonance," and the individual magnetic moments appear to be stationary in the rotating frame. Since the magnetic moments are stationary, it is as if $\mathbf{B}_0$ is absent, and the stationary $\mathbf{B}_1$ field is present. The magnetization vector, **M**, begins to precess about the stationary $\mathbf{B}_1$ field at a frequency of $\omega_1 = -\gamma B_1$. which known as the nutation frequency, and depends on the magnitude of B_1 produced by the rf coil.

The introduction of a pulse with a field magnitude of B_1 for a time period τ_p "tips" **M**, by an angle θ away from the *z*-axis:

$$\theta = \tau_p \cdot \gamma B_1 = -\tau_p \cdot \omega_1 \qquad (7)$$

Hence, to tip the magnetization into the *xy*-plane of the rotating frame, τ_p is set such that $\theta = \pi/2$. The phase of the pulse dictates the orientation of the magnetization vector within this plane, following the right hand rule. For example, a pulse applied along the *x*-axis will direct the magnetization vector to the $-y$-axis. Once the pulse is turned off, $\mathbf{B}_1$ is removed and the magnetic moments once again precess about $\mathbf{B}_0$ at the Larmor frequency. As **M** precesses about $\mathbf{B}_o$, it induces a current in the sample coil, which is recorded and digitized as the free induction decay (FID), which in turn is used to generate the NMR spectrum via Fourier transformation.

If $\omega_{rf} \neq \omega_0$, then the magnetic moments no longer appear stationary in the rotating frame, and $\mathbf{B}_0$ no longer appears to be absent, but rather, is attenuated by a factor of $(1 - \omega_{rf}/\omega_0)$. The result is an effective magnetic field, $\mathbf{B}_{eff}$:

$$\mathbf{B}_{eff} = (\mathbf{B}_0 - \omega_{rf}/\gamma)\cdot z + B_1/2\cdot x \qquad (8)$$

If $(\mathbf{B}_0 - \omega_{rf}/\gamma) >> \mathbf{B}_{eff}$, then ω_{rf} is considered to be "off resonance", and $\mathbf{B}_{eff}$ is ineffective at tipping the magnetization into the *xy*-plane (where the signal is detected). In the case of ultra-wideline (UW, *i.e.*, > 250 kHz broad) SSNMR spectra, resonances may be separated by hundreds of kHz, or more often, may spread over hundreds of kHz or tens of MHz, which makes it difficult (if not impossible) to acquire the entire powder pattern in a single experiment with traditional acquisition methods. Hence, specialized techniques are employed in such cases (*vide infra*).

1.2.4 Relaxation Processes

There are two types of nuclear spin relaxation that are essential for the NMR phenomenon. Spin-lattice relaxation (or longitudinal relaxation) is described by the T_1 relaxation time constant, and provides a measure of the time required for the magnetization to return to equilibrium along $\mathbf{B}_0$. The T_1 is measured experimentally with the inversion recovery pulse sequence.[21] Spin-spin relaxation (or transverse relaxation) is described by the T_2 relaxation time constant, and is a measure of the time required for complete dephasing of the magnetization in the *xy*-plane. The T_2 time constant is most often measured using the Carr-Purcell Meiboom-Gill (CPMG)[22,23] pulse sequence (*vide*

infra). All of the NMR interactions that are discussed in the next few sections can contribute to mechanisms which induce nuclear spin relaxation; a detailed discussion of relaxation mechanisms is beyond the scope of this introduction, and is well covered elsewhere.[24]

1.2.5 Chemical Shielding

The local magnetic field at a nucleus is dependent upon the external magnetic field, $\mathbf{B}_0$, and the induced magnetic field at the nucleus $\mathbf{B}_{ind}$:

$$\mathbf{B}_{loc} = \mathbf{B}_{ind} + \mathbf{B}_0 \qquad (9)$$

The $\mathbf{B}_{ind}$ varies between different nuclei, due to the induced circulation of electrons within the surrounding molecular orbitals. The effect that $\mathbf{B}_{ind}$ has on $\mathbf{B}_{loc}$ is referred to as the chemical shielding or nuclear magnetic shielding of the nucleus; if $\mathbf{B}_{ind}$ is aligned in the same direction as $\mathbf{B}_0$, causing $\mathbf{B}_{local}$ to increase, it is considered deshielding. If $\mathbf{B}_{ind}$ is aligned in the opposite direction to $\mathbf{B}_0$, causing $\mathbf{B}_{local}$ to decrease, it is considered shielding. The chemical shielding is reported in ppm with respect to the bare nucleus, which is assigned a value of 0 ppm. In practice, one cannot experimentally measure the chemical shielding of a bare nucleus for comparison to the chemical shielding of a nucleus in a sample of interest. In experimental NMR spectra, the chemical shift (CS) is measured which is the shielding of the nucleus, σ, with respect to that of a reference standard, σ_{ref}.[25]

$$\delta = \frac{\sigma_{ref} - \sigma}{1 - \sigma_{ref}} \approx \sigma_{ref} - \sigma \qquad (10)$$

An arbitrary standard reference compound is chosen for each nucleus, and all chemical shifts are reported with respect to this reference.

The chemical shielding or nuclear shielding (NS) interaction can be described by a second rank tensor (3 × 3 matrix):

$$\ddot{\boldsymbol{\sigma}} = \begin{pmatrix} \sigma_{xx} & \sigma_{xy} & \sigma_{xz} \\ \sigma_{yx} & \sigma_{yy} & \sigma_{yz} \\ \sigma_{zx} & \sigma_{zy} & \sigma_{zz} \end{pmatrix} \qquad (11)$$

This tensor is not traceless and is anti-symmetric. It can, however, be broken down into symmetric and anti-symmetric components. Only the former contributes to the observable chemical shifts, and it is represented by a symmetric second rank tensor which, in its own principal axis system (PAS), is written as:

$$\ddot{\boldsymbol{\sigma}} = \begin{pmatrix} \sigma_{11} & 0 & 0 \\ 0 & \sigma_{22} & 0 \\ 0 & 0 & \sigma_{33} \end{pmatrix} \qquad (12)$$

σ_{11}, σ_{22}, and σ_{33} are referred to as the principal components of the NS tensor, and are arranged such that $\sigma_{11} \leq \sigma_{22} \leq \sigma_{33}$ (*i.e.*, σ_{11} is the least shielded component, and σ_{33} is the most shielded component). This can be written equivalently in terms of chemical shift

as:

$$\ddot{\boldsymbol{\delta}} = \begin{pmatrix} \delta_{11} & 0 & 0 \\ 0 & \delta_{22} & 0 \\ 0 & 0 & \delta_{33} \end{pmatrix} \tag{13}$$

where $\delta_{11} \geq \delta_{22} \geq \delta_{33}$.

The CS interaction is orientation dependent or anisotropic, meaning the values of the tensor components can change depending upon the orientation of the tensor with respect to $\mathbf{B}_0$. There are several conventions available for describing the chemical shift anisotropy (CSA); herein, the Herzfeld-Berger convention[26,27] is used to describe the CSA. The isotropic shift, δ_{iso}, describes the isotropic or average chemical shift of the nucleus, and is found at the centre of gravity of the NMR powder patterns of spin-1/2 nuclides:

$$\delta_{iso} = \frac{(\delta_{11} + \delta_{22} + \delta_{33})}{3} \tag{14}$$

The span, Ω, describes the breadth of the pattern in ppm (often referred to as the magnitude of the CSA),

$$\Omega = \delta_{11} - \delta_{33} \tag{15}$$

and the skew, κ, gives the position of δ_{22} with respect to δ_{iso}, and describes the axial symmetry of the tensor:

$$\kappa = \frac{3\,(\delta_{22} - \delta_{iso})}{\Omega}, \quad 1 \leq \kappa \leq -1 \tag{16}$$

In solution NMR experiments, the CSA is averaged to zero due to the rapid tumbling of the molecules, and as a result, only the isotropic chemical shift is observed. In the solid state, where such rapid isotropic motion is absent, the orientation dependence of the CS tensor can be observed. Most solid state samples, including microcrystalline and amorphous or disordered solids have a vast number of tensor orientations which are represented within the bulk sample. The bulk of early SSNMR experiments were conducted upon microcrystalline powder samples, and as a result, the patterns arising from the distributions of these shifts are commonly referred to as powder patterns. Powder patterns represent the weighted sum of all of the resonances arising from individual CS tensor orientations (Figure 1.1), and its shape can be directly correlated to the principal components of the CS tensor.

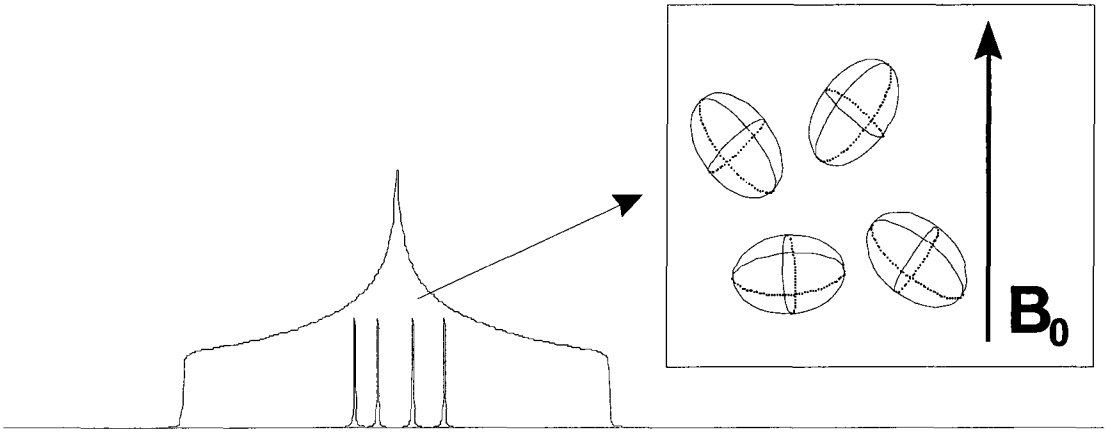

Figure 1.1. Depiction of the distribution of resonances arising from multiple CS tensor orientations.

1.2.6 The Quadrupolar Interaction

Nuclei with $I > ½$ are quadrupolar nuclei, and have an asymmetric distribution of the charge in the nucleus. This asymmetry in charge distribution is described by a scalar parameter known as the nuclear quadrupole moment (NQM or Q) which has dimensions of m^2 (or barn = 10^{-28} m^2). The nuclear quadrupole moment interacts with the electric field gradients (EFGs) in the molecule. The EFG at a nuclear site is described by a symmetric, traceless tensor, with principal components arranged such that $|V_{11}| \leq |V_{22}| \leq |V_{33}|$:

$$V_{EFG} = \begin{pmatrix} V_{11} & 0 & 0 \\ 0 & V_{22} & 0 \\ 0 & 0 & V_{33} \end{pmatrix} \quad \textbf{(17)}$$

The quadrupolar interaction (QI) is typically described by the quadrupolar coupling constant, C_Q,

$$C_Q = \frac{eQV_{33}}{h} \quad \textbf{(18)}$$

and the asymmetry parameter, η_Q,

$$\eta_Q = \frac{V_{11} - V_{22}}{V_{33}}, \quad 0 \leq \eta_Q \leq 1 \quad \textbf{(19)}$$

C_Q, which is usually reported in MHz, is a measure of the spherical symmetry of the

ground-state electronic environment at the quadrupolar nucleus, and it increases in magnitude as the degree of spherical symmetry decreases.[13] η_Q, which is a dimensionless parameter, is a measure of the axial symmetry of the EFG tensor; for an EFG tensor with a high degree of axial symmetry, η_Q is near zero or one. The magnitude of the QI is also sometimes reported as the quadrupolar frequency, ω_Q:

$$\omega_Q = \frac{3eQ}{2I(2I-1)\hbar}V_{33} = \frac{3C_Q}{2I(2I-1)\hbar} \quad \textbf{(20)}$$

The QI is described by the quadrupolar Hamiltonian, which is comprised of first and second order terms:

$$\mathcal{H}_Q = \mathcal{H}_Q^{(1)} + \mathcal{H}_Q^{(2)} \quad \textbf{(21)}$$

Under the high-field approximation, where $\omega_0 >> \omega_Q$, it is possible to treat the QI as a perturbation on the Zeeman Hamiltonian. To first order, the perturbation is given by:[28]

$$\omega_{m,m-1} = \frac{\omega_Q}{4}(1 - 2m)(3\cos^2\theta - 1 + \eta_Q\sin^2\theta cos2\varphi) \quad \textbf{(22)}$$

where θ and φ are polar angles which describe the relative orientation of $\mathbf{B}_0$ in the PAS of the EFG.

ΔE does not change for the $+1/2 \leftrightarrow -1/2$ transition (the central transition, CT) since the shift in energy is the same for both spin states. The remaining transitions (satellite transitions, STs), however, are altered significantly, which causes the NMR

signal of the satellite transitions to be broadened, typically over many MHz, so they are often not observed. The first order perturbation is also orientation dependent, and can be removed through the use of magic angle spinning (MAS) (*vide infra*). However, the second order term:[28]

$$\begin{aligned}\omega_{+1/2,-1/2} = \frac{\omega_Q^2}{12\omega_0}\{\frac{3}{2}\sin^2\theta[(A + B)\cos^2\theta - B] \\ - \eta_Q\cos 2\varphi\sin^2\theta[(A + B)\cos^2\theta + B] \\ + \frac{\eta_Q^2}{6}[A - (A + 4B)\cos^2\theta \\ - (A + B)\cos^2\varphi(\cos^2\theta - 1)^2 2]\}\end{aligned} \quad \textbf{(23)}$$

where:

$$\begin{aligned} A &= 24m(m - 1) - 4I(I+1) + 9 \\ \text{and} \quad B &= \frac{1}{4}[6m(m - 1) - 2I(I + 1) + 3] \end{aligned} \quad \textbf{(24)}$$

The orientation dependence of the second-order QI is such that MAS cannot completely average the pattern to a single sharp peak; rather, averaging of this interaction must be accomplished by rotating the sample about two axes simultaneously (e.g., the double-rotation or DOR technique),[29,30] or by selecting multiple-quantum (MQ) coherences in two-dimensional experiments for which the second-order QI can be averaged (e.g., dynamic-angle spinning, DAS[31-35] and MQ-MAS).[36-38]

1.2.7 Euler Angles

The relative orientation of the EFG and CS tensors can have a profound impact on

the appearance of a SSNMR spectrum. To best describe how these two tensors are aligned with respect to each other, three Euler angles, α, β, and γ, are employed. In this work the Euler angles are defined as follows: the two tensors are aligned so that, in a standard *xyz* coordinate system, V_{33} and σ_{33} are aligned along the *z-axis*, V_{22} and σ_{22} are aligned along the *y*-axis, and V_{11} and σ_{11} are aligned along the *x*-axis. First, the CS tensor is rotated about *z* by an angle, α. The CS tensor orientation is then taken as the reference frame, with σ_{33}, σ_{22} and σ_{11} becoming *x'*, *y'* and *z'*, respectively. A rotation of the new frame by an angle β is then made about the *y'*-axis, yielding a third frame of reference with axes of *x"*, *y"* and *z"*. A rotation by an angle of γ is then made about the *z"* axis, resulting in the final orientations of the tensors (Figure 1.2).

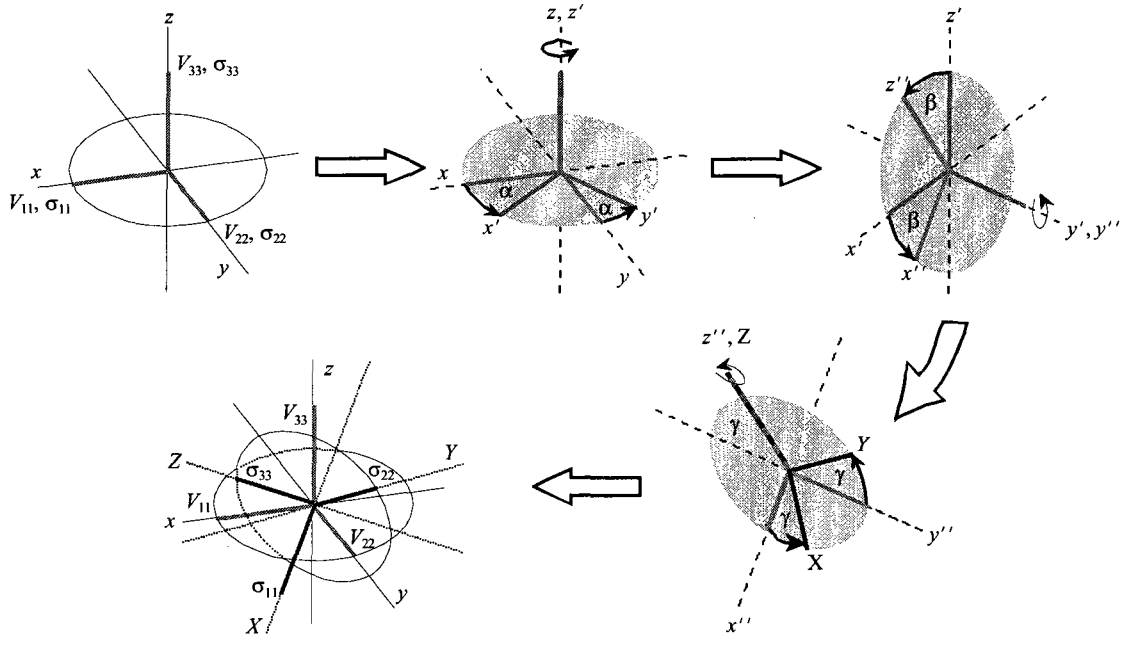

Figure 1.2. Diagram depicting the Euler angle convention used herein to describe the relative orientation of the CS and EFG tensors. Appended from Tang (2008).[39]

1.2.8 Dipolar and Scalar Coupling

Dipolar direct spin-spin coupling (or just dipolar coupling) and indirect spin-spin coupling (or scalar or *J*) coupling are two-spin NMR interactions. The dipolar interaction is a through space interaction, described by a traceless second rank tensor. Secular effects (i.e., frequency shifts) arising from the dipolar interaction are observed only in the solid state (and some oriented samples); in solution, the rapid isotropic motion of molecules average dipolar effects to zero.[40] For the purposes of this thesis, dipolar coupling will not be discussed further, as its effects have largely been removed through the use of decoupling schemes where applicable. It is also noted that the dipolar interaction is extremely important for the application of cross-polarization NMR experiments (vide infra). The interested reader may find a thorough description of the dipolar interaction elsewhere.[17]

J-coupling occurs between two nuclei, as for dipolar coupling; however, *J*-coupling is a through-bond interaction, mediated by electrons within the molecule.[41] *J*-coupling is described by a anti-symmetric tensor with a non-zero trace. The symmetric portion of the tensor makes both isotropic and anisotropic secular contributions, defined as the isotropic *J*-coupling, J or J_{iso}, and the *J*-anisotropy, ΔJ. While the former is very commonly observed in both solution- and solid-state NMR spectra, the latter is only observed in solid-state NMR spectra of nuclei which are *J*-coupled to heavy nuclei (or vice versa).[42] In this thesis, we are only concerned with isotropic contributions to *J*-couplings. The *J*-coupling of a nucleus A of spin I to a nucleus X of spin S results in a splitting of the resonance into $2(S + ½)$ peaks in the spectrum of A, and $2(I + ½)$ peaks in

the spectrum of X, with the spacing between the peaks in each spectrum equal to the value of the J_{iso} in Hz. Since *J*-coupling is a through-bond interaction, it provides valuable structural information about the bonding/connectivity within a given molecule.[41] Except for a few select cases, scalar couplings are not visible in the SSNMR spectra presented herein, as their relatively small magnitude (hundreds of Hz) are dwarfed by the broad (tens to hundreds of kHz) powder patterns.

1.3 Acquisition and enhancement techniques

There are a wide variety of techniques that can be employed to enhance the NMR signal and/or spectral resolution. Some involve specialized hardware, though many are simply pulse sequences that manipulate the spins in such a way as to increase the efficiency of the experiment. In this thesis, we are concerned with rapidly acquiring broad powder patterns with high S/N, and hence, will focus on techniques employed to that end.

1.3.1 Frequency-stepped NMR

The majority of the spectra in this work are either wideline NMR spectra (i.e., broad patterns ranging from ca. 20 to 250 kHz in breadth), or much broader spectra we designate as ultra-wideline (UW) NMR spectra (*i.e.* ≥ 250 kHz in breadth).[43] UW spectra exceed the excitation bandwidths of standard, high-power, rectangular pulses; as such, specialized hardware, pulse sequences or acquisition methodologies must be applied. Some UW NMR spectra must be acquired as a series of sub-spectra. Initially, this was

done with the "point-by-point" method, where the echo intensity of the free induction decay was plotted as a function of transmitter frequency[44,45] or magnetic field strength.[46,47] More recently, it has become common practice to co-add a series of Fourier transformed spectra, which have been acquired at evenly-spaced transmitter frequencies.[48,49] The acquisition of spectra in much larger frequency increments, combined with spectral processing prior to co-addition, greatly reduces experimental times and yields spectra with considerably higher S/N than conventional point-by-point acquisitions. This technique is known as the variable offset cumulative spectrum (VOCS) method,[48] or simply as a piecewise spectral acquisition. There are also some specialized pulse sequences which can be utilized to acquire UW NMR spectra in a single experiment, as well as to acquire extremely broad UW NMR spectra in a piecewise fashion (*vide infra*).

1.3.2 Magic-Angle Spinning

Magic-angle spinning (MAS) NMR spectroscopy[50] is a technique that involves rotating the sample holder (*i.e.*, rotor) about an axis at an angle of 54.74° from $\mathbf{B}_0$, which averages the CSA to zero (or at least enough that the effects of CSA are negligible, *vide infra*). The result is observation of solution-like NMR signals from spin-1/2 nuclei, and classic second-order quadrupolar lineshapes from quadrupolar nuclei. Hence, MAS allows for the isotropic shift and EFG tensor parameters to be determined with great accuracy.

In order for MAS to be most effective, a general rule is that the sample must be spun at a rate which is equal to, or greater than, the width of the SSNMR powder pattern.

For narrow patterns (i.e., ≤ 15 kHz), this is readily achieved with what have become standard NMR probes. However, for broad SSNMR spectra (like most of those contained within this work) limitations on NMR hardware make it difficult to spin the sample at a high enough rate to average the CSA to zero. Currently, the upper limit on spinning speed is ca. 70 kHz, which is attainable on specialized SSNMR probes.

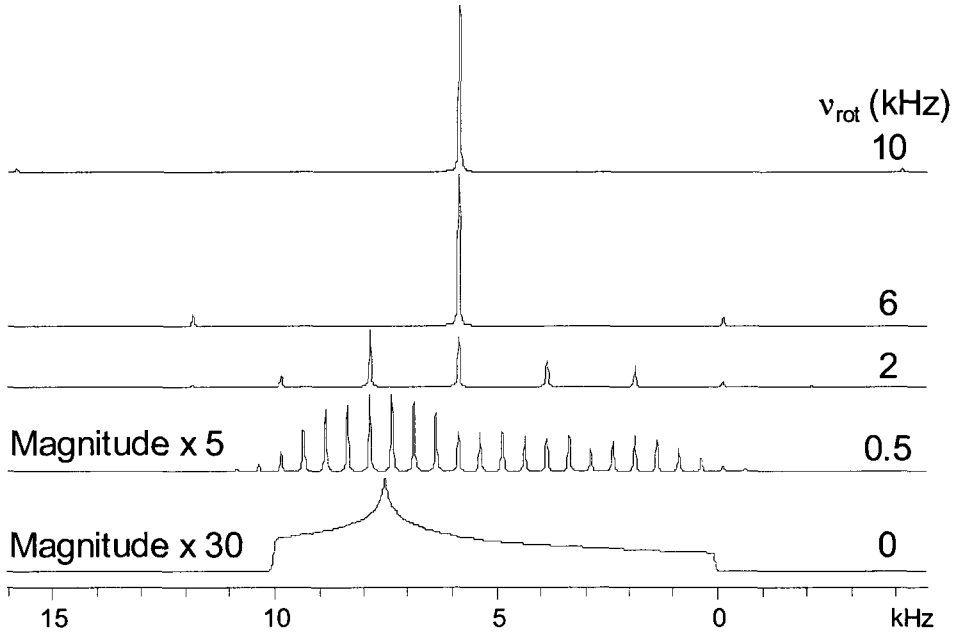

Figure 1.3. Simulation of the effect of MAS on a typical spin-1/2 powder pattern. Spinning speed is indicated to the right (υ_{rot}).

1.3.3 The Carr-Purcell Meiboom-Gill (CPMG) Pulse Sequence

The CPMG (Carr-Purcell Meiboom-Gill) pulse sequence,[22,23] also called QCPMG when applied to quadrupolar nuclei,[51-54] has become widely used in the acquisition of both wideline and UW SSNMR spectra.

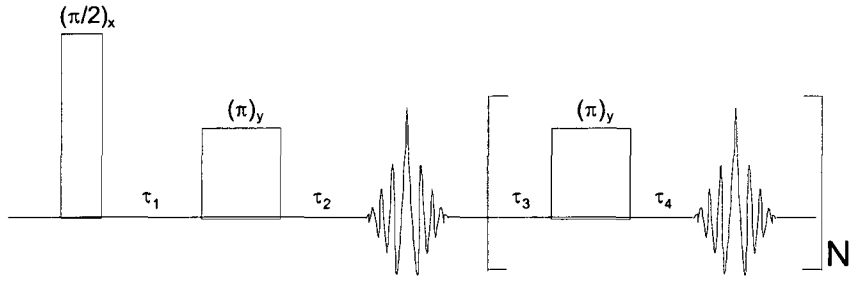

Figure 1.4. A block diagram of the Carr-Purcell Meiboom-Gill (CPMG) pulse sequence.

The sequence takes advantage of the large T_2 relaxation constants exhibited by some nuclei by continually refocusing the magnetization with a series of π pulses. As a result, a series of spin-echoes (Figure 1.5) is acquired in a single scan, significantly enhancing the signal intensity when compared to standard echo experiment,[55] in which a single refocusing pulse is made.

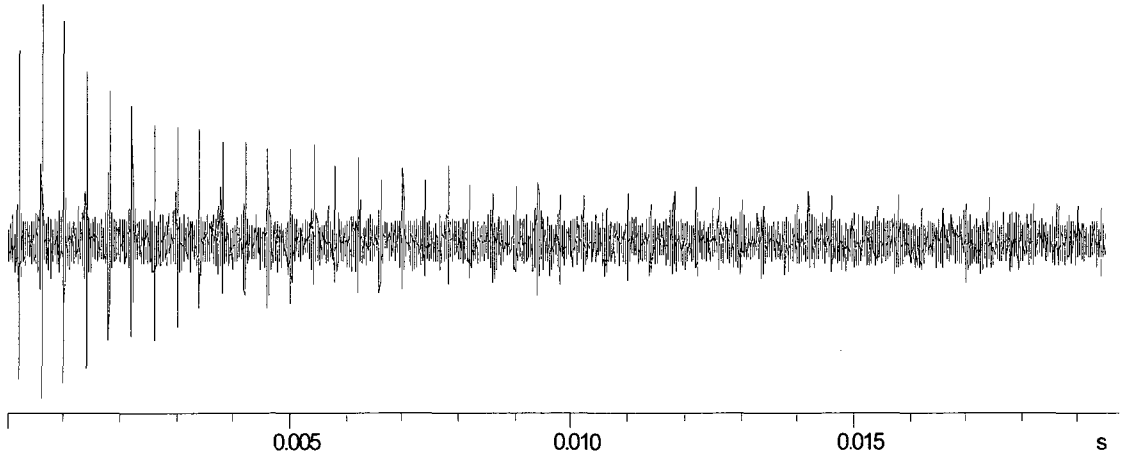

Figure 1.5. A free induction decay composed of multiple spin echoes.

This "echo train" can be directly processed by FT, results in a series of spikelets, the manifold of which takes the shape of a classic powder pattern. The spacings of the

spikelets (in Hz) are inversely proportional to the distance between the echoes (in s). Equivalently, the spin-echoes can be summed to produce an FID comprised of a single echo, which upon Fourier transformation, takes the form of a normal SSNMR powder pattern (Figure 1.6).

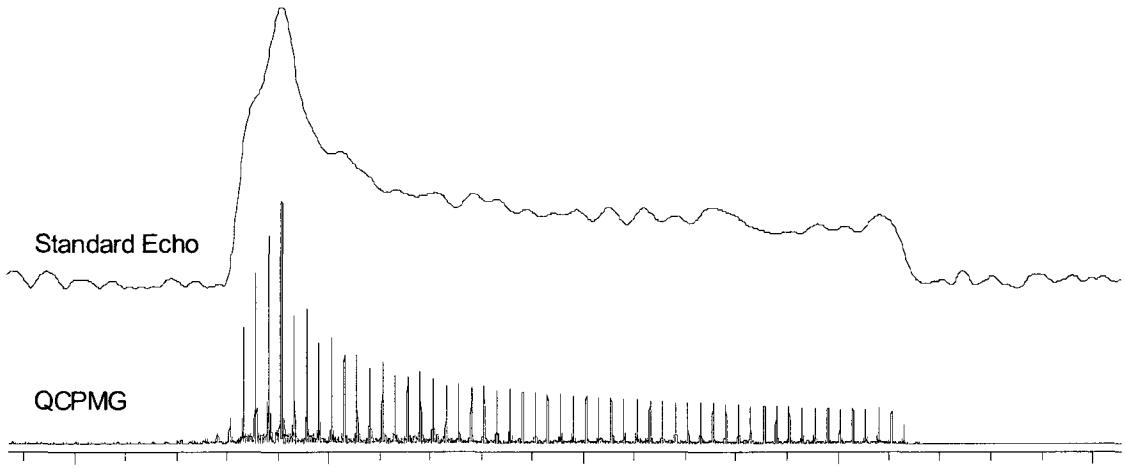

Figure 1.6. A comparison of a SSNMR spectrum acquired with a conventional echo seqeunce (top) and the CPMG sequence (bottom).

1.3.4. Wideband Uniform-Rate Smooth Truncation (WURST) QCPMG

In 2009, O'Dell et al. developed a new pulse sequence, wideband uniform-rate smooth truncation (WURST) QCPMG.[56] This sequence is a combination of the (WURST) pulse sequence[57,58] and a CPMG-type train of WURST pulses (Figure 1.7). The use of WURST pulses[57] in the acquisition of UW SSNMR spectra was proposed by Bhattacharyya and Frydman.[58] These pulses perform a frequency sweep which generates a $\mathbf{B}_{eff}$ field that sweeps from the $+z$ direction to the $-z$ (or to the xy-plane), which results in broadband excitation.[43] The CPMG-type train of WURST pulses then serves to refocus the magnetization in the xy-plane, providing significant signal enhancement when

compared to a standard echo experiment. This combination of broadband excitation and signal enhancement has made the WURST-CPMG sequence a valuable tool in the acquisition of UW SSNMR spectra, permitting acquisition of some spectra in a single experiment, and increasing the capacity to do UW NMR experiments on extremely broad patterns.[56,59]

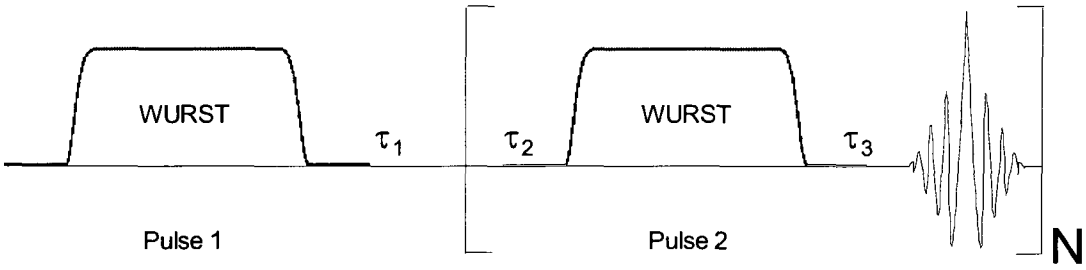

Figure 1.7. A block diagram of the wideband uniform-rate smooth truncation (WURST)-CPMG pulse sequence.

1.3.5. Cross Polarization

Cross polarization (CP) is employed in the acquisition of SSNMR spectra of nuclides which are considered unfavourable for NMR experiments due to a number of factors, such as low natural abundance and/or large T_1 relaxation constants.[60-62] Use of CP involves transferring magnetization from an abundant nucleus, I (*i.e.*, ^{1}H or ^{19}F), to the "dilute" nucleus of interest, S, which can significantly enhance the observed signal, by a maximum theoretical factor of γ_I/γ_S.[63]

A $(\pi/2)_x$ pulse is first made on the I channel, which is then followed by a lower power contact pulse that is made on both the I and S channels. To allow the transfer of magnetization to occur under static conditions, the contact pulses have the same rf field on both channels, to satisfy the Hartmann-Hahn (H-H) matching condition:[63]

$$\gamma_I B_{1I} = \gamma_S B_{1S} \quad (25)$$

The FID is then recorded by observing on the X channel. When MAS is employed, CP the H-H match is dependent upon the spinning speed. In addition, the efficiency of CP is decreased as spinning speed increases, because the I-S and I-I dipolar couplings are averaged when the spinning speed is of comparative magnitude.[63] If the combination of fast MAS and CP is required, it is possible to alleviate these averaging effects with pulse sequences such as variable-amplitude CP (VACP),[64,65] ramped-amplitude CP (RAMPCP),[66] and numerous others.

1.3.6 Optimal Control Theory

The most recent version of SIMPSON (Ver. 2.0)[67,68] NMR simulation software package includes an optimal control theory (OCT) functionality. OCT is capable of numerically optimizing a large number of variables, which makes it ideal for generating NMR pulses; one can input the spectral parameters of a given spectrum and generate a pulse designed specifically for the excitation of that spectrum. OCT studies on the optimization of NMR pulses have largely focussed on high-resolution solution experiments,[69-71] though recently our group examined the effectiveness of OCT at generating pulses for use in acquiring the solid-state spectra of quadrupolar nuclei.[72] Currently, the development of SSNMR pulses with OCT is still in its infancy and an in-depth treatment of the theory behind OCT is beyond the scope of this thesis, however it is discussed further in chapter 2, as applied to broad patterns of spin-1/2 nuclides.

1.4. Context of Research

The first research chapter of this thesis, Chapter 2, describes the application of the WURST-CPMG pulse sequence to various spin-1/2 nuclides (^{119}Sn, ^{207}Pb, ^{199}Hg and ^{195}Pt) in order to examine its effectiveness for acquiring wideline SSNMR patterns. WURST-CPMG is compared to the CP/CPMG and CPMG pulse sequences, and its usefulness in acquiring ultra-wideline (UW) SSNMR spectra in a piecewise fashion is explored. Additionally, the potential of pulses generated with SIMPSON 2.0[67,68] using optimal control theory (OCT) in acquiring wideline SSNMR spectra is investigated.; pulses generated with OCT are compared with standard, rectangular pulses at several pulse powers.

In Chapter 3, ^{207}Pb CP/CPMG and WURST-CPMG SSNMR experiments are carried out in the characterization of a series of $(2,6\text{-}Me_2C_6H_3S)_2Pb$ adducts which exhibit unique Pb(II) coordination environments. The ^{207}Pb SSNMR spectra are found to exhibit extremely large lead CSAs which span several hundred kHz, requiring piecewise acquisition with CP/CPMG. WURST-CPMG, however, is capable of exciting the entire powder pattern, eliminating the need for multiple subspectra to be acquired. ^{207}Pb NS tensor orientations are determined via *Amsterdam Density Functional* (ADF) calculations to examine the molecular origins of the experimentally determined CS tensor parameters.

In Chapter 4, ^{27}Al and ^{71}Ga solid-state NMR (SSNMR) are employed to examine a series of metal guanidinate (guan = MeN-C(N^{i}Pr$_2$)-NMe) complexes at 9.4 T and 21.1 T, to examine the relationships between the metal coordination environments and the

associated NMR interaction tensor parameters. The ^{27}Al CS and EFG tensor parameters are found to be greatly influenced by site symmetry at the metal centre; in particular, the magnitude of C_Q is determined to be strongly influenced by the nature of the bonding ligands, in addition to the aluminum coordination number. ^{71}Ga SSNMR experiments indicate that Ga(guan)$_3$ is less spherically symmetric and exhibits a much broader CSA than the similar Al analogue.

Initially, the focus of the study presented in Chapter 4 was to develop a methodology for the analysis of oriented surface-bound aluminum materials, which would require the application of signal-enhancing UW experiments. However, due to low sample loading levels and the inability to establish a lower detection limit, we chose to focus on a fundamental structural characterization of these compounds via ^{27}Al SSNMR and accompanying first principles calculations.

Bibliography

(1) Bloch, F.; Hansen, W. W.; Packard, M. *Phys. Rev.* 1946, 69, 127.

(2) Purcell, E. M.; Torrey, H. C.; Pound, R. V. *Phys. Rev.* 1946, 69, 37-38.

(3) Ashbrook, S. E. *Phys. Chem. Chem. Phys.* 2009, 11, 6892-6905.

(4) Lesage, A. *Phys. Chem. Chem. Phys.* 2009, 11, 6876-6891.

(5) Geppi, M.; Borsacchi, S.; Mollica, G.; Veracini, C. A. 2009, 44, 1-89.

(6) Singhal, A. 2009, 49-51, 149-192.

(7) Tishmack, P. A. 2009, 192, 381-435.

(8) Widdifield, C. M.; Chapman, R. P.; Bryce, D. L. 2009, 66, 195-326.

(9) Ketchem, R. R.; Hu, W.; Cross, T. A. *Science* 1993, 261, 1457-1460.

(10) Schmidt-Rohr, K.; Speiss, H. W. *Multidimentsional solid-state NMR and Polymers*; Academic Press: San Diego, 1994.

(11) Fitzgerald, J. J., Ed. *Solid-State NMR Spectroscopy of Inorganic Materials*; Oxford University Press: Washington, 1999.

(12) MacKenzie, K. J. D.; Smith, M. E. *Multinuclear Solid-state NMR of Inorganic Materials*; Pergamon: New York, 2002; Vol. 6.

(13) Kentgens, A. P. M. *Geoderma* 1997, 80, 271-306.

(14) Harris, R. K. *Nuclear Magnetic Resonance Spectroscopy*; Longman Scientific & Technical: New York, 1986.

(15) Mason, J., Ed. *Multinuclear NMR*; Plenum Press: New York, 1987.

(16) Slichter, C. P. *Principles of Magnetic Resonance*; 3rd ed. New York, 1990.

(17) Duer, M. J. *Introduction to Solid-State NMR Spectroscopy*; Blackwell Science Ltd.:

Oxford, 2004.

(18) Levitt, M. *Spin Dynamics: Basics of Nuclear Magnetic Resonance*; 2nd ed.; John Wiley and Sons: Chichester, 2008.

(19) Levitt, M. *J. Magn. Reson.* 1997, 126, 164-182.

(20) Dirac, P. A. M. *The Principles of Quantum Mechanics*; 4 ed.; Oxford University Press: Oxford, 1958.

(21) Keeler, J. *Understanding NMR Spectroscopy*; John Wiley and Sons: Chichester, 2005.

(22) Carr, H. Y.; Purcell, E. M. *Physical Review* 1954, 94, 630.

(23) Meiboom, S.; Gill, D. *Rev. Sci. Inst.* 1958, 29, 688-691.

(24) Wasylishen, R. E. In *NMR Spectroscopy Techniques*; Dybowski, C., Lichter, R. L., Eds.; Marcel Dekker, Inc.: New York, 1996, pp 45-85.

(25) Tang, J. A.; Kogut, E.; Norton, D.; Lough, A. J.; McGarvey, B. R.; Fekl, U.; Schurko, R. W. *J. Phys. Chem. B* 2009, 113, 3298-3313.

(26) Herzfeld, J.; Berger, A. E. *J. Chem. Phys.* 1980, 73, 6021-6030.

(27) Harris, R. K.; Becker, E. D.; De Menezes, S. M. C.; Granger, P.; Hoffman, R. E.; Zilm, K. W. *Magn. Reson. Chem.* 2008, 46, 582-598.

(28) Autschbach, J.; Zheng, S.; Schurko, R. W. *Conc. Magn. Reson* 2010, In Press.

(29) Samoson, A.; Lippmaa, E.; Pines, A. *Mol. Phys.* 1988, 65, 1013-1018.

(30) Wu, Y.; Sun, B. Q.; Pines, A.; Samoson, A.; Lippmaa, E. 1990, 89, 297-309.

(31) Llor, A.; Virlet, J. *Chem. Phys. Lett.* 1988, 152, 248-253.

(32) Mueller, K. T.; Sun, B. Q.; Chingas, G. C.; Zwanziger, J. W.; Terao, T.; Pines, A.

1990, 86, 470-487.

(33) Wu, Y.; Chmelka, B. F.; Pines, A.; Davis, M. E.; Grobet, P. J.; Jacobs, P. A. *Nature* 1990, 346, 550-552.

(34) Mueller, K. T.; Wooten, E. W.; Pines, A. 1991, 92, 620-627.

(35) Mueller, K. T.; Chingas, G. C.; Pines, A. *Rev. Sci. Instrum.* 1991, 62, 1445-1452.

(36) Frydman, L.; Harwood, J. S. *J. Am. Chem. Soc.* 1995, 117, 5367-5368.

(37) Medek, A.; Harwood, J. S.; Frydman, L. *J. Am. Chem. Soc.* 1995, 117, 12779-12787.

(38) Medek, A.; Frydman, L. *J. Braz. Chem. Soc.* 1999, 10, 263-277.

(39) Tang, J. A. *PhD Thesis*; University of Windsor: Windsor, 2008.

(40) Jameson, C. J.; Mason, J. In *Multinuclear NMR*; Mason, J., Ed.; Plenum Press: New York, 1987, pp 8-9.

(41) Jameson, C. J.; Mason, J. In *Multinuclear NMR*; Mason, J., Ed.; Plenum Press: New York, 1987, pp 9-11.

(42) Wasylishen, R. E. In *Encyclopedia of Nuclear Magnetic Resonance*; Grant, D. M., Harris, R. K., Eds.; Wiley Inc.: Chichester, UK, 1996; Vol. 3, pp 274-282.

(43) O'Dell, L. A.; Schurko, R. W. *Chem. Phys. Lett.* 2008, 464, 97-102.

(44) Rhodes, H. E.; Wang, P. K.; Stokes, H. T.; Slichter, C. P.; Sinfelt, J. H. *Phys. Rev. B* 1982, 26, 3559-3568.

(45) Bastow, T. J.; Smith, M. E. *Solid State Nucl. Magn. Reson.* 1992, 1, 165-174.

(46) Bryant, P. L.; Harwell, C. R.; Mrse, A. A.; Emery, E. F.; Gan, Z. H.; Caldwell, T.; Reyes, A. P.; Kuhns, P.; Hoyt, D. W.; Simeral, L. S.; Hall, R. W.; Butler, L. G. *J. Am. Chem. Soc.* 2001, 123, 12009-12017.

(47) Sampathkumaran, E. V.; Fujiwara, N.; Rayaprol, S.; Madhu, P. K.; Uwatoko, Y. *Phys. Rev. B* 2004, 70.

(48) Massiot, D.; Farnan, I.; Gautier, N.; Trumeau, D.; Trokiner, A.; Coutures, J. P. *Solid State Nucl. Magn. Reson.* 1995, 4, 241-248.

(49) Medek, A.; Frydman, V.; Frydman, L. *J. Phys. Chem. A* 1999, 103, 4830-4835.

(50) Andrew, E. R. *Philos. Trans. R. Soc. Lond. Ser. A-Math. Phys. Eng. Sci.* 1981, 299, 505-520.

(51) Larsen, F. H.; Jakobsen, H. J.; Ellis, P. D.; Nielsen, N. C. *J. Phys. Chem. A* 1997, 101, 8597-8606.

(52) Larsen, F. H.; Jakobsen, H. J.; Ellis, P. D.; Nielsen, N. C. *Mol. Phys.* 1998, 95, 1185-1195.

(53) Larsen, F. H.; Jakobsen, H. J.; Ellis, P. D.; Nielsen, N. C. *Chem. Phys. Lett.* 1998, 292, 467-473.

(54) Larsen, F. H.; Jakobsen, H. J.; Ellis, P. D.; Nielsen, N. C. *J. Magn. Reson.* 1998, 131, 144-147.

(55) Hahn, E. L. *Phys. Rev.* 1950, 80, 580-594.

(56) O'Dell, L. A.; Rossini, A. J.; Schurko, R. W. *Chem. Phys. Lett.* 2009, 468, 330-335.

(57) Kupce, E.; Freeman, R. *J. Magn. Reson. Ser. A* 1995, 115, 273-276.

(58) Bhattacharyya, R.; Frydman, L. *J. Chem. Phys.* 2007, 127.

(59) Tang, J. A.; O'Dell, L. A.; Aguiar, P. M.; Lucier, B. E. G.; Sakellariou, D.; Schurko, R. W. *Chem. Phys. Lett.* 2008, 466, 227-234.

(60) Siegel, R.; Nakashima, T. T.; Wasylishen, R. E. *Journal of Physical Chemistry B*

2004, 108, 2218-2226.

(61) Hung, I.; Rossini, A. J.; Schurko, R. W. *Journal of Physical Chemistry A* 2004, 108, 7112-7120.

(62) Briand, G. G.; Smith, A. D.; Schatte, G.; Rossini, A. J.; Schurko, R. W. *Inorg. Chem.* 2007, 46, 8625-8637.

(63) MacKenzie, K. J. D.; Smith, M. E. In *Pergamon Materials Series*; Pergamon: New York, 2002; Vol. 6, pp 85-90.

(64) Peersen, O. B.; Wu, X. L.; Kustanovich, I.; Smith, S. O. *J. Magn. Reson. Ser. A* 1993, 104, 334-339.

(65) Peersen, O. B.; Wu, X. L.; Smith, S. O. *J. Magn. Reson. Ser. A* 1994, 106, 127-131.

(66) Metz, G.; Wu, X. L.; Smith, S. O. *J. Magn. Reson. Ser. A* 1994, 110, 219-227.

(67) Bak, M.; Rasmussen, J. T.; Nielsen, N. C. *J. Magn. Reson.* 2000, 147, 296-330.

(68) Tosner, Z.; Vosegaard, T.; Kehlet, C.; Khaneja, N.; Glaser, S. J.; Nielsen, N. C. *J. Magn. Reson.* 2009, 197, 120-134.

(69) Skinner, T. E.; Reiss, T. O.; Luy, B.; Khaneja, N.; Glaser, S. J. *J. Magn. Reson.* 2003, 163, 8-15.

(70) Skinner, T. E.; Reiss, T. O.; Luy, B.; Khaneja, N.; Glaser, S. J. *J. Magn. Reson.* 2004, 167, 68-74.

(71) Kobzar, K.; Skinner, T. E.; Khaneja, N.; Glaser, S. J.; Luy, B. *J. Magn. Reson.* 2004, 170, 236-243.

(72) O'Dell, L. A.; Harris, K. J.; Schurko, R. W. *J. Magn. Reson.* 2010, 203, 156-166.

Chapter 2

New Methods for the Acquisition of Static CSA Patterns from Spin-1/2 Nuclides

2.1 Introduction

Solid-state NMR (SSNMR) powder patterns can vary in breadth from a few Hz to several MHz. In the former extreme, the widths of the spectral lines are on the order of those encountered in many solution-state NMR spectra. Such narrow lines occur in SSNMR spectra due to the absence of large anisotropic interactions or dipolar couplings, low magnetic susceptibility broadening, averaging via mechanical rotation and/or specialized pulse sequences, or combinations of these factors. However, the latter extreme describes the situation for many nuclides across the periodic table, where large anisotropic interactions dominate the appearance of the NMR powder patterns, and techniques for averaging (or partially averaging) these interactions are generally ineffective. Nonetheless, there is much information to be garnered from the acquisition of such patterns; in particular, analysis of the anisotropic NMR interaction tensors which give rise to these broad patterns can provide detailed information on structure and dynamics at the molecular level.

Wideline NMR spectroscopy is a term that has been in use since the 1950's to refer to NMR experiments conducted on nuclei with broad patterns arising from anisotropic dipole-dipole interactions (*e.g.*, ^{1}H, ^{19}F), quadrupolar interactions (*e.g.*, ^{2}H) and large chemical shift anisotropies (*e.g.*, ^{207}Pb, ^{199}Hg, etc.). Typically, these patterns range in

breadth from tens of kHz to *ca.* 300 kHz. However, there are numerous nuclei, both spin-1/2 and quadrupolar (*i.e.,* spin > 1/2), which can yield NMR patterns with breadths of hundreds of kHz to tens of MHz. Acquisition of such NMR spectra can be challenging, since (i) the signal intensity is spread over a wide spectral range, thereby decreasing the inherent signal to noise ratio (S/N), (ii) standard, high-power rectangular pulses are insufficient for uniform excitation of these broad patterns[1] and (iii) the probe detection bandwidths are often very limited. Such spectra cannot be acquired with routine NMR experiments, but require specialized methodologies, pulse sequences and/or hardware. We have previously suggested the term *ultra-wideline* (UW) *NMR spectroscopy* to describe the set of techniques designed to ensure uniform excitation of such extremely broad patterns.[2] Improvements in NMR hardware, the availability of ultra-high magnetic fields and the introduction of an array of different pulse sequences and experimental schemes have made the acquisition of UW NMR spectra feasible, and opened up the periodic table of NMR-active nuclides to investigation via SSNMR.[3-9]

Early UW NMR spectra were acquired using a "point-by-point" method, where the transmitter is stepped in even increments across the entire spectral range at constant magnetic field, and the echo intensity is plotted as a function of the transmitter frequency to obtain the total powder pattern.[10,11] There are recent reports that feature this acquisition technique, or describe experiments in which the magnetic field is incrementally stepped while holding the transmitter frequency constant.[3,12] This basic technique is very time-consuming, since a large number of experiments must be conducted to obtain an UW NMR spectrum of reasonable resolution. However, it was

later suggested that the total UW NMR experiment can be conducted more efficiently by acquiring echoes at evenly spaced transmitter offsets, Fourier transforming the individual echoes, and then co-adding[13,14] or skyline projecting[15] the resulting sub-spectra to produce the final pattern. This reduces the number of experiments required to obtain the complete powder pattern, and provides spectral resolution more closely associated with the dwell time of the echo experiment than the transmitter spacing.

There have been several modifications to the aforementioned UW NMR techniques that involve specialized pulse sequences or hardware. The quadrupolar Carr-Purcell Meiboom-Gill (QCPMG) pulse sequence, which was reintroduced for the acquisition of wideline NMR spectra of half-integer quadrupolar nuclei,[16] has been particularly useful in enhancing the S/N of individual sub-spectra and reducing total acquisition times in UW NMR experiments.[15,17-22] Another recently explored method for acquiring UW NMR spectra involves the use of microcoils,[2,23,24] which typically have a 1.5 mm inner diameter or less. Microcoils are capable of producing large, homogeneous B_1 fields from very modest power inputs. This feature partially offsets the loss in S/N from reduced sample size and allows for excitation pulses with correspondingly wider excitation bandwidths. In addition, the small coil size may also be advantageous in cases where only a limited amount of sample is available.

A recent development in the acquisition of UW spectra was initiated by Bhattacharyya and Frydman,[25] who proposed the use of WURST (Wideband Uniform Rate Smooth Truncation) broadband excitation pulses,[26] which greatly increase excitation bandwidths without the need for specialized hardware. Our group has recently expanded

upon this work with the WURST-QCPMG pulse sequence,[22] which utilizes a train of WURST pulses and acquisition windows in a fashion similar to the QCPMG sequence. The combination of the broad excitation bandwidths of WURST pulses with the signal enhancements of the QCPMG sequence has proven useful in the acquisition of NMR spectra of both half-integer and integer quadrupolar nuclei.[27]

Another potential method for acquiring UW NMR spectra lies in using optimal control theory (OCT), which was recently implemented in the SIMPSON (ver. 2.0) software package.[28,29] OCT can be used to numerically optimize a system composed of a very large number of variables, and can therefore be utilized to adjust pulse amplitudes, phases, transmitter offsets, etc. in order to obtain an "optimal NMR pulse sequence" in which the experimental efficiency is maximized. OCT has been used to generate broadband excitation schemes for high-resolution ^{13}C NMR at high fields, with excitation profiles of approximately 50 kHz,[30-32] as well as spectra of half-integer quadrupolar nuclei.[33] However, to the best of our knowledge, OCT has not yet been employed to optimize broadband excitation pulses for the acquisition of static UW powder patterns.

UW NMR studies to date have largely focussed on half-integer quadrupolar nuclei with broad central-transition NMR spectra resulting from large nuclear quadrupole moments and/or low gyromagnetic ratios coupled with sizeable electric field gradients (EFGs).[8,9,15,19,34-36] However, there are several heavy spin-1/2 nuclei such as ^{119}Sn, ^{195}Pt, ^{199}Hg and ^{207}Pb, which often have large chemical shift anisotropies (CSAs) and correspondingly broad patterns that could potentially be acquired efficiently using UW NMR experiments. For instance, Slichter and co-workers published several papers in the

1980's on ^{195}Pt NMR of catalytic platinum nanoparticles adsorbed on alumina, where the stepwise method was used to acquire ^{195}Pt NMR spectra up to 70 kHz in breadth.[10,37] Ellis and coworkers also carried out UW ^{195}Pt NMR experiments, though they employed MAS to acquire the extremely broad spectrum of K_2PtCl_4.[38] MAS techniques have also been used to acquire broad ^{119}Sn[39,40] and ^{199}Hg spectra.[41] However, we noted in two recent papers on UW ^{207}Pb and ^{195}Pt SSNMR[42,43] that MAS experiments on nuclei with extremely broad patterns are often unreliable, due to slight mis-sets of the magic angle[44] and/or incomplete excitation of the manifold of spinning sidebands, both of which yield patterns which do not allow for accurate assessments of the chemical shift tensor parameters.

In 2004, our research group, and Wasylishen *et al.*, examined the effectiveness of the CPMG pulse sequence in acquiring the NMR spectra of various spin-1/2 nuclei.[45,46] These experiments are especially useful when cross-polarization (CP)/MAS NMR experiments are limited by weak dipolar couplings and poor excitation bandwidths, or other complications arising from acquisition of broad powder patterns using MAS NMR.[44,47,48] ^{1}H-X (where X is a heavy spin-1/2 nucleus) CP/CPMG experiments are capable of yielding high quality UW NMR spectra from which chemical shift tensors can be readily extracted; however, the acquisitions of broad patterns are labour intensive, requiring the collection of many sub-spectra due to the limited excitation bandwidth associated with CP.[42] CPMG can also be used to directly excite the X nuclei with modest improvements in bandwidth; however, such experiments still require numerous sub-spectra to be acquired and are often hampered by large longitudinal (T_1) relaxation time

constants.

Herein, we improve upon the efficiency of previous UW NMR experiments on heavy spin-1/2 nuclides via application of the WURST-CPMG pulse sequence (WURST-CPMG is the exact same sequence as WURST-QCPMG, but since this paper does not deal with quadrupolar nuclei, we have omitted the "Q" as it does not apply here). UW ^{119}Sn, ^{207}Pb, ^{199}Hg and ^{195}Pt NMR spectra are acquired for some samples with large chemical shift anisotropies, and compared to data from analogous CPMG and CP/CPMG experiments, as appropriate. In addition, we also present the first attempt at utilizing pulses designed using OCT for uniform excitation of CSA-dominated powder patterns.

2.2 Experimental Details

All solid-state NMR experiments were carried out on a Varian InfinityPlus NMR spectrometer, equipped with an Oxford 9.4 T ($\nu_0(^1H)$ = 400 MHz) wide-bore magnet operating at $\nu_0(^{207}Pb)$ = 83.50 MHz, $\nu_0(^{195}Pt)$ = 85.76 MHz, $\nu_0(^{199}Hg)$ = 71.39 MHz and $\nu_0(^{119}Sn)$ = 149.29 MHz. All experiments were performed on a Varian/Chemagnetics 4 mm HXY triple resonance probe, with samples tightly packed into 4 mm (o.d.) zirconium oxide rotors. SnO was purchased from Strem Chemicals, and all other samples [$Pb(OAc)_2 \cdot 3H_2O$ (where OAc = CH_3CHOO), $Hg(OAc)_2$, and K_2PtCl_4] were purchased from Sigma-Aldrich. The $Pb(OAc)_2 \cdot 3H_2O$ was recrystallized from aqueous solution, and the remaining samples were used without further purification.

^{207}Pb NMR chemical shifts are reported with respect to tetramethyl lead ($Pb(CH_3)_4$, δ_{iso} = 0.0 ppm) by using an aqueous solution of 0.5 M lead acetate hydrate

($Pb(CH_3COO)_2 \cdot 3H_2O$) as a secondary standard with an isotropic chemical shift of -2941 ppm.[49] ^{195}Pt chemical shifts are referenced with respect to 1.0 M $NaPt(ClO_4)_2$ (aq) (δ_{iso} = 0.0 ppm).[50] ^{199}Hg chemical shifts are reported with respect to $Hg(CH_3)_2$ by setting the isotropic shift of a saturated aqueous solution of $Hg(ClO_4)_2$ to -2253 ppm.[51] Finally, tetramethyltin ($Sn(CH_3)_4$) was used as a reference standard for ^{119}Sn NMR experiments, with its isotropic shift set to 0.0 ppm.[52]

WURST-CPMG experiments employed recycle delays of 2, 7, 40 and 1450 s for the acquisition of all ^{119}Sn, ^{207}Pb, ^{195}Pt and ^{199}Hg NMR spectra, respectively. 50 μs pulse widths, and WURST-80 pulse shapes, were used for all WURST-CPMG experiments, with nutation frequencies of *ca.* 30, 67, 46 and 28 kHz for ^{119}Sn, ^{195}Pt, ^{207}Pb and ^{199}Hg, respectively. Between 64 and 250 Meiboom-Gill loops were acquired for the WURST-CPMG experiments, with an echo size of 200 points, sweep rate of in all cases. Further experimental details regarding the WURST-CPMG experiments can be found in the Appendix A (Table A1).

The CPMG pulse sequence was used to acquire the ^{119}Sn SSNMR spectrum of SnO. 10 sub-spectra were acquired by stepping the transmitter frequency at 45 kHz intervals, then Fourier transformed and co-added to yield the complete powder pattern. A 3.33 μs 90° pulse was employed, corresponding to an rf field of *ca.* 75 kHz. 64 Meiboom-Gill loops of 200 points were acquired for each transient, with a 2 s recycle delay. Further experimental details are summarized in Table A2.

The CP/CPMG sequence[45,46] was employed to obtain the ^{207}Pb NMR spectrum of $Pb(CH_3OO)_2 \cdot 3H_2O$. Nine echoes were acquired in a piecewise manner at 20 kHz offsets,

then co-added after being Fourier transformed to yield the complete spectrum. A Hartmann-Hahn matching condition of $\nu_{CP}(^{1}H) = \nu_{CP}(^{207}Pb) \approx 48$ kHz was used. Eighty Meiboom-Gill loops were acquired per scan, each of which was 200 points in length, and a 4 s pulse delay was employed between scans. Further experimental details regarding the CP/CPMG experiment can be found in Table A3.

The TPPM decoupling scheme[53] was employed for the acquisition of ^{207}Pb and ^{199}Hg CP/CPMG and CPMG NMR spectra, respectively, whereas CW decoupling was employed in all WURST-CPMG experiments. We note that in previous work by our group, we observed no noticeable difference in performance between CW and TPPM decoupling methods when recording UW spectra from static samples; therefore, choice of decoupling method should have no bearing on comparison of spectra acquired with different experiments.[54] Unless otherwise indicated, analytical simulations of static SSNMR spectra for the extraction of CS tensor parameters are based upon spectra produced from the time-domain co-addition of spin echos from WURST-CPMG experiments. This involves summing the spin-echoes in the time domain, which produces an FID resembling that of a standard echo sequence. This co-added echo is Fourier transformed, and a magnitude calculation is applied to obtain a spectrum of standard appearance (rather than spikelets), which has an outer manifold that is more easily simulated. WURST-CPMG spectra processed in this way can be found in the Appendix A (Figure A1), or in the case of $Hg(OAc)_2$, in Figure 2.3. Numerical simulations of WURST-CPMG powder patterns were also carried out using SIMPSON[28,29] to verify and refine the simulated parameter values. Additional

simulations of experimental spectra from CPMG and CP/CPMG experiments were also carried out using the WSolids simulation package[55] and/or DMFit[56] simulation software.

Optimized pulses employed during OCT experiments were generated using SIMPSON (ver. 2.0)[29] on a desktop computer with the Windows XP operating system. SnO was chosen as a test sample for all OCT experiments due to the receptive nature of the ^{119}Sn nucleus and its well known CS tensor parameters.[40] The CS tensor parameters used for the generation of all optimized pulses were Ω = 976 ppm and κ = 0.96, which are based on a simulation of a ^{119}Sn SSNMR spectrum acquired previously using the WURST-CPMG sequence. 376 crystallite orientations were used to optimize each pulse, and 28,656 crystallite orientations were used to produce corresponding numerical simulations. These orientations were calculated using the ZCW method.[57-59] Each pulse generated using OCT was composed of 200 elements of length 0.25 μs, with constant amplitude and phase during each of the constituent elements. The optimized pulses resulted from the optimization of initial, random pulse shapes, with the rf field limited by a maximum value. The pulse shapes were output as text files and manually converted into the P-code format required for use with the Varian Spinsight software. Simulations of all spectra related to the OCT portion of this work were carried out using SIMPSON (ver. 2.0).[28,29] All spectra were processed using NUTS (Acorn NMR).

2.3 Results and Discussion

2.3.1 ^{119}Sn NMR

Tin has three NMR active isotopes, ^{115}Sn, ^{117}Sn and ^{119}Sn; however, ^{119}Sn is generally chosen for tin NMR studies as it has the highest natural abundance (8.58%) and highest gyromagnetic ratio (-9.99760 x 10^7 rad T^{-1} s^{-1}, corresponding to 149.57 MHz at 9.4 T). Solid-state ^{119}Sn NMR has been used to study a wide variety of systems, including stannates,[39,60,61] nanoparticles,[62-64] and various organotin materials,[65-67] among others. We have chosen SnO to test ^{119}Sn WURST-CPMG because of its high tin content and its large (975 ppm) span.[40]

The ^{119}Sn NMR spectra of SnO acquired using the CPMG and WURST-CPMG pulse sequences are depicted in Figure 2.1. The powder patterns are *ca.* 160 kHz in breadth, and clearly indicate that the CS tensor is axially symmetric (*vide infra*). The pattern breadth is beyond the excitation bandwidth of standard rectangular pulses applied at commonly attainable rf powers; in this case, the CPMG experiment utilized $\pi/2$ pulses of *ca.* 3.3 μs ($\nu_1 \approx 75$ kHz). The CPMG spectrum (Figure 2.1A) was acquired in a piecewise frequency-stepped manner, with ten sub-spectra (80 transients per sub-spectrum) to complete the total pattern. The total spectrum was acquired in 27 minutes, not including the time required to retune the probe for each transmitter frequency. The WURST-CPMG (Figure 2.1B) spectrum was acquired in a single, 80 scan experiment which employed pulses with rf fields of 30 kHz and took *ca.* 3 minutes to complete; a reduction in experimental time of almost an order of magnitude (Table 2.1). In addition, there was a further (and substantial) reduction in experimental time, since the probe does

not have to be retuned. The S/N is comparable in the CPMG and WURST-CPMG spectra, but the latter is better defined in the region of δ_{33} (*i.e.,* the rightmost or low-frequency edge). There is also a pronounced modulation along the breadth of the CPMG spectrum which is not visible in the WURST-CPMG spectrum.

The CS tensor parameters are obtained by fitting a simulated pattern to either the outer manifold of the spikelet spectrum, or to a spectrum produced by Fourier transforming an FID produced from the co-addition of the WURST-CPMG spin-echoes in the time domain. Our simulation indicates that the CS parameters of SnO are δ_{iso} = −208 ppm, Ω = 988 ppm and κ = 0.95 (Table 2.2). These data agree well with the results of Cossement *et al.*, δ_{iso} = −208 ppm, Ω = 975 ppm and κ = 1.0.[40] A SIMPSON simulation of the WURST-CPMG spikelet manifold (Figure 2.1C) confirms the accuracy of the simulated parameters.

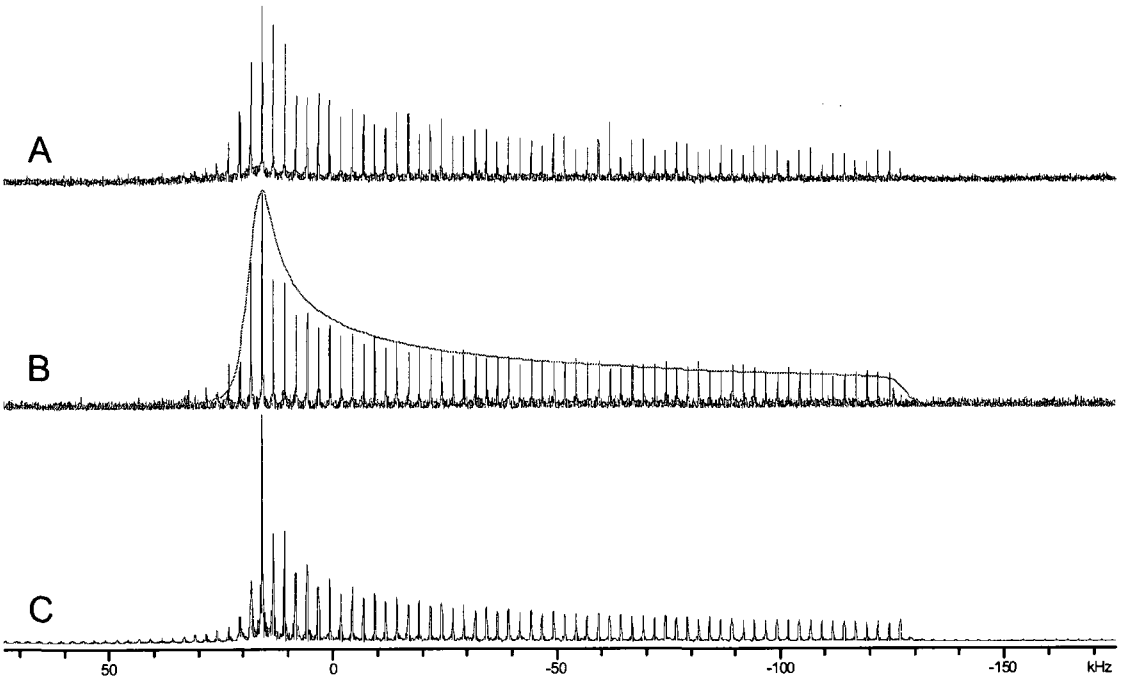

Figure 2.1. (A) ^{119}Sn CPMG NMR spectrum of SnO produced from the co-addition of 10 sub-spectra, each of which consists of 80 averaged transients. (B) Bottom trace: ^{119}Sn WURST-CPMG NMR spectrum of SnO. The spectrum consists of 80 averaged transients and was acquired in a single experiment. Top trace: analytical simulation based on the co-addition of the echoes from the WURST-CPMG experiment. (C) SIMPSON simulation of ^{119}Sn WURST-CPMG NMR spectrum of SnO.

Table 2.1. Comparison of total experimental times for CPMG, CP/CPMG and WURST-CPMG experiments.

	SnO		$Pb(OAc)_2 \cdot 3H_2O$		$Hg(OAc)_2$	K_2PtCl_4
	CPMG	WURST -CPMG	CP/CPMG	WURST -CPMG	WURST-CPMG	WURST -CPMG
Sub-spectra [a]	10	1	9	1	1	5
Scans per subspectrum	80	80	192	248	72	40
Recycle delay (s)	2	2	4	7	1450	40
Step size (kHz) [b]	45	N/A	20	N/A	N/A	400
Experimental time [c] (mins)	26.7	2.7	115.2	28.9	1740	133.3

[a] Denotes the number of sub-spectra required to collect the entire powder pattern with piecewise acquisition. A value of 1 indicates that piecewise acquisition was not required.
[b] Denotes the spacing between transmitter frequencies of sub-spectra in piecewise experiments.
[c] Experimental times listed do not account for the time required to retune the probe and change the transmitter frequency between sub-spectra in piecewise experiments.

Table 2.2. Comparison of experimental chemical shift parameters with values reported in the literature.[a]

Compound	δ_{iso} [b] (ppm)	Ω [c] (ppm)	κ [d]	ref. [e]
SnO (exp.)	**-208 (5)**	**988 (25)**	**0.95 (5)**	
SnO (lit.)	-208	975	1	40
$Pb(OAc)_2$ (exp.)	**-1890 (20)**	**1690 (30)**	**0.61 (4)**	
$Pb(OAc)_2$ (lit.)	-1904	1728	0.62	68
$Hg(OAc)_2$ (exp.)	**-2513 (20)**	**1810 (45)**	**0.89 (5)**	
$Hg(OAc)_2$ (lit.)	-2497	1826	0.9	69
K_2PtCl_4 (exp.)	**-1510 (100)**	**10425 (200)**	**-0.97 (3)**	
K_2PtCl_4 (lit.)	-1848	10414	-1	38

[a] The chemical shielding of each nucleus is represented as a tensor described by three principal components calculated from values of δ_{iso}, κ, and Ω. These principal components are arranged so that $\delta_{11} \geq \delta_{22} \geq \delta_{33}$.
[b] $\delta_{iso} = (\delta_{11} + \delta_{22} + \delta_{33})/3$. Values are with respect to reference standards given in the experimental section.
[c] $\Omega = (\delta_{11} - \delta_{33})$, based upon simulations of static WURST-CPMG spectra.
[d] $\kappa = 3(\delta_{22} - \delta_{iso})/\Omega$, $-1.0 \leq \kappa \leq 1.0$.
[e] Indicates the relevant reference for values reported in the literature.

2.3.2 ^{207}Pb NMR

^{207}Pb NMR experiments can be challenging to carry out because of the vast chemical shift range of lead, as well as the generally large lead chemical shift anisotropies and long T_1 relaxation times.[49,70-73] However, ^{207}Pb NMR is an extremely sensitive probe of the local Pb environment and has become an important tool in the characterization of lead-containing materials.[73] ^{207}Pb NMR has recently been applied to study technologically advanced materials such as waste disposal media[49] and materials relevant to lead-based superconductors.[49,70] The high sensitivity of the ^{207}Pb chemical shifts to small changes in sample temperature has contributed to the use of various lead-containing samples as "NMR thermometers."[74,75]

For lead-containing samples where protons are present, ^{1}H-^{207}Pb CP/MAS NMR experiments are typically applied, due to the enhancement afforded from CP and the dependence of the experimental recycle time on the T_1 of the protons (as opposed to the T_1 constants of ^{207}Pb, which are usually much longer).[71] In numerous cases where the CP efficiency is greatly reduced under conditions of MAS (even under slow spinning), static piecewise ^{1}H-^{207}Pb CP/CPMG NMR experiments are useful for the acquisition of ^{207}Pb NMR spectra. However, many ^{207}Pb NMR spectra are far too broad to be obtained in a single experiment, even under conditions of MAS.[38,42] $Pb(OAc)_2{\cdot}3H_2O$ is often used as a setup standard for stationary ^{1}H-^{207}Pb CP/CPMG NMR experiments, due to its relatively narrow pattern and short ^{1}H T_1 (*ca.* 7 s).[45,68,76] However, the breadth of the ^{207}Pb NMR spectrum of $Pb(OAc)_2{\cdot}3H_2O$ (at 9.4 T) far exceeds the excitation bandwidth of the CP/CPMG sequence, which is dependent upon the Hartmann-Hahn matching condition

(which can only be achieved across a relatively narrow range of frequencies). Direct excitation of the nucleus (*i.e.,* without CP), though also limited in bandwidth, has been shown to be more useful for the acquisition of broad NMR patterns.[77] Consequently, we employed WURST-CPMG to attempt an acquisition of the entire powder pattern of $Pb(OAc)_2 \cdot 3H_2O$ in a single experiment.

Figure 2.2 depicts the spectra of $Pb(OAc)_2 \cdot 3H_2O$ acquired with CP/CPMG (Figure 2.2A) and WURST-CPMG (Figure 2.2B). The spectra are *ca.* 138 kHz in breadth, with clearly defined discontinuities. The CSA-dominated powder pattern is too broad to be acquired with a single CP/CPMG experiment, necessitating the use of the piecewise frequency-stepped method. A total of nine sub-spectra were acquired to construct the complete powder pattern, each of which took just under 13 minutes to obtain, requiring *ca.* 115 minutes to acquire the complete pattern, not including the time required to retune the probe (Table 2.1).

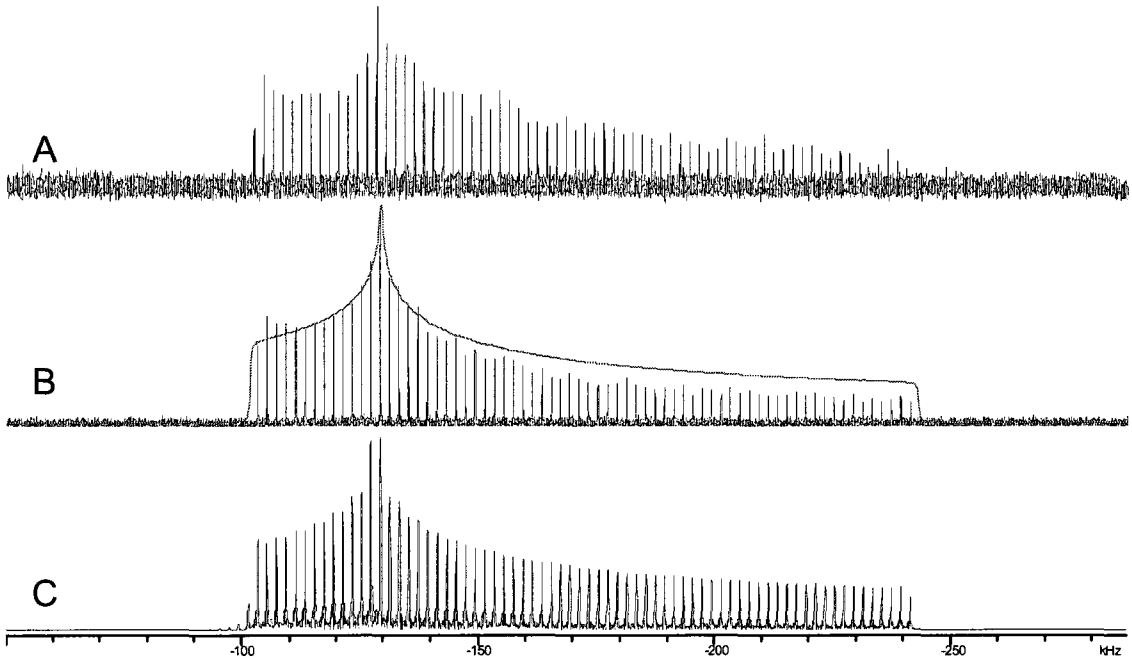

Figure 2.2 (A) ^{207}Pb CP/CPMG NMR spectrum of $Pb(OAc)_2 \cdot 3H_2O$ from the co-addition of 9 sub-spectra, each of which consists of 192 averaged transients. (B) Bottom trace: ^{207}Pb WURST-CPMG NMR spectrum of $Pb(OAc)_2 \cdot 3H_2O$ from the collection of 248 averaged transients in a single experiment. Top trace: analytical simulation based on the co-addition of the echoes from the WURST-CPMG experiment. (C) SIMPSON simulation of the ^{207}Pb WURST-CPMG NMR spectrum of $Pb(OAc)_2 \cdot 3H_2O$.

The WURST-CPMG ^{207}Pb NMR spectrum of $Pb(OAc)_2 \cdot 3H_2O$ was acquired in a single 248 scan experiment that required just under 30 minutes to complete. The WURST-CPMG pattern has a much higher signal-to-noise ratio and more clearly resolved discontinuities than the CP/CPMG pattern; in addition, the former required no special processing (*i.e.,* co-addition of sub-spectra). Simulation of the spectrum resulting from the time-domain co-added echoes of the WURST-CPMG experiment yields δ_{iso} = -1890 ppm, Ω = 1690 ppm and κ = 0.61, all of which agree very well with previously reported parameters (Table 2.2).[45,68,76] A SIMPSON simulation of the ^{207}Pb WURST-CPMG spikelet manifold (Figure 2.2B) using these parameters again further confirms the

accuracy of these values.

Due to the use of lead acetate as a ^{207}Pb SSNMR setup standard, it is worth noting that our first attempts to acquire these spectra resulted in distorted powder patterns with a pronounced "lump" at the high-frequency end of the pattern (Figure A2). However, recrystallization of the sample from aqueous solution significantly changed the appearance of the ^{207}Pb UW NMR spectrum, leading us to conclude that the initial sample was partially dehydrated. Indeed, the same phenomenon was acknowledged in our group's previous paper involving lead acetate hydrate, though a more pronounced shift to high frequency was noted.[45] This example illustrates the potential for WURST-CPMG experiments to enable the identification of impurities in samples where MAS experiments may not be suitable or possible.

2.3.3 ^{199}Hg NMR

Mercury has two NMR-active isotopes, ^{199}Hg and ^{201}Hg. The former is preferred for NMR spectroscopy due to its higher natural abundance (16.8%), higher gyromagnetic ratio (4.8458 x 10^7 rad T^{-1} s^{-1}, ν_0 = 72.5 MHz at 9.4 T) and the fact that it is a spin-1/2 nucleus (^{201}Hg is a spin 3/2 nucleus). ^{199}Hg NMR has been used extensively to probe the atomic environment of metal centres in biologically relevant materials by using ^{199}Hg as a surrogate nucleus for less receptive nuclei (*e.g.*, ^{67}Zn),[78] or to study model compounds of metal centres in proteins.[44] Solid-state ^{199}Hg NMR data has been collected for many different types of mercury-containing compounds, from dimercury (I) species[79] to organometallic molecules.[41] Like ^{207}Pb, ^{199}Hg also has an expansive chemical shift

range,[80] and many ^{199}Hg SSNMR spectra exhibit large CSAs, making ^{199}Hg SSNMR extremely sensitive to changes in local Hg environments. $Hg(OAc)_2$ was chosen as a test sample for ^{199}Hg WURST-CPMG NMR experiments because of its use as a CP setup standard in ^{199}Hg CP/MAS NMR experiments, as well as its well-characterized CS tensor parameters.[45,81]

Figure 2.3 shows the ^{199}Hg WURST-CPMG NMR spectrum of $Hg(OAc)_2$. The spectrum is *ca.* 130 kHz broad, and indicates a mercury CS tensor of nearly axial symmetry. 72 scans were used to acquire the ^{199}Hg WURST-CPMG NMR spectrum, resulting in a total experimental time of *ca.* 29 hours. A long recycle delay of 1450 s was applied for this experiment, due to the large $T_1(^{199}Hg)$ relaxation time constants.[69] Our group previously acquired the ^{199}Hg NMR spectrum of $Hg(OAc)_2$ with a piecewise ^{1}H-^{199}Hg CP/CPMG experiment that required the acquisition of six sub-spectra,[45] each subspectrum took 16 scans to acquire for the CP/CPMG experiments, and the entire experimental time required was *ca.* 2.4 hours (Table 2.1). Wasylishen *et. al* also acquired the ^{199}Hg NMR spectrum of $Hg(OAc)_2$ using CP/CPMG, which required the acquisition of nine sub-spectra and took *ca.* 5 hours.[46] The use of WURST-CPMG does not reduce the time required to obtain the ^{199}Hg NMR spectrum of $Hg(OAc)_2$ compared to the CP/CPMG experiment, largely due to the dependence of the recycle delay of the latter on the much shorter proton T_1. However, our experiment demonstrates that the WURST-CPMG sequence can be readily employed to acquire ^{199}Hg NMR spectra in cases where CP is not a viable option (*i.e.,* little or no CP efficiency due to the absence of abundant and/or mobile nuclei, etc.). Again, the other benefit of using WURST-CPMG is that the

entire powder pattern may be acquired without stepping the transmitter, and hence, no probe retuning is required. Fitting of the spectrum with SIMPSON yielded δ_{iso} = -2513 ppm, Ω = 1810 ppm and κ = 0.89, which match well with previous values (δ_{iso} = -2515, Ω = 1826 and κ= 0.90).[69]

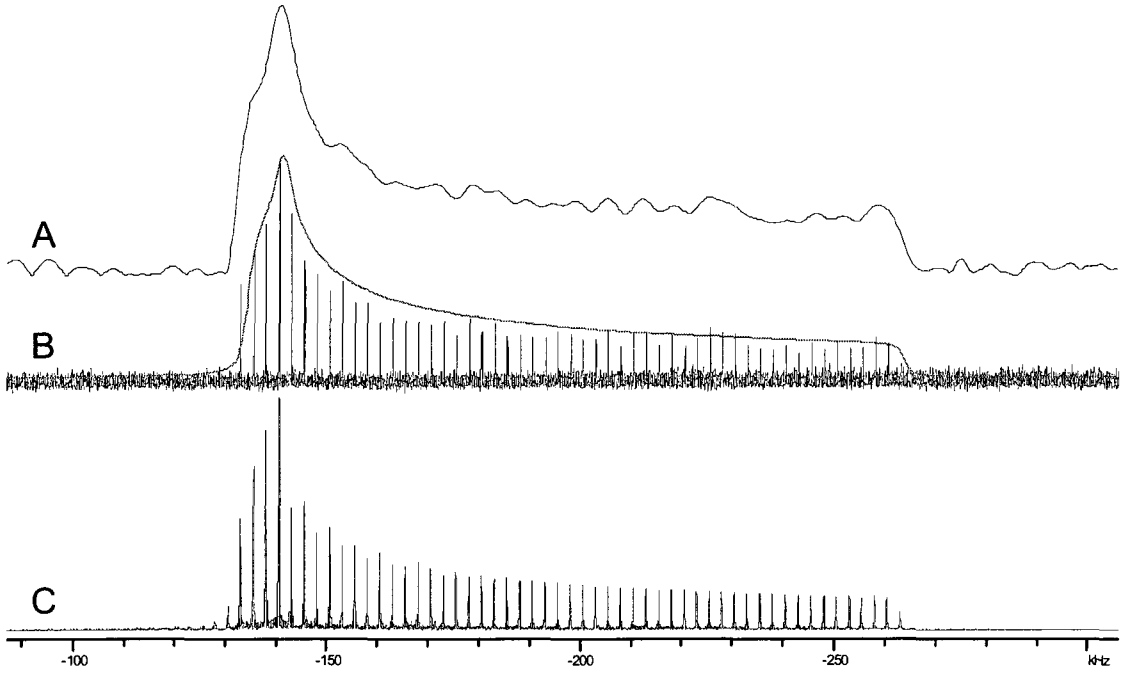

Figure 2.3. (A) Echo spectrum resulting from Fourier transformation of the sum of the spin-echoes of the ^{199}Hg WURST-CPMG experiment. (B) Bottom trace: ^{199}Hg WURST-CPMG NMR spectrum of $Hg(OAc)_2$. Top trace: analytical simulation based on the spectrum in A. (C) SIMPSON simulation of the ^{199}Hg WURST-CPMG NMR spectrum of $Hg(OAc)_2$.

2.3.4 ^{195}Pt NMR

^{195}Pt, the only NMR-active isotope of platinum, has a high natural abundance (33.8%) and a moderate gyromagnetic ratio (5.8383 × 10^7 rad T^{-1} s^{-1}, corresponding to a spectral frequency of 85.92 MHz at 9.4 T). ^{195}Pt NMR has been employed to study a broad range of platinum-containing materials including catalytic systems,[10,37,82,83] semi-

conductors,[84] and various platinum coordination complexes.[43,50,85-88] There is great variation in the magnitude of known platinum CSAs:[89] to date, the largest reported span obtained from ^{195}Pt SSNMR is that of K_2PtCl_4 (Ω =10414 ppm).[38] We chose K_2PtCl_4 to test the effectiveness of WURST-CPMG for patterns beyond the observable bandwidth of a WURST experiment.

Figure 2.4 depicts the ^{195}Pt NMR spectrum acquired with the WURST-CPMG pulse sequence. The pattern is too broad (*ca.* 980 kHz) to be collected in a single WURST-CPMG experiment; thus, piecewise acquisition is necessary. The collection of five sub-spectra at 400 kHz transmitter offsets was sufficient to obtain the entire powder pattern in just over 2 hours (Table 2.1). Based on similar experiments on SnO, we estimate that using the CPMG sequence to obtain a ^{195}Pt NMR spectrum of similar quality would require at least nine hours (please refer to the Appendix A for a full explanation of this estimate), as the reduced excitation bandwidth would necessitate the acquisition of more sub-spectra. Using an MAS experiment, Ellis *et al.* were able to acquire the total ^{195}Pt NMR spectrum in a piecewise fashion by collecting seven sub-spectra;[38] unfortunately, no experimental time is given for comparison. Not only does the WURST-CPMG experiment reduce the number of sub-spectra required to obtain the total powder pattern, it also provides a manifold of echo spikelets from which the platinum CS tensor can be accurately extracted, and avoids spectral artifacts from magic-angle mis-sets, resulting in a better overall powder pattern shape with a higher S/N. As with the previously discussed spectra, an echo spectrum resulting from the FT of spin-echoes co-added in the time domain was used for simulation purposes. The CS tensor parameters

(δ_{iso} = -1510 ppm Ω = 10425 ppm κ = -0.97) agree well with previously published results (δ_{iso} = -1848 ppm Ω = 10414 ppm κ = -1.0).[38]

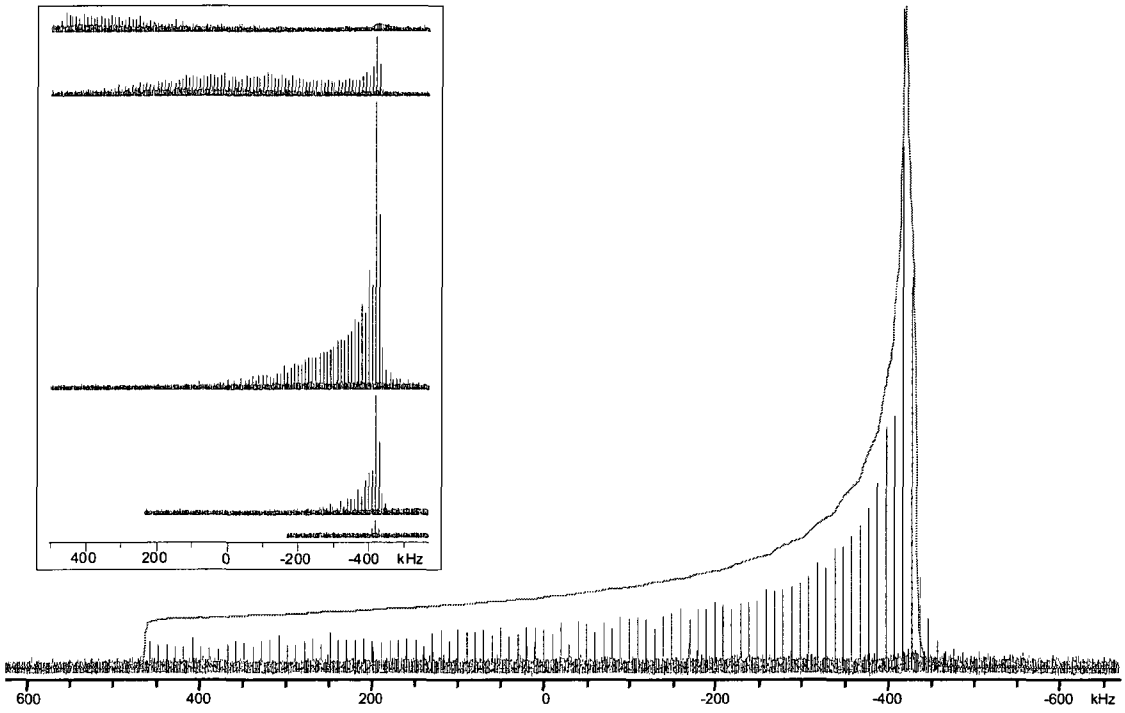

Figure 2.4. ^{195}Pt WURST-CPMG NMR spectrum of K_2PtCl_4. The spectrum was acquired in a piecewise manner and is the sum of 5 sub-spectra, each of which consists of 40 transients. Inset: The five subpectra obtained during the piecewise acquisition.

2.3.5 ^{119}Sn Ultra-Wideline SSNMR using pulses designed with Optimal Control Theory

Broadband excitation pulses generated using OCT thus far have been designed for high-resolution solution NMR experiments. BEBOP and BIBOP[30-32] pulses have been developed which can uniformly excite or invert spin magnetization over the full ^{13}C chemical shift range at moderate B_1 field strengths (*ca.* 50 kHz). Constant-amplitude "calibration-free" pulses have also been reported,[90] as well as ICEBERG pulses that result in transverse magnetization with a constant phase dispersion as a function of offset

frequency,[91] and studies that use OCT to optimize pulses for use with a quadrupolar nucleus in solution samples (*e.g.*, ^{23}Na).[92,93] As a preliminary investigation of the potential of optimized pulses for the acquisition of UW SSNMR spectra of spin-1/2 nuclei, we employed the open-source NMR simulation program SIMPSON to attempt to generate pulses capable of exciting the full width of the ^{119}Sn SSNMR spectrum of SnO at 9.4 T (*ca.* 150 kHz).

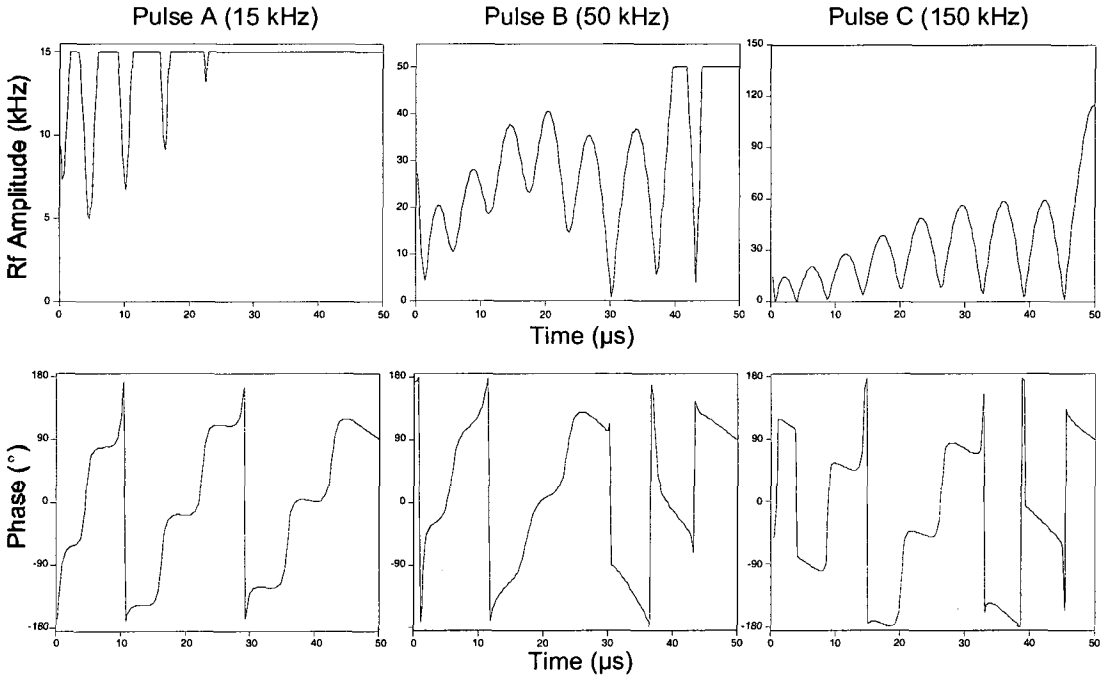

Figure 2.5. Visual descriptions of the rf amplitude (top) and phase (bottom) of the pulses generated using OCT which were employed for this work.

A variety of pulses were generated with different restrictions placed on their lengths and maximum rf amplitudes. We focus the discussion on the three best-performing pulses (Figure 2.5), each of which are 50 μs in length and restricted to maximum rf powers of 15, 50 and 150 kHz (hereafter referred to as pulses A, B and C,

respectively). Other pulse lengths (25 and 100 μs) were also tested; however, the 50 μs pulses were found to yield the best experimental lineshapes. The rf amplitude profiles of these optimized pulses resemble trains of "Gaussian-like" shapes which generally increase in amplitude with time, though, for the pulse limited to 15 kHz rf power, this "Gaussian-train" shape is severely truncated. This motif was observed in all of the pulses generated for this application. It is of interest to note that these pulse shapes closely resemble the polychromatic pulses published by Kupče and Freeman in 1994,[94] which were employed for broadband excitation of ^{13}C and ^{1}H solution NMR spectra. Kobzar *et al.* also observed similar shapes in a previous report on pulses generated with OCT.[95] The phase modulations of the pulses reported here are similar in each case; the phase is swept smoothly and relatively slowly through a range of *ca.* 10 to 50 degrees over the course of each Gaussian-like amplitude modulation, but undergoes rapid jumps of 90 to 180 degrees between each modulation. In particular, the phase profiles of the 50 kHz and 150 kHz pulses are nearly identical. All three pulses end with a phase very close to 90°.

Figure 2.6A shows the ^{119}Sn pattern acquired from SnO using pulse A, and experimental and numerically simulated spectra obtained with a 15 kHz rectangular, monochromatic $\pi/2$ pulses for comparison. In each case the transmitter frequency was applied near the center of gravity of the pattern (−167 ppm). Pulse A results in a spectrum with all discontinuities clearly visible, and a more uniform excitation profile than that of the lineshape predicted by SIMPSON 2.0. The 15 kHz square pulse produces a spectrum that is clearly inferior, with only one clearly resolved discontinuity, and a signal intensity that drops significantly with increasing distance from the isotropic shift,

as would be expected given its limited bandwidth. Figure 2.6B compares the ^{119}Sn NMR spectra acquired with pulse B and a 50 kHz rectangular $\pi/2$ pulse. The 50 kHz rectangular pulse shows an improved performance over the 15 kHz rectangular pulse, as it is capable of exciting the full width of the spectrum such that all three discontinuities are resolved, although a drop in intensity is observed at the low frequency end of the pattern. The spectrum acquired with pulse B has a slightly rounded shoulder on the low frequency side, implying that either its excitation bandwidth is not quite as wide as the pattern, or that magnetization vectors corresponding to different orientations in different regions of the powder patterns are nutating at variable rates, similar to nutation phenomena in central transition spectra of half-integer quadrupoles (a full numerical treatment is beyond the scope of this work).[96-98] Both spectra are reasonable representations of the simulated powder pattern, though the spectrum acquired using pulse B more closely resembles the lineshape predicted by SIMPSON. Figure 2.6C depicts the ^{119}Sn NMR spectrum of SnO acquired using pulse C, which was generated with a maximum permitted rf field of 150 kHz. In this case the maximum rf amplitude calculated by the OCT optimization is *ca.* 115 kHz, well below the maximum permitted value; hence, for comparison, a spectrum was obtained using a 115 kHz rectangular $\pi/2$ pulse. The spectrum acquired with pulse C is disproportionately intense on the low frequency end when compared to the lineshape predicted by SIMPSON 2.0, whereas the 115 kHz rectangular pulse produces a spectrum that matches the simulated lineshape reasonably well (though high-frequency discontinuity is still less intense than the idealized simulated lineshape).

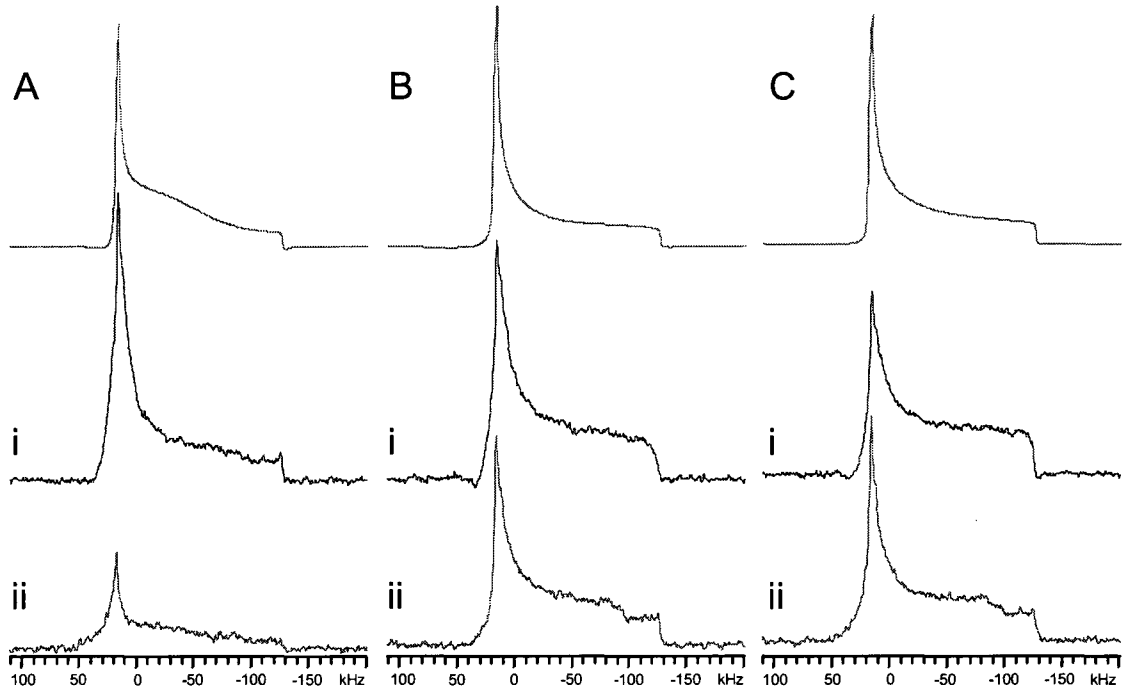

Figure 2.6. ^{119}Sn NMR spectra of SnO acquired with an OCT pulse with (Ai) a 15 kHz maximum rf field, (Aii) a 15 kHz rectangular pulse, (Bi) an OCT pulse with a 50 kHz maximum rf field, (Bii) a 50 kHz rectangular pulse, (Ci) an OCT pulse with a 150 kHz maximum rf field, and (Cii) a 150 kHz rectangular pulse. SIMPSON simulations of powder patterns resulting from a rectangular pulse at each respective pulse strength are shown above the experimental spectra.

Table 2.3 gives selected experimental details for the OCT experiments. The measured S/N ratios confirm that the OCT pulses outperform standard rectangular pulses of similar pulse power. Of the OCT pulses, pulses A and B yield spectra with similar S/N values (70 and 71, respectively), while the spectrum resulting from pulse C has a somewhat lower S/N (58). Of the standard rectangular pulses, the 15 kHz pulse has the worst S/N (27), while the 50 kHz and 115 kHz pulses has S/N values of 54 and 51, respectively. We also note that the WURST-CPMG (and CPMG) experiments produced spectra with nearly half the S/N of the best OCT and rectangular- pulse experiments,

despite being acquired with only one tenth the number of scans. In large part, this is due to the signal enhancement from acquiring many echoes with a train of refocusing pulses in the CPMG-type experiments. In cases where T_2 relaxation constants are very small (i.e., where the CPMG-type experiments are not useful), pulses generated with OCT offer a useful, low-power alternative.

Table 2.3. Comparison of selected ^{119}Sn SSNMR spectral parameters

	S/N[a]	Experimental Time (min.)	# of Scans
15 kHz rectangular pulse	27	26.7	800
15 kHz OCT pulse	70	26.7	800
50 kHz rectangular pulse	54	26.7	800
50 kHz OCT pulse	71	26.7	800
115 kHz rectangular pulse	51	26.7	800
115 kHz OCT pulse	58	26.7	800
30 kHz WURST-CPMG	32	2.7	80
75 kHz CPMG[b]	29	2.7	80

[a] S/N ratios are based on the most intense discontinuity of the ^{119}Sn SSNMR pattern. For CPMG-type experiments, the most intense spikelet was used for S/N determination.
[b] The data given for the CPMG spectrum is based on the sub-spectrum centred closest to δ_{22}.

These preliminary results indicate that broadband excitation pulses optimized using OCT for the acquisition of broad CSA patterns are particularly advantageous at low rf powers, and therefore should be suitable for studying low-γ spin-1/2 nuclides such as ^{15}N, ^{57}Fe, ^{89}Y, ^{103}Rh and $^{107/109}$Ag, samples sensitive to rf heating, or in solid state NMR studies of biological samples where high concentrations of ionic salts are present which can result in arcing within the probe. When high rf powers can be employed, these

pulses offer little or no advantage over regular $\pi/2$ pulses in terms of excitation, at least over a range of up to *ca.* 150 kHz (we have yet to test this approach over greater frequency ranges). However, of all six spectra presented in this section, the spectrum acquired with pulse A most closely resembles the powder pattern predicted by SIMPSON 2.0. Hence, in terms of lineshape accuracy, the use of such optimized pulses may be advantageous (this was also noted in a study of excitation pulses generated for half-integer quadrupoles using OCT).[33] Finally, we note that in order to take advantage of the significant signal enhancement available from the CPMG protocol, this approach will require the optimization of broadband refocusing pulses, which is not straightforward.[29] We are currently making preliminary investigations of such refocusing pulses.

2.4 Conclusions

The WURST-CPMG pulse sequence has successfully been applied in the acquisition of wideline and UW SSNMR patterns of various spin-1/2 nuclides. In comparison to the CPMG sequence, WURST-CPMG offers a significant reduction in experimental time in the acquisition of the ^{119}Sn SSNMR spectrum of SnO, removing the need for piecewise acquisition. Similarly, ^{207}Pb WURST-CPMG NMR proves to be more efficient than the ^{1}H-^{207}Pb CP/CPMG sequence in acquiring the ^{207}Pb SSNMR spectrum of $Pb(OAc)_2 \cdot 3H_2O$, as the entire pattern could be acquired in a single experiment, and in a shorter period of time. In cases where the T_1 of the X nucleus is very long compared to the $T_1(^1H)$ (*e.g.,* for ^{199}Hg SSNMR experiments on $Hg(OAc)_2$), CP/CPMG may prove to be more efficient; however, CP is not always feasible (*i.e.,* ^{1}H or ^{19}F are not present in the

sample), in which case WURST-CPMG is an extremely useful alternative. For SSNMR spectra that exceed the excitation bandwidth of WURST-CPMG pulses (*e.g.*, ^{195}Pt NMR of K_2PtCl_4), piecewise acquisition can be readily employed to obtain the total powder pattern.

Preliminary experiments making use of pulses generated with OCT indicate that low-power pulses can be created which outperform standard, rectangular pulses of the same power for the acquisition of broad spin-1/2 SSNMR patterns. The improvements in signal intensity and powder-pattern shape provided by OCT pulses at low power levels are reduced as the pulse power is increased, though for samples sensitive to increases in temperature, samples containing low-γ nuclei or solution samples with high salt concentrations, these pulses may be a useful alternative to standard rectangular pulses. For the acquisition of the ^{119}Sn SSNMR spectrum of SnO, WURST-CPMG is the best method of acquisition; however, in cases where T_2 relaxation constants are very small, pulses generated using OCT offer a reasonable alternative.

We hope that this work encourages further investigations of the broad powder patterns of heavy spin-1/2 nuclides, since their acute sensitivity to the surrounding electronic structure could greatly enhance our understanding of structure and dynamics for a broad array of materials. These techniques will be very useful for further NMR investigations of a number of additional spin-1/2 nuclei which may have broad patterns arising from CSA or disorder at the atomic/molecular level, including metal nuclides like ^{77}Se, ^{29}Si, ^{125}Te, ^{181}Yb, and of course low-gamma nuclides such as as ^{15}N, ^{57}Fe, ^{89}Y, ^{103}Rh and $^{107/109}$Ag.

Bibliography

(1) Neue, G.; Dybowski, C.; Smith, M. L.; Barich, D. H. *Solid State Nucl. Magn. Reson.* 1994, 3, 115-119.

(2) Tang, J. A.; O'Dell, L. A.; Aguiar, P. M.; Lucier, B. E. G.; Sakellariou, D.; Schurko, R. W. *Chem. Phys. Lett.* 2008, 466, 227-234.

(3) Bryant, P. L.; Harwell, C. R.; Mrse, A. A.; Emery, E. F.; Gan, Z. H.; Caldwell, T.; Reyes, A. P.; Kuhns, P.; Hoyt, D. W.; Simeral, L. S.; Hall, R. W.; Butler, L. G. *J. Am. Chem. Soc.* 2001, 123, 12009-12017.

(4) Lipton, A. S.; Buchko, G. W.; Sears, J. A.; Kennedy, M. A.; Ellis, P. D. *J. Am. Chem. Soc.* 2001, 123, 992-993.

(5) Hamaed, H.; Lo, A. Y. H.; Lee, D. S.; Evans, W. J.; Schurko, R. W. *J. Am. Chem. Soc.* 2006, 128, 12638-12639.

(6) Forgeron, M. A. M.; Wasylishen, R. E. *Magn. Reson. Chem.* 2008, 46, 206-214.

(7) Crewdson, P.; Bryce, D. L.; Rominger, F.; Hofmann, P. *Angew. Chem.-Int. Edit.* 2008, 47, 3454-3457.

(8) Michaelis, V. K.; Aguiar, P. M.; Terskikh, V. V.; Kroeker, S. *Chem. Commun.* 2009, 4660-4662.

(9) Rossini, A. J.; Mills, R. W.; Briscoe, G. A.; Norton, E. L.; Geier, S. J.; Hung, I.; Zheng, S.; Autschbach, J.; Schurko, R. W. *J. Am. Chem. Soc.* 2009, 131, 3317-3330.

(10) Rhodes, H. E.; Wang, P. K.; Stokes, H. T.; Slichter, C. P.; Sinfelt, J. H. *Phys. Rev. B* 1982, 26, 3559-3568.

(11) Bastow, T. J.; Smith, M. E. *Solid State Nucl. Magn. Reson.* 1992, 1, 165-174.

(12) Sampathkumaran, E. V.; Fujiwara, N.; Rayaprol, S.; Madhu, P. K.; Uwatoko, Y. *Phys. Rev. B* 2004, 70.

(13) Massiot, D.; Farnan, I.; Gautier, N.; Trumeau, D.; Trokiner, A.; Coutures, J. P. *Solid State Nucl. Magn. Reson.* 1995, 4, 241-248.

(14) Medek, A.; Frydman, V.; Frydman, L. *J. Phys. Chem. A* 1999, 103, 4830-4835.

(15) Lipton, A. S.; Wright, T. A.; Bowman, M. K.; Reger, D. L.; Ellis, P. D. *J. Am. Chem. Soc.* 2002, 124, 5850-5860.

(16) Larsen, F. H.; Jakobsen, H. J.; Ellis, P. D.; Nielsen, N. C. *J. Phys. Chem. A* 1997, 101, 8597-8606.

(17) Lipton, A. S.; Sears, J. A.; Ellis, P. D. *J. Magn. Reson.* 2001, 151, 48-59.

(18) Hung, I.; Schurko, R. W. *J. Phys. Chem. B* 2004, 108, 9060-9069.

(19) Tang, J. A.; Masuda, J. D.; Boyle, T. J.; Schurko, R. W. *ChemPhysChem* 2006, 7, 117-130.

(20) Tang, J. A.; Ellis, B. D.; Warren, T. H.; Hanna, J. V.; Macdonald, C. L. B.; Schurko, R. W. *J. Am. Chem. Soc.* 2007, 129, 13049-13065.

(21) Lipton, A. S.; Heck, R. W.; Primak, S.; McNeill, D. R.; Wilson, D. M.; Ellis, P. D. *J. Am. Chem. Soc.* 2008, 130, 9332-9341.

(22) O'Dell, L. A.; Schurko, R. W. *Chem. Phys. Lett.* 2008, 464, 97-102.

(23) Yamauchi, K.; Janssen, J. W. G.; Kentgens, A. P. M. *J. Magn. Reson.* 2004, 167, 87-96.

(24) Kentgens, A. P. M.; Bart, J.; van Bentum, P. J. M.; Brinkmann, A.; Van Eck, E. R. H.; Gardeniers, J. G. E.; Janssen, J. W. G.; Knijn, P.; Vasa, S.; Verkuijlen, M. H. W. *J.*

Chem. Phys. 2008, 128.

(25) Bhattacharyya, R.; Frydman, L. *J. Chem. Phys.* 2007, 127.

(26) Kupce, E.; Freeman, R. *J. Magn. Reson. Ser. A* 1995, 115, 273-276.

(27) O'Dell, L. A.; Rossini, A. J.; Schurko, R. W. *Chem. Phys. Lett.* 2009, 468, 330-335.

(28) Bak, M.; Rasmussen, J. T.; Nielsen, N. C. *J. Magn. Reson.* 2000, 147, 296-330.

(29) Tosner, Z.; Vosegaard, T.; Kehlet, C.; Khaneja, N.; Glaser, S. J.; Nielsen, N. C. *J. Magn. Reson.* 2009, 197, 120-134.

(30) Skinner, T. E.; Reiss, T. O.; Luy, B.; Khaneja, N.; Glaser, S. J. *J. Magn. Reson.* 2003, 163, 8-15.

(31) Skinner, T. E.; Reiss, T. O.; Luy, B.; Khaneja, N.; Glaser, S. J. *J. Magn. Reson.* 2004, 167, 68-74.

(32) Kobzar, K.; Skinner, T. E.; Khaneja, N.; Glaser, S. J.; Luy, B. *J. Magn. Reson.* 2004, 170, 236-243.

(33) O'Dell, L. A.; Harris, K. J.; Schurko, R. W. *J. Magn. Reson.* 2010, 203, 156-166.

(34) Siegel, R.; Nakashima, T. T.; Wasylishen, R. E. *Concepts Magn. Reson. Part A* 2005, 26A, 47-61.

(35) Bowers, G. M.; Lipton, A. S.; Mueller, K. T. *Solid State Nucl. Magn. Reson.* 2006, 29, 95-103.

(36) Hamaed, H.; Laschuk, M. W.; Terskikh, V. V.; Schurko, R. W. *J. Am. Chem. Soc.* 2009, 131, 8271-8279.

(37) Makowka, C. D.; Slichter, C. P.; Sinfelt, J. H. *Phys. Rev. B* 1985, 31, 5663-5679.

(38) Sparks, S. W.; Ellis, P. D. *J. Am. Chem. Soc.* 1986, 108, 3215-3218.

(39) Grey, C. P.; Dobson, C. M.; Cheetham, A. K.; Jakeman, R. J. B. *J. Am. Chem. Soc.* 1989, 111, 505-511.

(40) Cossement, C.; Darville, J.; Gilles, J. M.; Nagy, J. B.; Fernandez, C.; Amoureux, J. P. *Magn. Reson. Chem.* 1992, 30, 263-270.

(41) Bowmaker, G. A.; Harris, R. K.; Oh, S. W. *Coord. Chem. Rev.* 1997, 167, 49-94.

(42) Briand, G. G.; Smith, A. D.; Schatte, G.; Rossini, A. J.; Schurko, R. W. *Inorg. Chem.* 2007, 46, 8625-8637.

(43) Tang, J. A.; Kogut, E.; Norton, D.; Lough, A. J.; McGarvey, B. R.; Fekl, U.; Schurko, R. W. *J. Phys. Chem. B* 2009, 113, 3298-3313.

(44) Santos, R. A.; Gruff, E. S.; Koch, S. A.; Harbison, G. S. *J. Am. Chem. Soc.* 1991, 113, 469-475.

(45) Hung, I.; Rossini, A. J.; Schurko, R. W. *J. Phys. Chem. A* 2004, 108, 7112-7120.

(46) Siegel, R.; Nakashima, T. T.; Wasylishen, R. E. *J. Phys. Chem. B* 2004, 108, 2218-2226.

(47) Menger, E. M.; Raleigh, D. P.; Griffin, R. G. *J. Magn. Reson.* 1985, 63, 579-582.

(48) Groombridge, C. J. *Magn. Reson. Chem.* 1993, 31, 380-387.

(49) Fayon, F.; Farnan, I.; Bessada, C.; Coutures, J.; Massiot, D.; Coutures, J. P. *J. Am. Chem. Soc.* 1997, 119, 6837-6843.

(50) Harris, R. K.; Reams, P.; Packer, K. J. *J. Chem. Soc.-Dalton Trans.* 1986, 1015-1020.

(51) Hook, J. M.; Dean, P. A. W.; Vangorkom, L. C. M. *Magn. Reson. Chem.* 1995, 33, 77-79.

(52) Harris, R. K.; Becker, E. D.; De Menezes, S. M. C.; Goodfellow, R.; Granger, P. *Pure Appl. Chem.* 2001, 73, 1795-1818.

(53) Bennett, A. E.; Rienstra, C. M.; Auger, M.; Lakshmi, K. V.; Griffin, R. G. *J. Chem. Phys.* 1995, 103, 6951-6958.

(54) O'Dell, L. A.; Schurko, R. W. *Phys. Chem. Chem. Phys.* 2009, 11, 7069-7077.

(55) Eichele, K.; Wasylishen, R. E., WSolids: Solid-State NMR Spectrum Simulation, 2001.

(56) Massiot, D.; Fayon, F.; Capron, M.; King, I.; Le Calve, S.; Alonso, B.; Durand, J. O.; Bujoli, B.; Gan, Z. H.; Hoatson, G. *Magn. Reson. Chem.* 2002, 40, 70-76.

(57) Zaremba, S. *Ann. Mat. Pura. Appl.* 1966, 73, 293-317.

(58) Conroy, H. *J. Chem. Phys.* 1967, 47, 5307-&.

(59) Cheng, V. B.; Suzukawa, H. H.; Wolfsber.M *J. Chem. Phys.* 1973, 59, 3992-3999.

(60) Cheetham, A. K.; Dobson, C. M.; Grey, C. P.; Jakeman, R. J. B. *Nature* 1987, 328, 706-707.

(61) Clayden, N. J.; Dobson, C. M.; Fern, A. *J. Chem. Soc.-Dalton Trans.* 1989, 843-847.

(62) de Monredon, S.; Cellot, A.; Ribot, F.; Sanchez, C.; Armelao, L.; Gueneau, L.; Delattre, L. *J. Mater. Chem.* 2002, 12, 2396-2400.

(63) O'Dell, L. A.; Savin, S. L. P.; Chadwick, A. V.; Smith, M. E. *Nanotechnology* 2005, 16, 1836-1843.

(64) Sepelak, V.; Becker, K. D.; Bergmann, I.; Suzuki, S.; Indris, S.; Feldhoff, A.; Heitjans, P.; Grey, C. P. *Chem. Mat.* 2009, 21, 2518-2524.

(65) Harris, R. K.; Sebald, A.; Furlani, D.; Tagliavini, G. *Organometallics* 1988, 7, 388-

394.

(66) Apperley, D. C.; Davies, N. A.; Harris, R. K.; Brimah, A. K.; Eller, S.; Fischer, R. D. *Organometallics* 1990, 9, 2672-2676.

(67) Bai, H. P.; Harris, R. K.; Reuter, H. *J. Organomet. Chem.* 1991, 408, 167-172.

(68) Kye, Y. S.; Connolly, S.; Herreros, B.; Harbison, G. S. *Main Group Met. Chem.* 1999, 22, 373-383.

(69) Eichele, K.; Kroeker, S.; Wu, G.; Wasylishen, R. E. *Solid State Nucl. Magn. Reson.* 1995, 4, 295-300.

(70) Zhao, P. D.; Prasad, S.; Huang, J.; Fitzgerald, J. J.; Shore, J. S. *J. Phys. Chem. B* 1999, 103, 10617-10626.

(71) Grutzner, J. B.; Stewart, K. W.; Wasylishen, R. E.; Lumsden, M. D.; Dybowski, C.; Beckmann, P. A. *J. Am. Chem. Soc.* 2001, 123, 7094-7100.

(72) Van Bramer, S. E.; Glatfelter, A.; Bai, S.; Dybowski, C.; Neue, G.; Perry, D. L. *Magn. Reson. Chem.* 2006, 44, 357-365.

(73) Dybowski, C.; Neue, G. *Prog. Nucl. Magn. Reson. Spectrosc.* 2002, 41, 153-170.

(74) Van Gorkom, L. C. M.; Hook, J. M.; Logan, M. B.; Hanna, J. V.; Wasylishen, R. E. *Magn. Reson. Chem.* 1995, 33, 791-795.

(75) Bielecki, A.; Burum, D. P. *J. Magn. Reson. Ser. A* 1995, 116, 215-220.

(76) Irwin, A. D.; Chandler, C. D.; Assink, R.; Hampdensmith, M. J. *Inorg. Chem.* 1994, 33, 1005-1006.

(77) Larsson, A. C.; Ivanov, A. V.; Pike, K. J.; Forsling, W.; Antzutkin, O. N. *J. Magn. Reson.* 2005, 177, 56-66.

(78) Utschig, L. M.; Bryson, J. W.; Ohalloran, T. V. *Science* 1995, 268, 380-385.

(79) Bowmaker, G. A.; Harris, R. K.; Apperley, D. C. *Inorg. Chem.* 1999, 38, 4956-4962.

(80) Goodfellow, R. J. In *Multinuclear NMR*; 1st ed.; Mason, J., Ed.; Plenum Press: New York, 1987, pp 563-584.

(81) Harris, R. K.; Sebald, A. *Magn. Reson. Chem.* 1987, 25, 1058-1062.

(82) Tong, Y. Y.; Rice, C.; Wieckowski, A.; Oldfield, E. *J. Am. Chem. Soc.* 2000, 122, 11921-11924.

(83) Tong, Y. Y.; Wieckowski, A.; Oldfield, E. *J. Phys. Chem. B* 2002, 106, 2434-2446.

(84) Grykalowska, A.; Nowak, B. *Solid State Nucl. Magn. Reson.* 2005, 27, 223-227.

(85) Doddrell, D. M.; Barron, P. F.; Clegg, D. E.; Bowie, C. *J. Chem. Soc.-Chem. Commun.* 1982, 575-576.

(86) Dechter, J. J.; Kowalewski, J. *J. Magn. Reson.* 1984, 59, 146-149.

(87) Harris, R. K.; McNaught, I. J.; Reams, P.; Packer, K. J. *Magn. Reson. Chem.* 1991, 29, S60-S72.

(88) Austin, E. J. W.; Barrie, P. J.; Clark, R. J. H. *J. Chem. Soc.-Chem. Commun.* 1993, 1404-1405.

(89) Goodfellow, R. J., Ed. *Group VIII Transition Metals*; 1st ed.; Plenum Press: New York, 1987.

(90) Skinner, T. E.; Kobzar, K.; Luy, B.; Bendall, M. R.; Bermel, W.; Khaneja, N.; Glaser, S. J. *J. Magn. Reson.* 2006, 179, 241-249.

(91) Gershenzon, N. I.; Skinner, T. E.; Brutscher, B.; Khaneja, N.; Nimbalkar, M.; Luy, B.; Glaser, S. J. *J. Magn. Reson.* 2008, 192, 235-243.

(92) Lee, J. S.; Regatte, R. R.; Jerschow, A. *J. Chem. Phys.* 2008, 129.

(93) Lee, J. S.; Regatte, R. R.; Jerschow, A. *J. Chem. Phys.* 2009, 131.

(94) Kupce, E.; Freeman, R. *J. Magn. Reson. Ser. A* 1994, 108, 268-273.

(95) Kobzar, K.; Skinner, T. E.; Khaneja, N.; Glaser, S. J.; Luy, B. *J. Magn. Reson.* 2008, 194, 58-66.

(96) Samoson, A.; Kundla, E.; Lippmaa, E. *J. Magn. Reson.* 1982, 49, 350-357.

(97) Samoson, A.; Lippmaa, E. *Chem. Phys. Lett.* 1983, 100, 205-208.

(98) Samoson, A.; Lippmaa, E. *Phys. Rev. B* 1983, 28, 6567-6570.

Chapter 3

^{207}Pb SSNMR Spectroscopic Investigations of Pb(II) Thiolates

3.1 Introduction

Lead (II) is a heavy *p*-block element capable of adopting a broad array of coordination environments and high coordination numbers, due to its large atomic radius and stereochemically active lone pair of electrons.[1-4] However, the propensity of Pb(II) to form such highly coordinated species can result in the formation of polymeric structures, and in turn, a reduction in solubility as observed in a number of Pb(II) thiolate species.[5-8] In an effort to improve the solubility of such compounds, $(2,6\text{-}Me_2C_6H_3S)_2Pb$ and several substituted adducts were developed and characterized.[9,10] As an extension of this work, and to explore the potential for new dative bonding arrangements about the Pb centre, $[(2,6\text{-}Me_2C_6H_3S)_2Pb]_2$(dppe) (**2**), $[(2,6\text{-}Me_2C_6H_3S)_2Pb]_2$(tmeda) (**3**), and $[(2,6\text{-}Me_2C_6H_3S)_2Pb]_3$(dmpe) (**4**) (where dppe = bis(diphenylphosphinoethane), tmeda = *N,N,N',N'* - tetramethylethylenediamine, and dmpe = bis(dimethylphosphino)ethane) were synthesized and isolated. This series of novel Pb(II) thiolates exhibits a unique array of Pb coordination environments, though a common feature is the formation of pseudo-trigonal pyramidal Pb bonding arrangements, similar to that of the $[(PhS)Pb]^-$ anion (**1**),[11,12] as shown in Scheme 1.

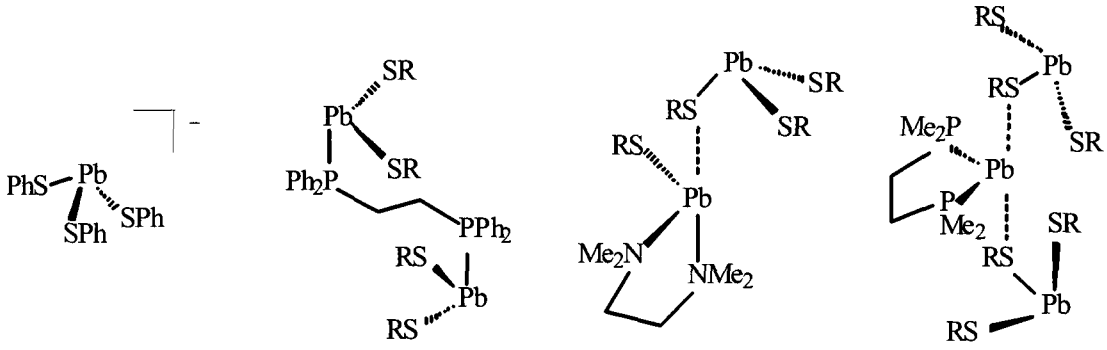

1 2 3 4

Scheme 1. Note that the dashed lines in 3 and 4 indicate dative bonds.

Owing to the insolubility of many of this class of Pb complexes, it is of importance to further examine well-characterized systems with ^{207}Pb solid state NMR (SSNMR). The utility of ^{207}Pb SSNMR as a probe of structure and dynamics has long been known to be of great importance.[10,13-16] ^{207}Pb SSNMR spectra are most often acquired under conditions of magic-angle spinning (MAS) owing to the broad patterns arising from large lead chemical shift anisotropies (CSA).[13,17] Such experiments are sometimes problematic, since (i) the lead chemical shift is highly temperature dependent and may change due to frictional heating of the rotor,[13,18-20] and (ii) for very large lead CSAs, the magic angle must be set with great precision to avoid "doubling" of the spinning sidebands (SSBs) and other related spectral artifacts.[21-23] In addition, it has been observed that short, high-power pulses on the ^{207}Pb channel are often incapable of uniformly exciting the entire manifold of SSBs, leading to reduced peak intensities on the outside limits of the spectrum, and hence, to spurious Herzfeld-Berger analyses of the chemical shift tensors.[10] In samples with sources of abundant nuclei (i.e., ^{1}H and ^{19}F) which are proximate to the ^{207}Pb centres, ^{1}H-^{207}Pb and ^{19}F-^{207}Pb cross-polarization magic

angle spinning (CP/MAS) NMR experiments are the norm.[24-27] These experiments provide large increases in signal-to-noise ratios (S/N) and reduced experimental times, due to signal enhancement via CP and the (typically) shorter longitudinal relaxation constants (T_1) of the abundant nuclei upon which the recycle times depend. Since many ^{207}Pb T_1's are known to be very long (on the order of minutes to hours) in solid systems[20,28-30], these experiments are of great value. However, the excitation profiles of CP experiments are usually reduced compared to those achieved in standard Bloch decay experiments; therefore, CP/MAS experiments are of limited utility for extremely broad patterns.[10,31]

Owing to the broad (i.e., >250 kHz) nature of many Pb NMR patterns, as well as decreased CP efficiency under MAS conditions resulting from distant and/or immobile ^{1}H or ^{19}F nuclei, frequency-stepped piecewise acquisitions on static (i.e., stationary) samples have proven particularly useful.[10,14,31-33] We designate such patterns as ultra-wideline (UW) NMR patterns, since they typically cannot be uniformly excited with rectangular pulses at currently achievable power levels. Traditional piecewise acquisitions involve stepping the transmitter at constant field (or sweeping the field at constant frequency) and plotting the spin echo intensities as a function of frequency (field).[33,34] The efficiency of piecewise acquisitions can be greatly improved by Fourier transforming the individual sub-spectra, followed by co-addition or skyline projection (this technique has been applied to numerous quadrupolar nuclei).[35,36] Further improvement stems from the use of the quadrupolar Carr-Purcell Meiboom-Gill (QCPMG) pulse sequence, which was reintroduced for the acquisition of broad, central-

transition, powder patterns of quadrupolar nuclei.[37] Though predominantly applied for quadrupolar nuclei,[38-41] our research group and others have employed the CPMG sequence (or CP/CPMG for systems with abundant nuclei such as ^{1}H and ^{19}F) to acquire SSNMR spectra of heavy spin-1/2 nuclei (e.g., ^{113}Cd, ^{195}Pt, ^{199}Hg, ^{207}Pb).[10,14,31,32,42,43] Though effective, the use of the CPMG and CP/CPMG sequences for piecewise acquisition of broad NMR patterns is labour intensive, as the probe must be retuned for the acquisition of each sub-spectrum. As mentioned above, an alternative method for acquisition of UW SSNMR spectra is to sweep the magnetic field at a constant transmitter frequency; however, this requires specialized coils and controllers to be installed within the bore of the magnet.[44,45] More recently, the wideband uniform-rate smooth truncation (WURST)[46] pulse sequence has been introduced as a method for acquiring UW SSNMR patterns.[47,48] This sequence has been modified into the form of a CPMG-type sequence called WURST-QCPMG,[49] which provides the benefits of broadband excitation of WURST and S/N enhancements of CPMG. This modification enables one to acquire UW spectra with fewer subspectra, or sometimes even in a single experiment, depending upon the Larmor frequency and quadrupolar parameters.

Herein, we present ^{207}Pb SSNMR spectra of **1** - **4**, acquired in a piecewise fashion with the CP/CPMG pulse sequence. We also employ the WURST-CPMG sequence the obtain the ^{207}Pb SSNMR spectra, in an effort to improve upon the efficiency of acquisition. DFT calculations are carried out with the *Amsterdam Density Functional* (ADF) software,[50-52] to determine the nuclear shielding (NS) tensor orientations and relate the experimentally observed CS parameters to the molecular structures.

3.2 Experimental Details

3.2.1 Solid-State ^{207}Pb NMR Spectroscopy

All Pb (II) thiolate samples were prepared by the group of Prof. Glen Briand at Mount Allison University. Solid-state ^{207}Pb and ^{31}P NMR spectra were acquired on a Varian Infinity Plus spectrometer with an Oxford 9.4 T wide-bore magnet (ν_0 (^{1}H) = 400 MHz, ν_0 (^{207}Pb) = 83.74 MHz, ν_0 (^{31}P) = 161.82 MHz. ^{207}Pb chemical shifts were referenced to tetramethyllead ($Pb(CH_3)_4$, δ_{iso} = 0.0 ppm) by using a 0.5M aqueous solution of $Pb(NO_3)_2$ (δ_{iso} = -2941 ppm) as a secondary standard.[28] Phosphorous chemical shifts are referenced to 0.5M H_3PO_4 (aq) (δ_{iso} = 0.0 ppm).

Solid-state NMR experiments were carried out using either a 4 mm HX double resonance Varian/Chemagnetics probe or a 4mm HXY triple resonance Varian/Chemagnetics probe. Lead acetate [$Pb(OAc)_2 \cdot xH_2O$] was used to optimize parameters for cross-polarization/Carr-Purcell-Meiboom-Gill (CP/CPMG)[14,32] and WURST-CPMG[49] experiments. The total spectrum for each CP/CPMG experiment was obtained by co-adding individual subspectra that were collected at evenly spaced transmitter offsets. 19-23 subspectra were required, and pulse delays for CP/CPMG experiments ranged from 20 - 45 s. Other experimental details regarding CP/CPMG experiments can be found in the Appendix B (Table B1). TPPM ^{1}H decoupling[53] was used for all CP/CPMG experiments. WURST-CPMG[49] experiments were able to be completed without piecewise acquisition and employed 50 μs WURST pulses with a pulse power of *ca.* 47 kHz. Further experimental details regarding WURST-CPMG experiments may be found in Appendix B (Table B2) All ^{207}Pb spectra were simulated

using the WSolids NMR simulation program,[54] and processed with NUTS (Acorn NMR).

3.2.2 Density Functional Theory Calculations

The NMR and EPR modules[55-57] of the *Amsterdam Density Functional* (ADF) program package[50-52] on the Shared Hierarchical Academic Research Computing Network (SHARCNET)[58] were used to carry out all theoretical calculations. Relativistic effects were accounted for using the Zeroth-Order regular approximation (ZORA).[59-63] All-electron gauge including atomic orbitals (GIAO)[64] triple-ζ doubly-polarized basis sets were used for all atoms, except for the Pb atom(s) in each structure for which a quadruple-ζ doubly polarized basis set was employed. All calculations were carried out using atomic coordinates from single-crystal X-ray experiments, with proton bond lengths set to experimentally optimal values.

3.3 Results and Discussion

3.3.1 Solid-State ^{207}Pb NMR Spectroscopy

In this section we examine the ^{207}Pb SSNMR spectra of **1**, **2**, **3** and **4**. ^{1}H - ^{207}Pb CP/MAS experiments were attempted on these samples, and were unsuccessful, yielding incompletely excited spectra much like those discussed in our previous work on analogous systems.[10] Examples of these CP/MAS spectra can be found in Appendix B (Figure B1). Hence, all ^{207}Pb SSNMR spectra were acquired from stationary samples in a piecewise fashion using the CP/CPMG pulse sequence. The WURST-CPMG pulse sequence was also employed, in order to see if the number of sub-spectra required for an

accurate lineshape could be reduced, and the need for CP from ^{1}H nuclei could be eliminated (which would aid in quantification of signal intensity in samples with multiple sites). The lead isotropic chemical shifts of all of the compounds are similar (Table 3.1), in spite of the large chemical shift range of lead, which is currently thought to be on the order of 18000 ppm.[13] However, the anisotropic CS parameters vary greatly between compounds, indicating unique electronic environments for each ^{207}Pb nucleus. Since each compound has a unique coordination environment(s) for the Pb atoms, the Pb chemical shift (CS) tensor should reflect changes in molecular geometry and the nature of the bonding ligands.

The co-added ^{1}H-^{207}Pb CP/CPMG NMR spectrum of **1** (Figure 3.1) has a breadth of ca. 280 kHz and required the acquisition of 20 subspectra (totaling 32 hours of acquisition). The lengthy experimental time prohibited the acquisition of spikelets which are more closely spaced (i.e., further spacing of echoes in the CPMG echo train), due to the associated reductions in signal-to-noise (S/N). Also depicted in Figure 3.1 is the ^{207}Pb WURST-CPMG NMR spectrum of **1**, which was acquired in a single experiment taking only 19 hours, and appears similar to that obtained with the CP/CPMG sequence. Though it does not offer the reduced pulse delay times and population enhancements associated with CP, the excitation bandwidth of WURST-CPMG is far superior to that of CP/CPMG, allowing the entire spectrum to be acquired in a single experiment as opposed to a piecewise manner. Eliminating the need for piecewise experiments also has the added benefit of removing the requirement that personnel be present to retune the probe between acquisitions of subspectra.

Table 3.1. Experimental ^{207}Pb Chemical Shift Parameters[a]

Compound	δ_{11} (ppm)	δ_{22} (ppm)	δ_{33} (ppm)	δ_{iso} [c] (ppm)	Ω[d] (ppm)	κ[e]
(1) (PbS_3)	4262	3176	812	2750 (20)[f]	3400 (70)	0.37 (5)
(2) (PbS_2P)	4458	3314	58	2610 (40)	4400 (100)	0.48 (5)
(3) Site 1 (PbS_3)	4522	3856	922	3100 (75)	3600 (150)	0.63 (5)
(3) Site 2 (PbS_2N_2)	4503	2620	453	2525 (75)	4050 (125)	0.07 (5)
(4) Site 1 (PbS_2P_2)	477	36	-993	-160 (50)	1470 (100)	0.40 (5)
(4) Site 2 (PbS_3)	4282	3986	582	2950 (100)	3700 (300)	0.84 (5)
(4) Site 3 (PbS_3)	4395	3795	645	2945 (100)	3750 (300)	0.68 (5)

[a] The principal components of the chemical shift tensor are defined as $\delta_{11} \geq \delta_{22} \geq \delta_{33}$, where δ_{11} and δ_{33} are oriented along the directions of lowest and highest shielding, respectively.

[b] The nuclear environment of each site is denoted in parentheses.

[c] $\delta_{iso} = (\delta_{11} + \delta_{22} + \delta_{33})/3$. Values are with respect to $(CH_3)_4Pb$ ($\delta_{iso} = 0.0$ ppm).

[d] $\Omega = (\delta_{11} - \delta_{33})$, based upon simulations of static CP/CPMG spectra.

[e] $\kappa = 3(\delta_{22} - \delta_{iso})/\Omega$, $-1.0 \leq \kappa \leq 1.0$.

[f] Values in parentheses denote the uncertainty in the last digit of each parameter where indicated.

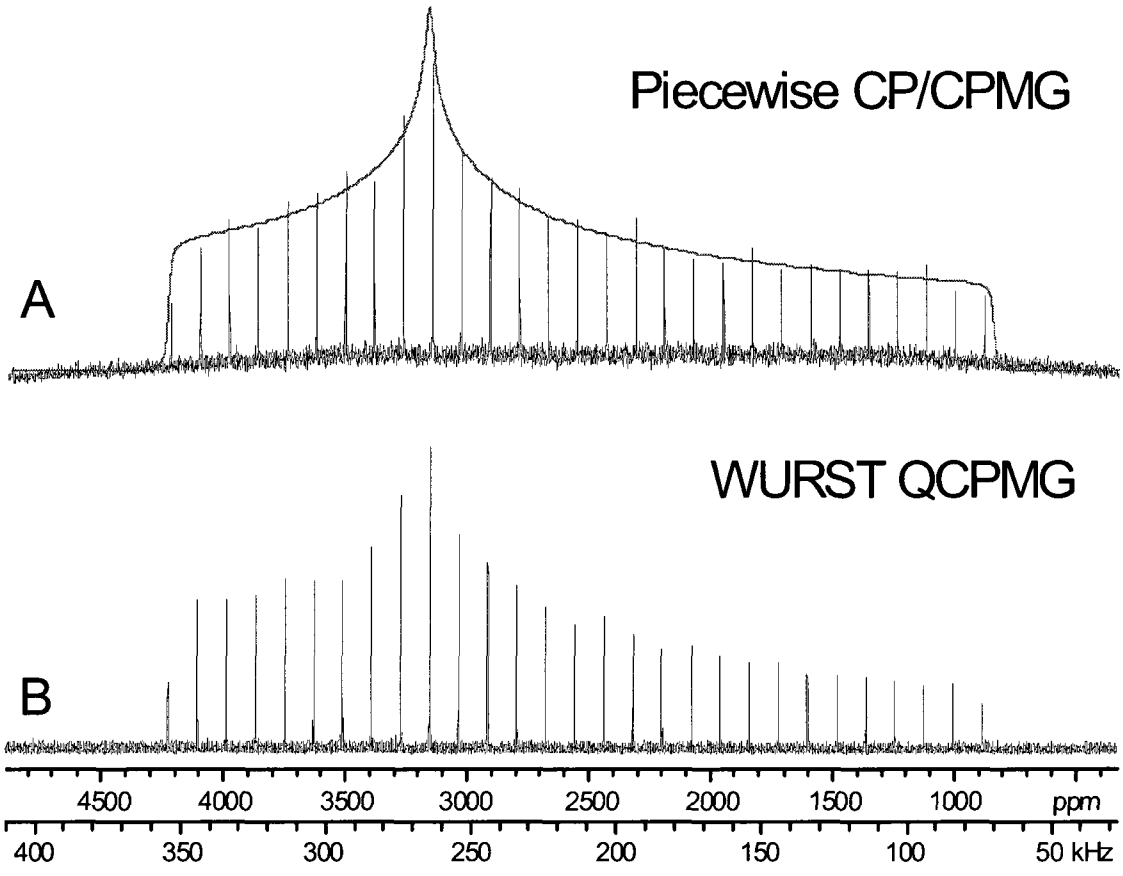

Figure 3.1. (A) ^{1}H - ^{207}Pb CP/CPMG and (B) WURST-QCPMG ^{207}Pb NMR spectra of $[(PhS)_3Pb][As\ Ph_3]$, **1,** with WSolids simulation (top trace).

Compound **1** contains a single Pb site in a three-coordinate pyramidal PbS_3 environment. Simulation of a CSA powder pattern which fits the outer manifold of the spikelet spectrum yields the ^{207}Pb chemical shift tensor parameters, which include an isotropic shift of δ_{iso} = 2750 ppm, a span of Ω = 3400 ppm and a skew of κ = 0.37 (see Table 3.1 for definitions of these parameters). The isotropic shift represents the average chemical shift value that would be observed if the molecule was rapidly tumbling in an isotropic fashion (δ_{iso} is normally what is measured in solution NMR experiments, and can sometimes be influenced by the solvent, temperature, viscosity, etc.). The span indicates the breadth of the chemical shielding (CS) pattern in ppm, and reports the

magnitude of the CSA. Finally, the skew is a dimensionless parameter which indicates the degree of axial symmetry of the CS tensor ($-1 \leq \kappa \leq +1$, where $\kappa = +1$ and -1 represent the two extremes of axial symmetry). In this case, the positive value of κ indicates that δ_{33} is the distinct component of the CS tensor (i.e., δ_{11} and δ_{22} are similar in magnitude). Based on the site symmetry, and our previous studies of lead coordination compounds of this sort,[10] it is predicted that δ_{33}, which corresponds to the direction of highest nuclear shielding, is aligned along or near the direction of the lone electron pair. The CS tensor parameters, as well as the orientation of the CS tensor in the molecular frame, are discussed in detail in the theoretical section below.

Figure 3.2 shows the ^{207}Pb CP/CPMG and WURST-CPMG NMR spectra of **2**. The two spectra are similar in appearance, though the low-frequency end of the spectrum acquired with WURST-CPMG is lower in intensity than that acquired with CP/CPMG. However, the discontinuities of the WURST-CPMG spectrum are still clearly visible, and allow for the determination of CS tensor parameters. As with the SSNMR experiments conducted on **1**, WURST-CPMG is advantageous as it allows the entire spectrum of **2** (breadth of ca. 390 kHz) to be acquired in a single experiment, whereas the CP/CPMG experiment required the acquisition of 19 subspectra. WURST-CPMG also offers a moderate reduction in experimental time (Table 3.2). Compound **2** has a Pb environment which is similar to that of **1** except one sulfur atom has been replaced by a phosphorous atom. **2** has a comparable skew to that of **1**, $\kappa = 0.48$, but a significantly larger span, $\Omega =$ 4400 ppm. Again, δ_{33} is the distinct component of the CS tensor.

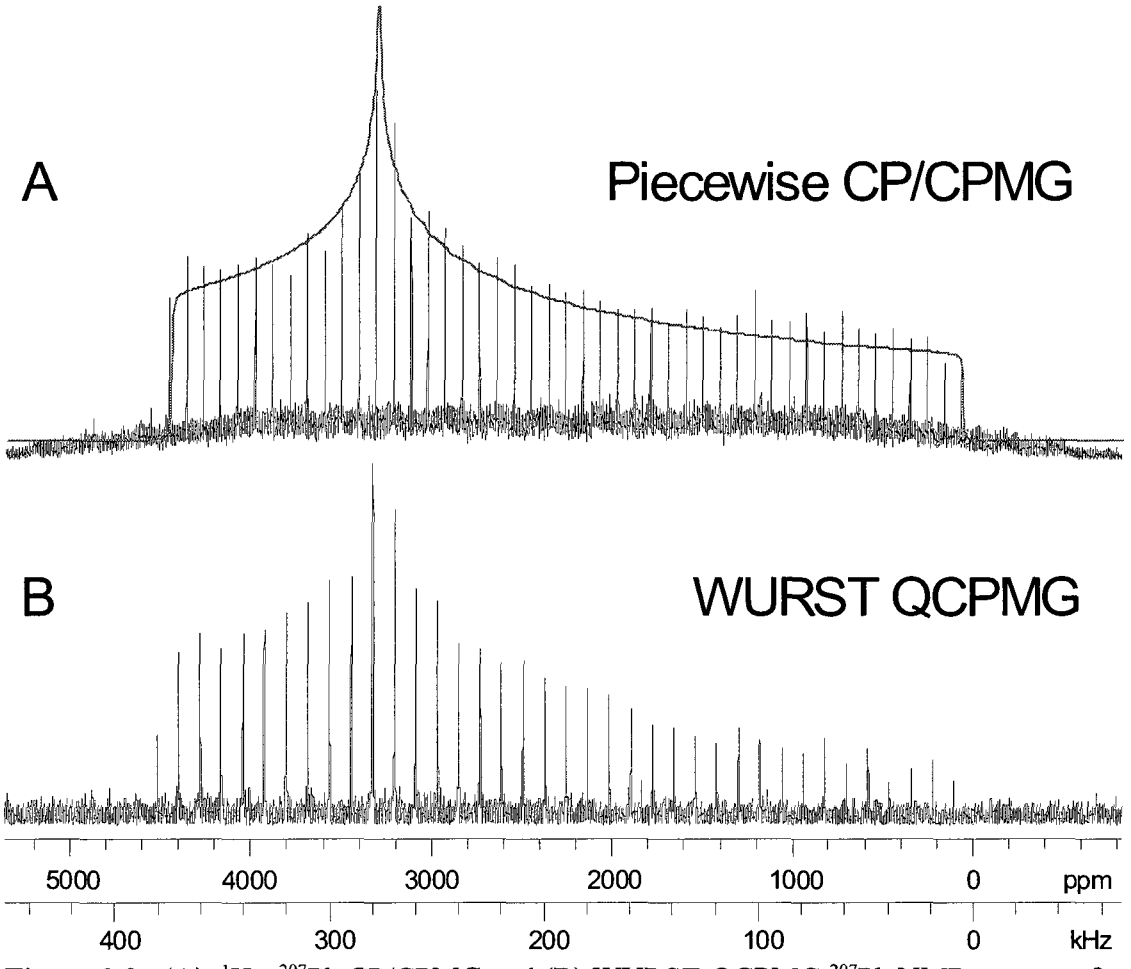

Figure 3.2. (A) ^{1}H - ^{207}Pb CP/CPMG and (B) WURST-QCPMG ^{207}Pb NMR spectra of $[(2,6\text{-}Me_2C_6H_3S)_2Pb]_2(dppe)$ (**2**) with WSolids simulation (top trace).

Table 3.2. Comparison of experimental times (hours) between CP/CPMG and WURST-CPMG

	1	**2**	**3**	**4**
CP/CPMG	32	23	20.3	22
WURST-CPMG	19	20.2	41.6	60

^{1}H-^{31}P CP/MAS NMR spectra were acquired for **2** (Figure 3.3), in the hope of observing indirect spin-spin coupling between ^{207}Pb and neighbouring ^{31}P nuclei. A single resonance with δ_{iso} = 17(1) ppm is observed. Since the natural abundance of ^{207}Pb is 22.6%, the coupling is manifested in the form of two satellite peaks, comprising a doublet of 22.6% of the total integrated intensity, with ^{1}J (^{207}Pb, ^{31}P) = 1895(100) Hz. This coupling is not visible in the ^{207}Pb CP/CPMG NMR spectrum, due to its small magnitude relative to the lead CSA (Ω = 4400 ppm) and the inherently low resolution in the CPMG spectrum. It is possible that this coupling might be observed in ^{207}Pb MAS or CP/MAS NMR spectra; unfortunately, these experiments were unsuccessful (refer to Appendix B, Figure B1) due to lengthy ^{207}Pb T_1 constants and inefficient CP at even very slow spinning rates.

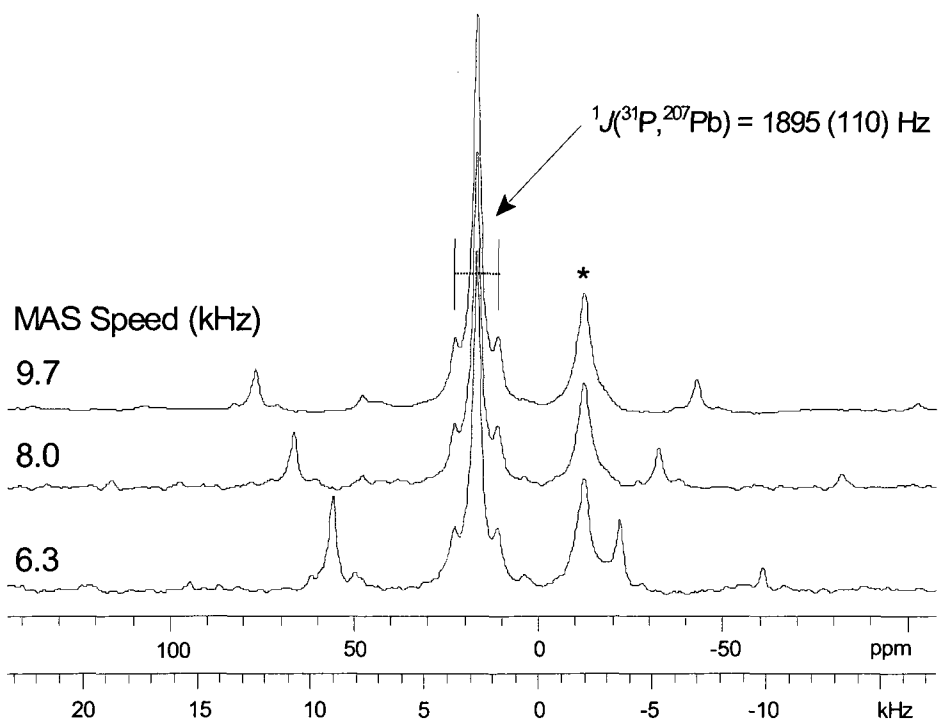

Figure 3.3. ^{1}H-^{31}P CP/MAS NMR of $[(2,6\text{-}Me_2C_6H_3S)_2Pb]_2(dppe)$, **2**. * denotes impurity

Two distinct but overlapping powder patterns are observed in the ^{1}H-^{207}Pb CP/CPMG and ^{207}Pb WURST-CPMG NMR spectra of compound **3** (Figure 3.4), which is consistent with its crystal structure. As with **1** and **2**, the spectrum of **3** was able to be acquired in a single experiment with the WURST-CPMG pulse sequence, but required piecewise acquisition with CP/CPMG. Unlike the previously discussed compounds, the spectrum of **3** obtained with the WURST-CPMG pulse sequence required a much longer experimental time (Table 3.2) than that acquired with CP/CPMG, even with lower spectral resolution. This is likely due to the much longer T_1 constant of the ^{207}Pb nucleus than that of ^{1}H. CP is also very efficient for **3**, owing to the presence of multiple methyl groups within the molecule. DFT calculations (*vide infra*) were used to assign each experimental CS tensor to a crystallographic site. Site 1 (PbS_3) has a Ω = 3600 ppm, similar to that of **1**, and κ = 0.63, which is slightly larger in magnitude than those of **1** and **2**. δ_{33} is again the distinct component of the CS tensor, and is likely oriented in a similar manner to that described for **1** and **2**. Site 2 of **3** has a distinct four-coordinate PbS_2N_2 environment, with a pseudo-trigonal bipyramidal geometry including the stereo-chemically active lone pair. Accordingly, this site has markedly different CS tensor parameters, with Ω = 4050 ppm and κ = 0.07 (though the isotropic shift is still in the same region as all of the other sites). The value of κ indicates that all three principal components of the CS tensor are significantly different from one another, making a prediction of the CS tensor orientation based on molecular symmetry alone more difficult. We also note that the poorly resolved low-frequency edge of the spectrum leads to a significant error range in the reported values of the most shielded CS tensor element,

δ_{33}, for the two tensors.

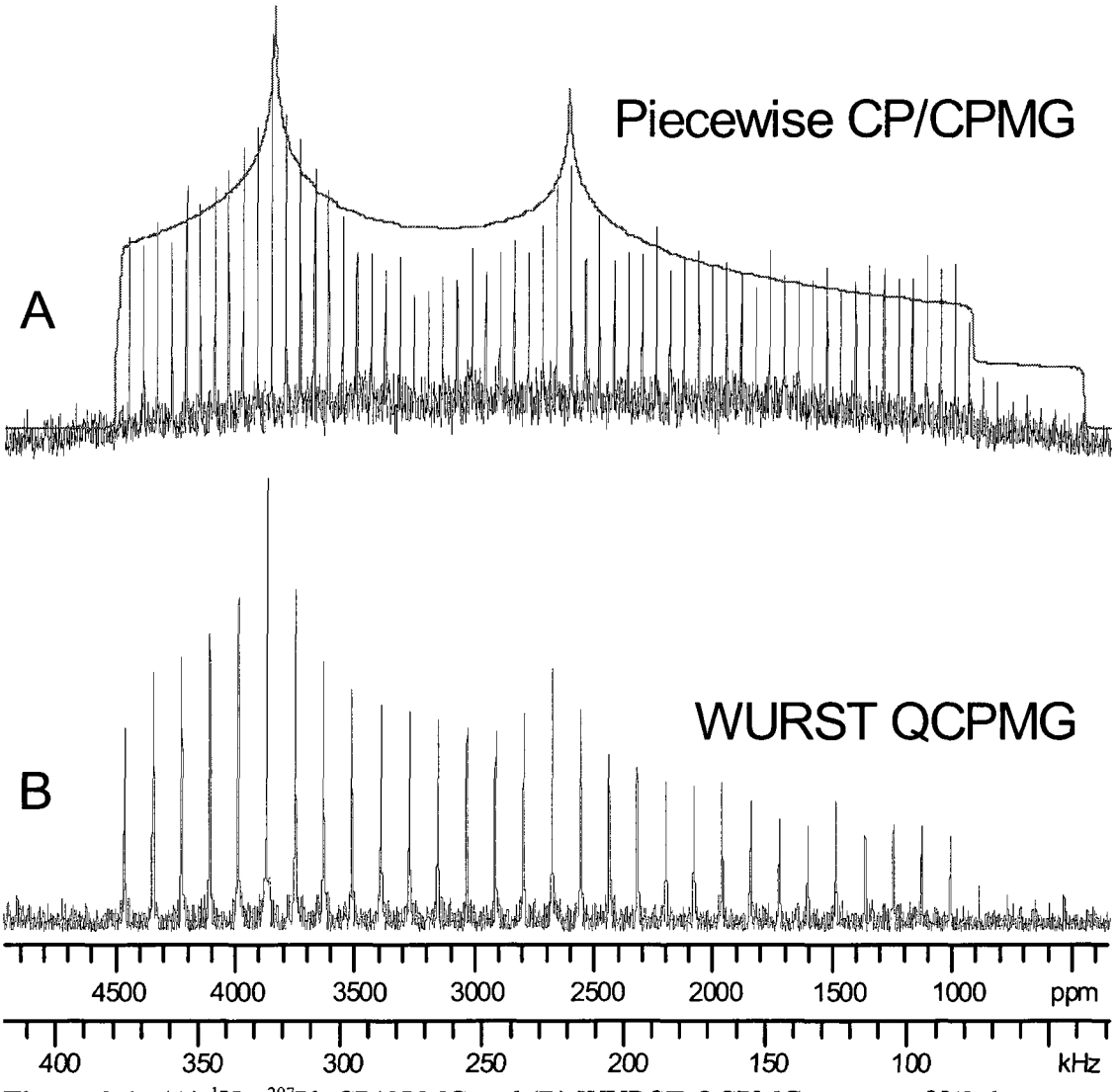

Figure 3.4. (A) ^{1}H - ^{207}Pb CP/CPMG and (B) WURST-QCPMG spectra of $[(2,6\text{-}Me_2C_6H_3S)_2Pb]_2(tmeda)$, **3**, with WSolids simulation (top trace).

The ^{1}H-^{207}Pb CP/CPMG and ^{207}Pb WURST-CPMG NMR spectra of **4** also have two distinct CSA patterns (Figure 3.5); however, the patterns are well separated and resolved. Despite the extreme breadth (ca. 485 kHz) of the powder patterns, the entire spectrum was acquired in a single WURST-CPMG experiment, and the resulting powder patterns closely resemble those of the CP/CPMG experiment. As with **3**, however, the piecewise CP/CPMG experiment offered a more efficient method of acquisition, as it took 22 hours to acquire the spectrum, as opposed to the 60 hour experimental time of the WURST-CPMG experiment (we note that the spikelet spacing in the latter experiment offers higher spectral resolution, and accounts for some of the increase in experimental time). There are three Pb sites predicted from the crystal structure: Site 1 is a PbS_2P_2 centre and Sites 2 and 3 are similar PbS_3 environments. The CS tensor parameters of sites 2 and 3 closely resemble those of **1**, **2** and site 1 of **3**. Site 2 has Ω = 3700 ppm and κ = 0.84, and site 3 has Ω = 3750 ppm and κ = 0.68; however, there are large errors associated with these parameters as the two spectra are difficult to resolve due to the inherently low spectral resolution. As in the cases above, the σ_{33}'s are the distinct components of the CS tensors, and are likely oriented along the pseudo three-fold rotational symmetry axes of each unit. The CS tensor parameters of site 1 (PbS_2P_2) are Ω = 1470 ppm, which is much smaller than those of any of the other systems, and κ = 0.4, again indicating that δ_{33} is the distinct component. Prediction of the orientation of the CS tensor for site 1 is again difficult because of the unique coordination environment of the Pb centre; the disparate parameters and tensor orientations will be discussed below.

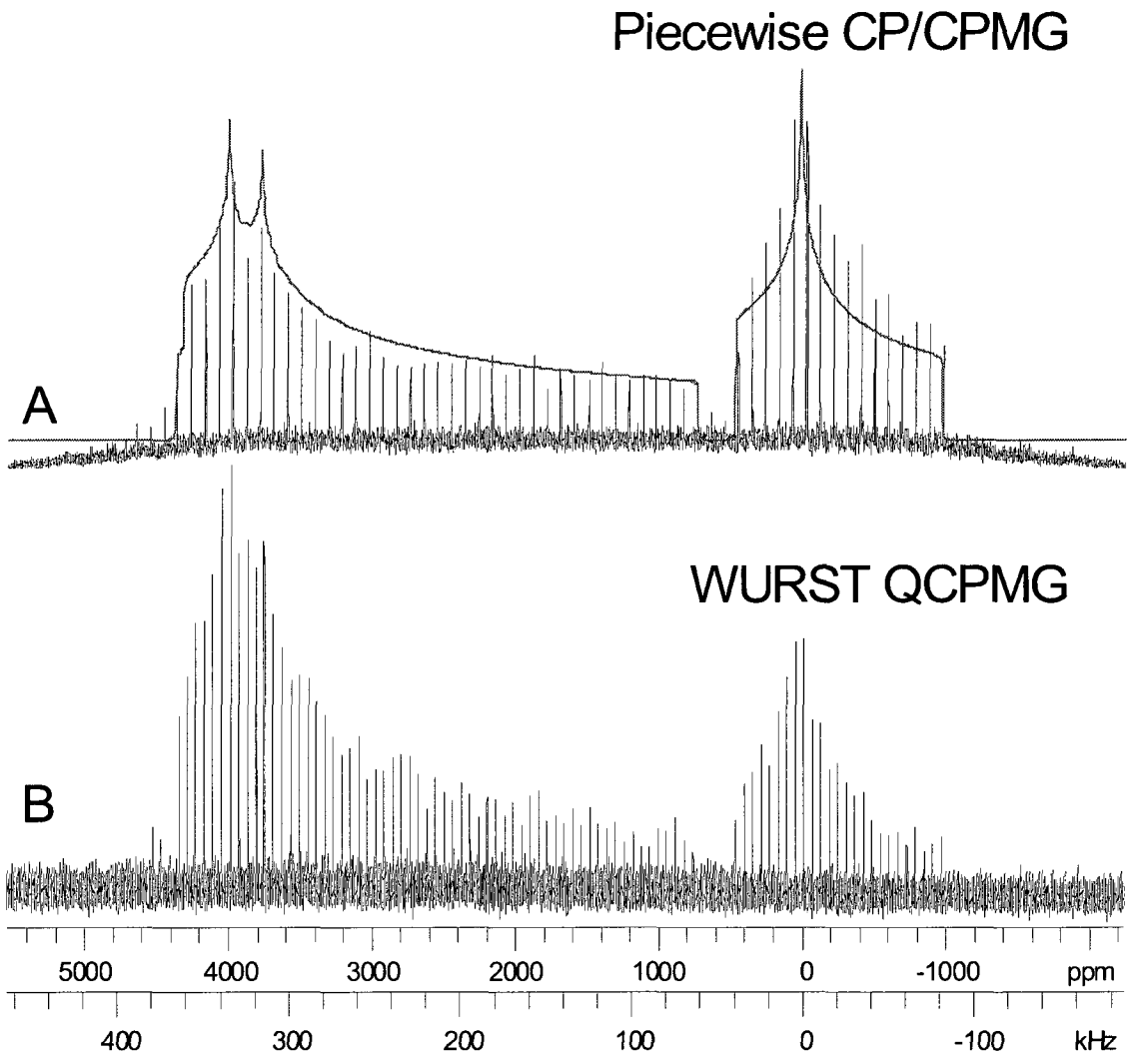

Figure 3.5. (A) ^{1}H - ^{207}Pb CP/CPMG and (B) WURST-QCPMG spectrum of $[(2,6\text{-}Me_2C_6H_3S)_2Pb]_3(dmpe)$, **4**, with WSolids simulation.

^{31}P CP/MAS NMR spectra reveal two resonances of approximately equal intensity with δ_{iso} of 35.8(10) ppm and 0.1(10) ppm, with values of $^{1}J(^{207}Pb, ^{31}P)$ of 2474 (80) Hz and 1363 (50) Hz, respectively (Figure 3.6). The large values of $^{1}J(^{207}Pb, ^{31}P)$ and corresponding satellite intensities clearly indicate the presence of Pb-P bonds. As with **2**, the ^{1}J couplings are not visible in the ^{207}Pb CP/CPMG NMR spectrum due to the inherently low resolution. The presence of two ^{31}P resonances with very different values of δ_{iso} and $^{1}J(^{207}Pb, ^{31}P)$ is puzzling; one would not expect this given the crystal structure of **4**, since the two phosphorus sites of the dmpe group are chemically similar (and long range solid-state interactions are not expected to result in such differences). Preliminary DFT computations of the ^{31}P chemical shifts in a structural model of **4** indicate the chemical shifts of the two sites should differ by only ca. 5 ppm, in contrast to the difference of ca. 36 ppm observed experimentally (Table B3). Further, the two shifts measured in the solid state bear no resemblance to those observed in solution ^{31}P NMR experiments mentioned above, where a δ_{iso} of ca. -34 ppm is thought to correspond to dmpe weakly interacting with the Pb site, and free dmpe has a δ_{iso} = -47.55 ppm. At this time, we have no definitive explanation for the large differences in the parameters measured in the solid state. Since the powder XRD pattern of sample **4** matches closely, but not exactly, with simulated patterns (Figure B2), it is possible that there is an additional crystalline solid phase which is currently unaccounted for.

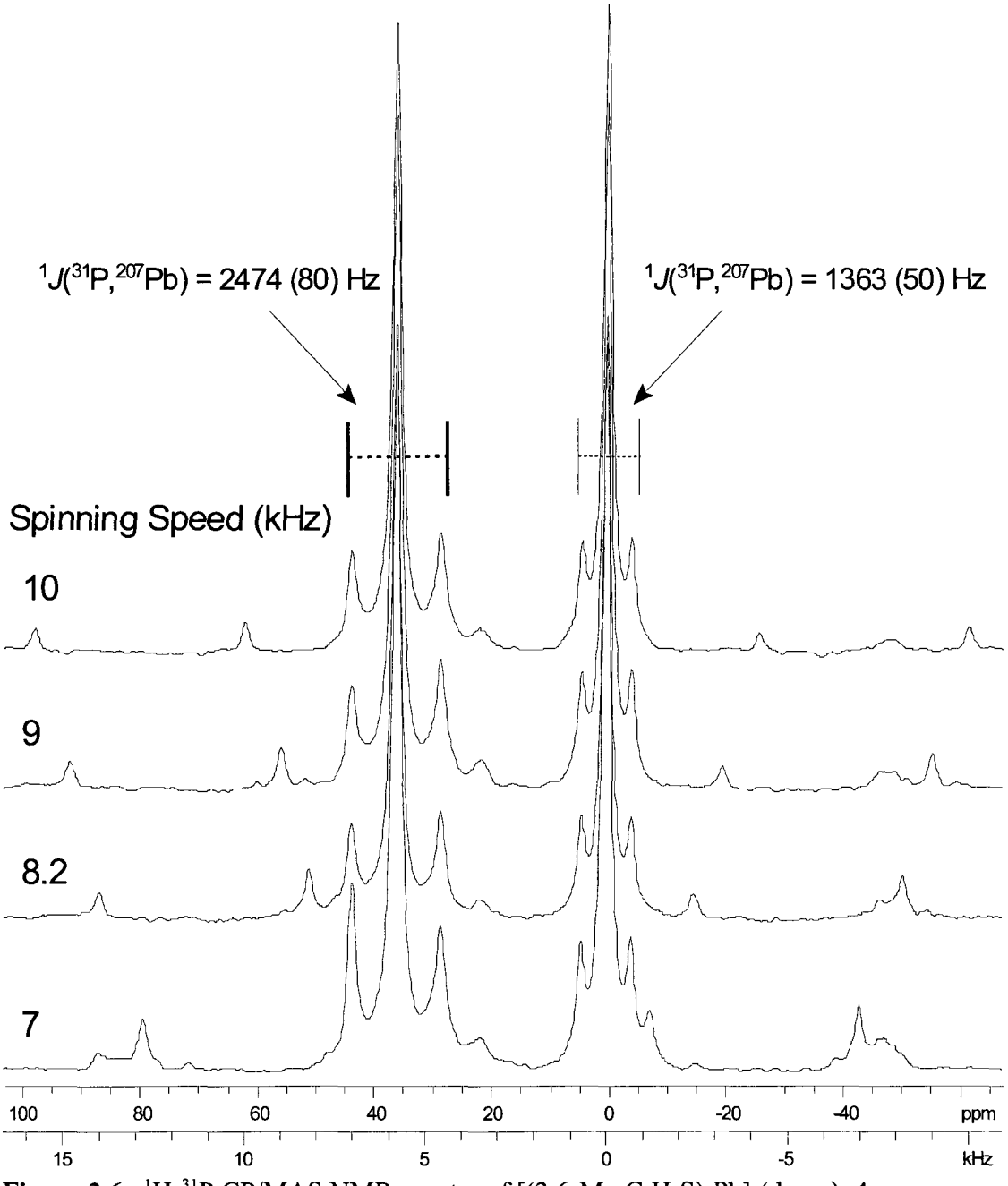

Figure 3.6. ^1H-^{31}P CP/MAS NMR spectra of $[(2,6\text{-}Me_2C_6H_3S)_2Pb]_3(dmpe)$, **4**.

We have demonstrated that both CP/CPMG and WURST-CPMG pulse sequences are useful for acquiring ^{207}Pb UW SSNMR spectra. The WURST-QCPMG sequence enables acquisition of these extremely broad ^{207}Pb NMR patterns in a single experiment (i.e., without the need for stepping the transmitter frequency) and offers considerable time savings (Table 3.2) for samples **1** and **2**. Perhaps most importantly, it is unnecessary to have personnel present to monitor the experiment and re-tune the probe, allowing more efficient 24 hour acquisition. However, for samples **3** and **4**, CP/CPMG is a more efficient for acquiring the UW ^{207}Pb SSNMR spectra. The WURST-CPMG pulse sequence, which relies on direct excitation of the ^{207}Pb nuclei, is less successful in these cases due to the much longer $T_1(^{207}\text{Pb})$ values. However, by directly exciting the ^{207}Pb nucleus, WURST-CPMG avoids inaccurate distributions of signal intensity in samples with multiple sites, which can occur in CP experiments due to varying CP efficiency between sites. Though not always the most efficient method of acquisition where cross-polarization is possible, WURST-CPMG may be very useful for acquiring UW SSNMR spectra of samples where ^{1}H (or ^{19}F) is not present, or in cases where personnel are not available to acquire multiple spectra for piecewise experiments.

3.3.2 Calculation of Lead Nuclear Shielding (NS) Tensors with Density Functional Theory

Calculations of NMR parameters using density functional theory (DFT) allow for the correlation of observed NMR parameters to molecular structure, as well as for the exploration of the origins of nuclear magnetic shielding interactions. It is crucial to develop such understandings for unique coordination environments such as the ones

described herein, since this will afford rapid structural interpretation for many current and future systems for which crystallographic data is unavailable (i.e., sub-microcrystalline and disordered systems). Furthermore, in compounds containing multiple sites, NMR parameters gleaned from DFT calculations can aid in the assignment of the spectra. In cases where MAS NMR experiments are impractical, these calculations are an invaluable tool for making spectral assignments. Since the current work deals with Pb chemical shifts, which arise from nuclear shielding (NS) of the Pb nuclei (i.e., magnetic shielding of the nucleus induced by electron circulation, which can be described in terms of mixing occupied and virtual molecular orbitals), the Zeroth-Order-Relativistic-Approximation (ZORA)[61-63] was employed for all DFT calculations. This methodology is essential for systems containing heavy atoms, as relativistic effects on the NS tensor become pronounced for heavy nuclei.[59,60,65,66]

The theoretical anisotropic NS parameters for **1** and site 1 of **3** (Table 3.3) agree well with experimentally determined results. For the remaining Pb sites, Ω is generally overestimated, except for site 1 of **4** where it is slightly underestimated. Calculated values of κ generally agree well with experimental results, with the exception of **2**. Despite the vast chemical shift range of ^{207}Pb, predicted values of δ_{iso} agree well (i.e., deviate by *ca.* 250 ppm or less) with those observed experimentally, with the exception of Site 1 of **4** and, to a lesser extent, Site 1 of **3**.

Table 3.3. Theoretical and Experimental ^{207}Pb NS and CS tensor parameters.

	σ_{11}	σ_{22}	σ_{33}	σ_{iso}	δ_{iso}[a] (ppm)	Ω	κ
1							
Paramagnetic	-7494	-6071	-5545	-6370		1948	-0.5
Diamagnetic	9956.3	9959.2	9964.2	9959.9		8	0.27
Spin-Orbit	1028.8	1210.5	2788.4	1675.9		1760	0.79
Total	3785.3	4930.6	7082	5266	2592	3297	0.31
Experimental					**2750**	**3400**	**0.37**
2							
Paramagnetic	-7969	-5990	-4455	-6138		3514	-0.1
Diamagnetic	9956.9	9960.6	9963	9960.1		6	-0.2
Spin-Orbit	1070	1255.4	3146.2	1823.8		2076	0.82
Total	3140.3	8559.5	8559.5	5646.2	2438	5419	0.23
Experimental					**2610**	**4400**	**0.48**
3 (site 1)							
Paramagnetic	-7049.7	-6660.2	-5091.7	-5267.2		1958	0.6
Diamagnetic	9955.7	9960.9	9961.7	9959.4		6	-0.8
Spin-Orbit	763.8	1128.7	2855.4	1582.6		2092	0.65
Total	3816.4	4452.2	7556.1	5274.9	2812	3740	0.66
Experimental					**3100**	**3600**	**0.63**
3 (site 2)							
Paramagnetic	-8199.4	-5994.9	-4126.1	6106.8		4073	0.0
Diamagnetic	9950.2	9955.7	9958.5	9954.8		8	-0.3
Spin-Orbit	837.6	1204	3233.1	1758.2		2396	0.69
Total	2621.3	5170.4	9027.1	5806.2	2479	6406	0.2
Experimental					**2610**	**3685**	**0.0**
4 (site 1)							
Paramagnetic	-4536	-4400	-3756	-4231		780.4	0.65
Diamagnetic	9952	9952.8	9964	9956.3		12	0.87
Spin-Orbit	3035.9	3193.8	3329.2	3186.3		293.2	0
Total	8564.5	8670.4	9500.9	8911.9	-854	936.3	0.77
Experimental					**-160**	**1475**	**0.38**

Table 3.3. (continued)							
4 (site 2)							
Paramagnetic	-7800	-6676	-5123	-6533		2677	0.16
Diamagnetic	9956.8	9960.1	9962.9	9959.9		6.2	0
Spin-Orbit	658.3	948.1	2789.5	1465.3		2131	0.73
Total	3020.7	4092.0	7563.9	4892.2	3198	4543	0.53
Experimental					**3045**	**3625**	**0.79**
4 (site 3)							
Paramagnetic	-7825	-6637	-5118	-6526		2707	0.12
Diamagnetic	9957.1	9960.5	9963.6	9960.4		6.51	0
Spin-Orbit	724.9	1001.9	2759.7	1495.5		2035	0.73
Total	3121.6	4130.4	7536.2	4929.4	3160	4415	0.54
Experimental					**2950**	**3600**	**0.67**

[a]The principal nuclear shielding components are related to the chemical shift components by the equation $\delta_{iso} = (\sigma_{ref} - \sigma_{iso})/(1-\sigma_{ref})$, where σ_{ref} corresponds to the isotropic shielding value of a reference compound (tetramethyllead, $\sigma_{ref} = 8064.8$).

Calculated Pb NS tensor orientations are depicted in Figures 3.7 and 3.8. The Pb site of **1** (PbS_3, Figure 3.7A, 3.7B) is in a trigonal pyramidal environment. As predicted from our experimental data, the NS tensor is oriented such that σ_{33}, the distinct principal component, is aligned along the direction of the lone pair, similar to results reported previously.[10,67] Compound **2** also contains a single, three coordinate Pb site (PbS_2P, Figure 3.7C, 3.7D), which is in an environment of lower symmetry than that of compound **1**, due to the distinct Pb-P bond which is significantly longer than the Pb-S bonds. In this case, σ_{33} is aligned close to the plane of the two Pb-S bonds (Table 3.4) in the direction of the lone pair.

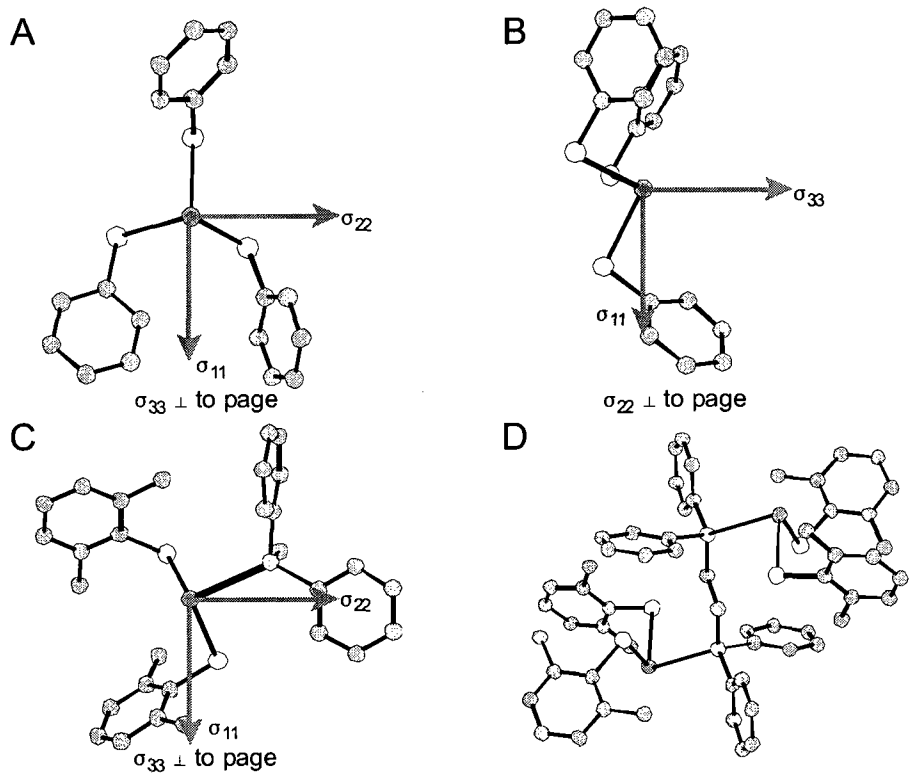

Figure 3.7. (A) "Top" view and (B) "side" view of NS tensor orientation of **1**, (C) NS tensor orientation of **2**, and (D) **2** shown as dimer.

Table 3.4. Angles describing the orientation of NS tensor components with respect to key structural and symmetry elements.

Compound 1					
σ_{33}-Pb-S (1)	119.28°				
σ_{33}-Pb-S (2)	133.37°				
σ_{33}-Pb-S (3)	116.16°				
Compound 2					
σ_{33}-Pb-S (1)	141.04°				
σ_{33}-Pb-S (2)	122.00°				
σ_{33}-Pb-P	98.40°				
Compound 3 (Site 1)		(Site 2)			
σ_{33}-Pb-S (1)	113.91°	σ_{33}-Pb-S (1)	163.50°		
σ_{33}-Pb-S (2)	138.04°	σ_{33}-Pb-S (2)	94.07°		
σ_{33}-Pb-S (3)	108.90°	σ_{33}-Pb-N (1)	103.42°		
		σ_{33}-Pb-N (2)	81.52°		
Compound 4 (Site 1)		(Site 2)		(Site 3)	
σ_{33}-Pb-S (1)	10.74°	σ_{33}-Pb-S (1)	142.42°	σ_{33}-Pb-S (1)	102.91°
σ_{33}-Pb-S (2)	163.49°	σ_{33}-Pb-S (2)	121.73°	σ_{33}-Pb-S (2)	143.48°
σ_{33}-Pb-P (1)	88.31°	σ_{33}-Pb-S (3)	98.40°	σ_{33}-Pb-S (3)	120.62°
σ_{33}-Pb-P (2)	86.82°				

Two distinct Pb sites are present in **3** (Figure 3.8A, 3.8B): one three-coordinate environment (PbS_3, Site 1), and one four-coordinate environment (PbS_2N_2, Site 2). Site 1, much like compound **1**, has a trigonal pyramidal coordination geometry; however, one of the three S atoms is datively coordinated, forming a longer Pb-S bond than the other two. As a result, there is a reduced symmetry compared to **1**, and σ_{33} is not clearly aligned along a particular symmetry element. The coordination sphere of Site 2 contains two nitrogen atoms and two sulfur atoms, (one of the latter is bound to the Pb in a dative manner). σ_{33} is oriented *ca.* 165° from the shorter, covalent Pb-S bond, near the position of the lone pair. σ_{11} is in the same plane as the N-Pb-N bonding arrangement, and bisects the N-Pb-N angle. Compound **4** has three distinct Pb centres (Figure 3.8C, 3.8D): one four coordinate (PbS_2N_2) site (Site 1), and two three coordinate (PbS_3) sites (Sites 2 and 3) which are nearly identical (Table 3.4). As with Site 1 of **3**, one coordinating sulfur atom from each of Sites 2 and 3 forms a dative bond with Site 1, which lengthens the Pb-S bond and reduces the local symmetry at the Pb centre. Accordingly, σ_{33} is shifted away from the pseudo three-fold axis of rotation (Figure 3.8). Site 1 adopts a unique four coordinate environment, with bonds to a bidentate DMPE ligand, and dative bonds to two sulfur atoms from neighbouring sites.

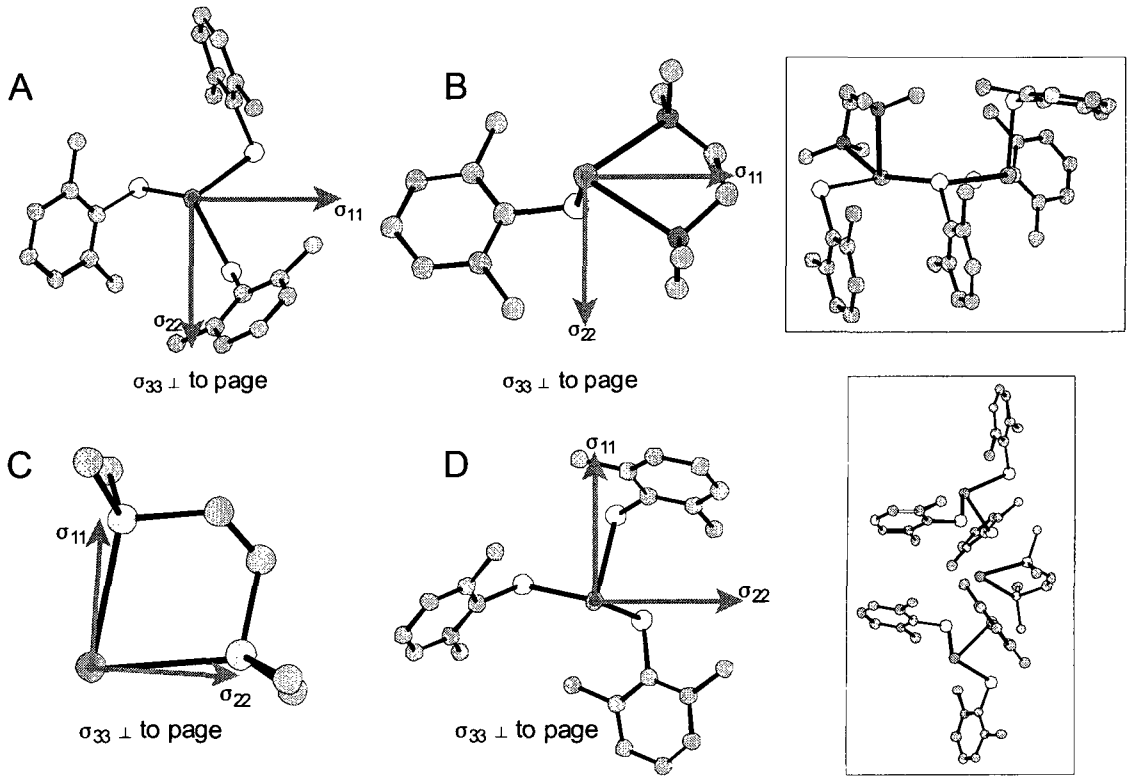

Figure 3.8. NS Tensor orientations of (A) Site 1and (B) Site 2 of **3**, and (C) Site 1 and (D) Site 2 of **4**. The full molecules are shown in the insets. Note that Site 3 of **4** has been omitted due to its similarity to Site 2.

In comparing the Pb NS tensor parameters and orientations, some interesting trends emerge. First, consider the PbS_3 environments in compounds **1**, **3** and **4**. Close examination of the Pb-S bond lengths and S-Pb-S bond angles indicate that **1** is the most symmetric, possessing a local pseudo three-fold rotational axis, and **4** is the least symmetric. It is interesting to note that as the sites deviate farther from a rotational axis, the values of κ increase when one would expect them to decrease. The orientation of the σ_{33} component of the NS tensor seems to move from the pseudo-C_3 axis in **1** into the S-Pb-S plane in **3** and **4**. Clearly, simple symmetry arguments cannot be made to describe these changes in NS tensor parameters and orientations; rather, it is a delicate interplay

between paramagnetic shielding contributions involving the Pb lone pair which is a major factor in determining the nature of these tensors, as we have noted in previous work.[10]

If the PbS_2P type environment of site of **2** is then examined, one can see that the bond angles are similar to those of the PbS_3 site of **1**; in essence, the difference between the two sites is a phosphorous atom in place of a sulfur atom within the coordination sphere of the Pb centre in **2**. This relatively minor change results in drastically different Ω and κ values (Table 3.1), with Ω increasing significantly and κ taking on an intermediate value, relative to the other Pb compounds. The next Pb environment to consider is the PbS_2P_2 site of **4**. The major difference between this site and the PbS_2P site of **2** is the difference in coordination number (the extra P ligand in the site of **4** makes it four coordinate). The Ω value for the PbS_2P_2 site of **4** is reduced by a great deal compared to the PbS_2P site of **2**, which may be related to the fact that the Pb-S bonds in the four coordinate site of **4** are dative bonds. The lone pair is not stereochemically active due to the local geometry of the Pb atom in this site. The smaller span associated with this site arises from the absence of the large paramagnetic deshielding terms associated with high *p*-character of the lone pair. This is distinct from the other sites where these deshielding terms give rise to large spans and serve to orient σ_{33} near or along the stereochemically active lone pairs. The final site is the PbS_2N_2 site of **3**, which exhibits a relatively large Ω value relative to the aforementioned Pb environments, and a κ value near zero. The PbS_2N_2 environment has an unusual geometry, and undoubtedly has closely spaced occupied and virtual molecular orbitals which are induced to mix by the external magnetic field, thereby producing the large span (a full discussion of this is

beyond the scope of the current work). The skew is easier to rationalize: each of the CS tensor components are completely different from one another, meaning they are directed into distinct electronic environments, consistent with the asymmetric nature of this site. Though there are no clear general trends regarding the Ω values, PbS_3-type environments tend to have CS tensors which are close to being axially symmetric, whereas the PbS_2P, PbS_2P_2 and PbS_2N_2 sites each have CS tensors with three distinct tensor components, in line with their local symmetries.

3.4 Conclusions

^{207}Pb SSNMR experiments have been successfully carried out on compounds **1** - **4** using both the CP/CPMG and WURST-CPMG pulse sequences. The sensitivity of ^{207}Pb SSNMR as a probe of molecular structure is evident, as the resulting ^{207}Pb SSNMR spectra differ greatly with small changes in the coordination environment of the Pb centre. The CP/CPMG pulse sequence allows for these spectra to be readily acquired in a piecewise fashion, though employment of the WURST-CPMG sequence allows for each of the spectra to be acquired in a single experiment. Theoretical investigations with ADF and ZORA agree reasonably well with experimental data, and aid in spectral assignment in cases where overlapping patterns of multiple sites exist. Such calculations also allow for the determination of NS tensor orientations, which correlate spectral parameters to the molecular structure. These NS tensor orientations, and the magnitude of the associated NS parameters, are highly dependent upon the coordination environment of the Pb centre; varying the number, and nature, of coordinating ligands has a profound impact on these

parameters, and by extension, the spectral appearance. Smaller variations in coordination environment, such as varying bond distance and bond angle, have a lesser effect, though such subtle variations still alter the NS parameters. Consequently, we believe that the use of these two pulse sequences for signal enhancement, in combination with DFT calculations of nuclear shielding properties, will allow for many Pb-containing materials to be studied using ^{207}Pb SSNMR. We are hopeful that this work inspires further research in this area, and aids others in shedding new light on the nature of lead-containing materials.

Bibliography

(1) Parr, J. *Polyhedron* 1997, 16, 551-566.

(2) Tsubomura, T.; Ito, M.; Sakai, K. *Inorganica Chimica Acta* 1999, 284, 149-157.

(3) Cramer, R. E.; Waddling, C. A.; Fujimoto, C. H.; Smith, D. W.; Kim, K. E. *Journal of the Chemical Society-Dalton Transactions* 1997, 1675-1683.

(4) Shimoni-Livny, L.; Glusker, J. P.; Bock, C. W. *Inorganic Chemistry* 1998, 37, 1853-1867.

(5) Rae, A. D.; Craig, D. C.; Dance, I. G.; Scudder, M. L.; Dean, P. A. W.; Kmetic, M. A.; Payne, N. C.; Vittal, J. J. *Acta Crystallographica Section B-Structural Science* 1997, 53, 457-465.

(6) Krebs, B.; Brommelhaus, A.; Kersting, B.; Nienhaus, M. *European Journal of Solid State and Inorganic Chemistry* 1992, 29, 167-180.

(7) Dean, P. A. W.; Vittal, J. J.; Payne, N. C. *Inorganic Chemistry* 1985, 24, 3594-3597.

(8) Shaw, R. A.; Woods, M. 1971, 1569-&.

(9) Appleton, S. E.; Briand, G. G.; Decken, A.; Smith, A. S. *Dalton Transactions* 2004, 3515-3520.

(10) Briand, G. G.; Smith, A. D.; Schatte, G.; Rossini, A. J.; Schurko, R. W. *Inorg. Chem.* 2007, 46, 8625-8637.

(11) Dean, P. A. W.; Vittal, J. J.; Payne, N. C. *Inorganic Chemistry* 1984, 23, 4232-4236.

(12) Christou, G.; Folting, K.; Huffman, J. C. *Polyhedron* 1984, 3, 1247-1253.

(13) Dybowski, C.; Neue, G. *Progress in Nuclear Magnetic Resonance Spectroscopy* 2002, 41, 153-170.

(14) Siegel, R.; Nakashima, T. T.; Wasylishen, R. E. *Journal of Physical Chemistry B* 2004, 108, 2218-2226.

(15) Katz, M. J.; Aguiar, P. M.; Batchelor, R. J.; Bokov, A. A.; Ye, Z. G.; Kroeker, S.; Leznoff, D. B. *Journal of the American Chemical Society* 2006, 128, 3669-3676.

(16) Willans, M. J.; Demko, B. A.; Wasylishen, R. E. *Physical Chemistry Chemical Physics* 2006, 8, 2733-2743.

(17) Duncan, T., Michael *A Compilation of Chemical Shift Anisotropies*; The Farragut Press: Chicago, 1990.

(18) Van Gorkom, L. C. M.; Hook, J. M.; Logan, M. B.; Hanna, J. V.; Wasylishen, R. E. *Magnetic Resonance in Chemistry* 1995, 33, 791-795.

(19) Bielecki, A.; Burum, D. P. *Journal of Magnetic Resonance Series A* 1995, 116, 215-220.

(20) Grutzner, J. B.; Stewart, K. W.; Wasylishen, R. E.; Lumsden, M. D.; Dybowski, C.; Beckmann, P. A. *Journal of the American Chemical Society* 2001, 123, 7094-7100.

(21) Menger, E. M.; Raleigh, D. P.; Griffin, R. G. *J. Magn. Reson.* 1985, 63, 579-582.

(22) Santos, R. A.; Gruff, E. S.; Koch, S. A.; Harbison, G. S. *J. Am. Chem. Soc.* 1991, 113, 469-475.

(23) Groombridge, C. J. *Magn. Reson. Chem.* 1993, 31, 380-387.

(24) Harris, R. K.; Sebald, A. *Magn. Reson. Chem.* 1987, 25, 1058-1062.

(25) Harris, R. K.; Sebald, A. *Magn. Reson. Chem.* 1989, 27, 81-87.

(26) Sebald, A.; Harris, R. K. *Organometallics* 1990, 9, 2096-2100.

(27) Bureau, B.; Silly, G.; Buzare, J. Y. *Solid State Nucl. Magn. Reson.* 1999, 15, 79-89.

(28) Fayon, F.; Farnan, I.; Bessada, C.; Coutures, J.; Massiot, D.; Coutures, J. P. *Journal of the American Chemical Society* 1997, 119, 6837-6843.

(29) Zhao, P. D.; Prasad, S.; Huang, J.; Fitzgerald, J. J.; Shore, J. S. *Journal of Physical Chemistry B* 1999, 103, 10617-10626.

(30) Van Bramer, S. E.; Glatfelter, A.; Bai, S.; Dybowski, C.; Neue, G.; Perry, D. L. *Magnetic Resonance in Chemistry* 2006, 44, 357-365.

(31) Tang, J. A.; Kogut, E.; Norton, D.; Lough, A. J.; McGarvey, B. R.; Fekl, U.; Schurko, R. W. *Journal of Physical Chemistry B* 2009, 113, 3298-3313.

(32) Hung, I.; Rossini, A. J.; Schurko, R. W. *Journal of Physical Chemistry A* 2004, 108, 7112-7120.

(33) Rhodes, H. E.; Wang, P. K.; Stokes, H. T.; Slichter, C. P.; Sinfelt, J. H. *Phys. Rev. B* 1982, 26, 3559-3568.

(34) Bastow, T. J.; Smith, M. E. *Solid State Nucl. Magn. Reson.* 1992, 1, 165-174.

(35) Massiot, D.; Farnan, I.; Gautier, N.; Trumeau, D.; Trokiner, A.; Coutures, J. P. *Solid State Nucl. Magn. Reson.* 1995, 4, 241-248.

(36) Medek, A.; Frydman, V.; Frydman, L. *J. Phys. Chem. A* 1999, 103, 4830-4835.

(37) Larsen, F. H.; Jakobsen, H. J.; Ellis, P. D.; Nielsen, N. C. *Journal of Physical Chemistry A* 1997, 101, 8597-8606.

(38) Lipton, A. S.; Wright, T. A.; Bowman, M. K.; Reger, D. L.; Ellis, P. D. *J. Am. Chem. Soc.* 2002, 124, 5850-5860.

(39) Siegel, R.; Nakashima, T. T.; Wasylishen, R. E. *Concepts Magn. Reson. Part A* 2005, 26A, 62-77.

(40) Bowers, G. M.; Lipton, A. S.; Mueller, K. T. *Solid State Nucl. Magn. Reson.* 2006, 29, 95-103.

(41) Tang, J. A.; Masuda, J. D.; Boyle, T. J.; Schurko, R. W. *ChemPhysChem* 2006, 7, 117-130.

(42) Kogut, E.; Tang, J. A.; Lough, A. J.; Widdifield, C. M.; Schurko, R. W.; Fekl, U. *Inorg. Chem.* 2006, 45, 8850-8852.

(43) Thibault, M. H.; Lucier, B. E. G.; Schurko, R. W.; Fontaine, F. G. *Dalton Trans.* 2009, 7701-7716.

(44) Bryant, P. L.; Harwell, C. R.; Mrse, A. A.; Emery, E. F.; Gan, Z. H.; Caldwell, T.; Reyes, A. P.; Kuhns, P.; Hoyt, D. W.; Simeral, L. S.; Hall, R. W.; Butler, L. G. *J. Am. Chem. Soc.* 2001, 123, 12009-12017.

(45) Sampathkumaran, E. V.; Fujiwara, N.; Rayaprol, S.; Madhu, P. K.; Uwatoko, Y. *Phys. Rev. B* 2004, 70.

(46) Kupce, E.; Freeman, R. *J. Magn. Reson. Ser. A* 1995, 117, 246-256.

(47) Bhattacharyya, R.; Frydman, L. *J. Chem. Phys.* 2007, 127.

(48) Bohlen, J. M.; Rey, M.; Bodenhausen, G. 1989, 84, 191-197.

(49) O'Dell, L. A.; Schurko, R. W. *Chem. Phys. Lett.* 2008, 464, 97-102.

(50) Guerra, C. F.; Snijders, J. G.; te Velde, G.; Baerends, E. J. *Theoretical Chemistry Accounts* 1998, 99, 391-403.

(51) Velde, G. T.; Bickelhaupt, F. M.; Baerends, E. J.; Guerra, C. F.; Van Gisbergen, S. J. A.; Snijders, J. G.; Ziegler, T. *Journal of Computational Chemistry* 2001, 22, 931-967.

(52) ADF2005.01, ADF2005.01, SCM, Theoretical Chemistry, Vrije Universiteit,

Amsterdam,

(53) Bennett, A. E.; Rienstra, C. M.; Auger, M.; Lakshmi, K. V.; Griffin, R. G. *Journal of Chemical Physics* 1995, 103, 6951-6958.

(54) Eichele, K.; Wasylishen, R. E., WSolids: Solid-State NMR Spectrum Simulation, 2001.

(55) Schreckenbach, G.; Ziegler, T. *Journal of Physical Chemistry* 1995, 99, 606-611.

(56) Schreckenbach, G.; Ziegler, T. *International Journal of Quantum Chemistry* 1997, 61, 899-918.

(57) Wolff, S. K.; Ziegler, T. *Journal of Chemical Physics* 1998, 109, 895-905.

(58) This work was made possible by the facilities of the Shared Hierarchical Academic Research Computing Network (SHARCNET:www.sharcnet.ca) and Compute/Calcul Canada.

(59) Autschbach, J. In *Calculation of NMR and EPR Parameters*; Wiley-VCH: Weinheim, 2004, pp 227-247.

(60) Autschbach, J.; Ziegler, T. In *Calculation of NMR and EPR Parameters*; Wiley-VCH: Weinheim, 2004, pp 249-264.

(61) van Lenthe, E.; Baerends, E. J.; Snijders, J. G. *Journal of Chemical Physics* 1993, 99, 4597-4610.

(62) van Lenthe, E.; Baerends, E. J.; Snijders, J. G. *Journal of Chemical Physics* 1994, 101, 9783-9792.

(63) van Lenthe, E.; van Leeuwen, R.; Baerends, E. J.; Snijders, J. G. *International Journal of Quantum Chemistry* 1996, 57, 281-293.

(64) Ditchfield, R. *Molecular Physics* 1974, 27, 789-807.

(65) Autschbach, J.; Ziegler, T. *Journal of Chemical Physics* 2000, 113, 936-947.

(66) Autschbach, J.; Ziegler, T. *Journal of Chemical Physics* 2000, 113, 9410-9418.

(67) Katz, M. J.; Michaelis, V. K.; Agular, P. M.; Yson, R.; Lu, H.; Kaluarachchi, H.; Batchelor, R. J.; Schreckenbach, G.; Kroeker, S.; Patterson, H. H.; Leznoff, D. B. *Inorg. Chem.* 2008, 47, 6353-6363.

Chapter 4

Solid-state NMR Investigations of Metal Guanidinates

4.1 Introduction

Recently, the synthesis of a series of group 13 amidinates (i.e. containing a bidentate N-C-N ligand) (Scheme 1) was reported.[1-3] Similar group 13 amidinates have shown promise in several applications, including catalysis,[4] C-H bond activation[5] and as precursors in chemical vapour deposition.[1,6] These molecules offer a wide variety of unique coordination environments, including four-, five- and six-coordinate metal centres with several different coordinating ligands. Though all of the molecules in the series

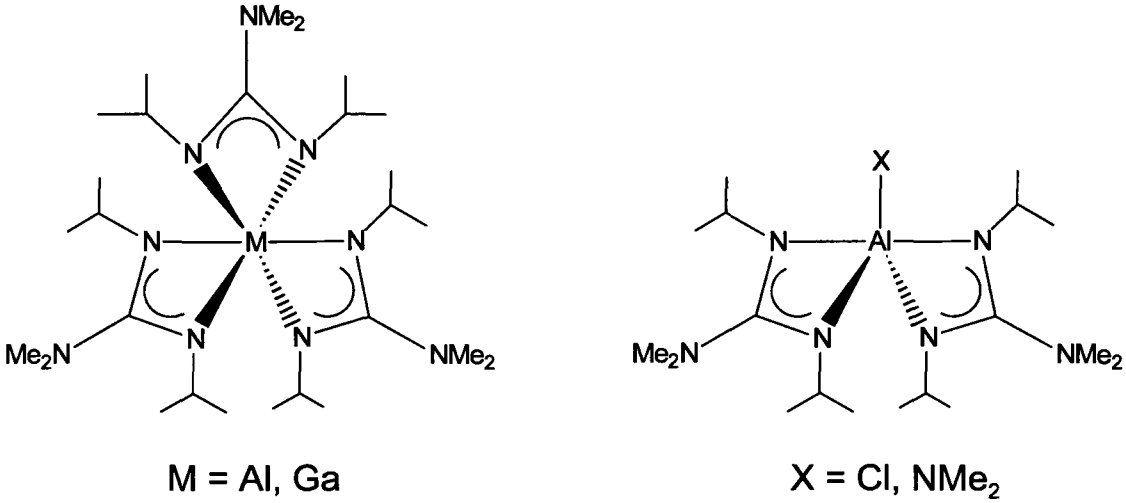

Scheme 1

discussed herein can be recrystallized to produce high quality crystals suitable for structural characterization by single-crystal X-ray diffraction, it is unlikely that these same molecules (or other molecules with similar structural motifs) will be amenable to

such characterization when used in the applications described above; hence, it is very useful to gain an understanding of the relationships between these well-characterized structures and NMR parameters which can be obtained through a variety of solid-state NMR (SSNMR) experiments.

^{27}Al solid-state NMR spectroscopy is widely used for the structural characterization of a wide variety of aluminum-containing materials,[7,8] such as glasses,[9] minerals,[10] microporous materials such as zeolites[11] and aluminophosphates,[12] and to a much lesser extent, molecular compounds.[13-17] ^{27}Al, which is a quadrupolar nucleus with a nuclear spin of 5/2, is favourable for SSNMR experimentation, owing to its 100% natural abundance, moderate quadrupole moment (14.66×10^{-28} m^2) and relatively high gyromagnetic ratio (6.97×10^7 rad T^{-1}s^{-1}).[18] It is well known that ^{27}Al SSNMR spectra are extremely sensitive to structural differences between aluminum environments: for instance, it is easy to distinguish between four-, five- and six-coordinate Al sites on the basis of their chemical shifts. However, there is often little variation between the isotropic chemical shifts of aluminum centres with the same coordination number.

In addition to information on the isotropic chemical shift, ^{27}Al SSNMR allows for the measurement of electric field gradient (EFG) and chemical shift (CS) tensor parameters, which is useful for distinguishing between compounds exhibiting similar chemical shifts. The quadrupolar interaction, which is the interaction between a nuclear spin with a non-zero quadrupole moment, and the local EFGs, can be probed directly with ^{27}Al SSNMR spectroscopy, allowing one to explore the ground-state electronic structure, symmetry and bonding at each Al site.

Though not employed as extensively as ^{27}Al SSNMR, ^{71}Ga SSNMR has also been used to study various materials,[19] including gallium oxides,[20] zeolites, [21] molecular sieves[22] and coordination complexes.[23] ^{71}Ga has a moderately high gyromagnetic ratio (8.18×10^7 rad $T^{-1}s^{-1}$), moderate quadrupole moment (10.7×10^{-28} m^2), and moderate natural abundance (39.89%) which make it suitable for SSNMR experiments. However, ^{71}Ga SSNMR experiments can be challenging to perform as the resulting spectra are often very broad, owing to the fact that ^{71}Ga is a spin-3/2 quadrupole.[19]

Herein we examine a series of guanidinate (guan = Me_2N-$C(N^iPr)_2$) compounds with ^{27}Al SSNMR spectroscopy, including $Al(guan)_3$, $Al(guan)_2Cl$ and $Al(guan)_2NMe_2$, in order to determine whether they can be differentiated on the basis of their EFG and CS tensor parameters. ^{71}Ga SSNMR experiments are also performed on $Ga(guan)_3$ in order to examine the alteration of the metal EFG tensor parameters resulting from this much heavier metal element. Two field strengths, 9.4 T and 21.1 T, are employed to ensure the accuracy of the EFG and CS tensor parameters which are extracted. *Ab initio* calculations of EFG and nuclear shielding (NS) tensors have also been conducted to ascertain their effectiveness at predicting the experimentally obtained parameters, and to determine the orientations of these tensors within the molecular frames.

4.2 Experimental Details

All guanidinate compounds were provided by Dr. Séan T. Barry and Julie Delahunt at Carleton university, and were prepared as described elsewhere.[1] $Al(NO_3)_3 \cdot 9H_2O$ and $Ga(NO_3)_x H_2O$ were purchased from Aldrich and used without further purification. Samples were powdered under an inert dinitrogen atmosphere, and tightly packed into 4 mm (o.d.) zirconium oxide rotors.

Solid-state NMR experiments were performed using a Varian InfinityPlus NMR spectrometer equipped with an Oxford 9.4 T ($\nu_0(^1H)$ = 400 MHz) wide-bore magnet at the University of Windsor operating at $\nu_0(^{27}Al)$ = 104.16 MHz and $\nu_0(^{71}Ga)$ = 121.89 MHz, or at the National Ultra-high Field Facility for Solids (www.nmr900.ca) in Ottawa, ON, on a Bruker Avance II NMR spectrometer equipped with a Bruker 21.15 T ($\nu_0(^1H)$ = 900 MHz) magnet operating at $\nu_0(^{27}Al)$ = 234.53 MHz and $\nu_0(^{71}Ga)$ = 274.49 MHz. Experiments conducted at 9.4 T were carried out using a Varian/Chemagnetics 4 mm HXY triple-resonance probe or a Varian/Chemagnetics 4 mm HX double-resonance probe. Experiments performed at 21.1 T employed a Bruker 4 mm double resonance probe. ^{27}Al NMR chemical shifts are reported with respect to a 1.0 M aqueous solution of $Al(NO_3)_3 \cdot 9H_2O$ (δ_{iso} = 0.0 ppm). A 1.0 M aqueous solution of $Ga(NO_3)_3 \cdot xH_2O$ (δ_{iso} = 0.0 ppm) was used as a reference for all ^{71}Ga SSNMR experiments.

The standard Hahn-echo pulse sequence ($(\pi/2)_x$ - τ_1 - $(\pi)_y$ - τ_2 - acq) was employed for the acquisition of all spectra at 9.4 T, where τ_1 and τ_2 represent short delays (i.e., 20 to 100 μs). $\pi/2$ pulse powers of *ca.* 4 - 27 kHz were used for ^{27}Al NMR experiments, and of *ca.* 34 kHz for the ^{71}Ga NMR experiment. A sequence of the form ($(\pi/2)_x$ - τ_1 - $(\pi/2)_y$ - τ_2

- acq) was employed at 21.1 T, with *ca.* 42 kHz and *ca.* 80 kHz $\pi/2$ pulses for ^{27}Al and ^{71}Ga experiments, respectively. Further experimental details can be found in Appendix C (Tables C1 and C2). The TPPM decoupling scheme[24] was employed in the acquisition of all SSNMR spectra. Analytical simulations of all spectra were carried out using the WSolids Simulation package,[25] and NUTS (Acorn NMR) was used for all spectral processing. EFG shield[26] was employed to calculate EFG and NS tensor parameters using the formulae given in Table 4.1.

Ab initio calculations were performed using Gaussian 03[27] operating on a dual-733 MHz Pentium III Dell Precision 420 workstation, a dual-2.0 GHz Xenon Dell Precision 650 workstation, or the Shared Hierarchical Academic Research Computing Network (SHARCNET). The restricted Hartree-Fock (RHF) and hybrid density functional (B3LYP)[16,20,28] methodologies were used, with the (6-311G**) and (6-31G**) basis sets employed on all Al, Ga and N atoms. The aug-cc-pVDZ-6-311g basis set was employed on the Cl atom of $Al(guan)_2Cl$. The (3-21G**) basis set was used on all other atoms present in the molecules in an effort to reduce computational expense, and protons were placed in idealized positions based on known literature values. Predicted isotropic chemical shifts were determined using $\delta = \sigma_{ref} - \sigma_{sample}$ and are given with respect to $Al(H_2O)_6^{3+}$ ($\delta_{iso} = 0.0$ ppm); the isotropic shielding of the cation was calculated with each method and basis set employed.

4.3 Results and Discussion

4.3.1. ^{27}Al and ^{71}Ga Solid-state NMR Spectroscopy

The compounds studied in this work comprise an interesting series of structural motifs arising from coordination of guanidinate ligands, with various metal coordination environments and coordinating ligands. It is well known that ^{27}Al NMR can be used to differentiate between four-, five- and six-coordinate aluminum environments based on chemical shifts; however, chemical shift differentiation between different aluminum compounds containing the same number of coordinating ligands is more difficult. Such compounds, though superficially similar in symmetry and coordination number, have drastically different CS and EFG tensor parameters, due to the nature of the coordinating ligands. In this section, we describe the use of ^{27}Al and ^{71}Ga SSNMR experiments for the extraction of CS and EFG tensor parameters, as well as the first principles calculation of the NMR interaction tensor components and their orientation in the molecular frames.

In many instances, determination of accurate CS and EFG tensor parameters from the central transition second-order quadrupolar NMR patterns can be challenging. The chemical shielding anisotropy (CSA) and quadrupolar interaction (QI) manifest themselves in very distinct manners in such patterns, depending upon their relative magnitude, as well as the relative orientation of their interaction tensors.[29,30] The tensor orientations with respect to the molecular frames are only experimentally obtainable from NMR experiments on single crystals or oriented samples; fortunately, these orientations can often be inferred from local symmetry and structure, and predicted with great accuracy by theoretical calculations.

For microcrystalline powder samples, several techniques are commonly employed to distinguish between the contributions of the CSA and QI to the central transition spectrum. In this work, magic-angle spinning (MAS) NMR spectroscopy was employed in tandem with standard Hahn-echo NMR experiments on stationary samples (i.e., static NMR experiments). By rapidly spinning the sample about an axis oriented at 54.74° with respect to the static magnetic field, it is possible to average the effects of CSA, provided that the spinning rate, ν_{rot} (in Hz), is greater than the span, $\Omega = \delta_{11} - \delta_{33}$ (in Hz), of the pattern. Since MAS only partially averages the orientation dependence of the second-order quadrupolar interaction, clear discontinuities and shoulders are observed in the MAS NMR pattern which can easily be simulated to yield the quadrupolar parameters, C_Q and η_Q, as well as the isotropic chemical shift, δ_{iso}. In practice, for MAS NMR of half-integer quadrupoles, it is only necessary to spin fast enough to ensure that the spinning sidebands are well separated from the isotropic pattern, in order to ensure that the positions of the discontinuities and shoulders can be determined with accuracy. The anisotropic CS tensor parameters, Ω and κ, and the Euler angles which describe the relative orientation of the EFG and CS tensors can then be determined from spectra obtained under static conditions. In this section, the ^{27}Al SSNMR spectra of $Al(guan)_3$, $Al(guan)_2NMe_2$, and $Al(guan)_2Cl$, as well as the ^{71}Ga SSNMR spectrum of $Ga(guan)_3$ are presented, and their NMR interaction tensor parameters discussed in the context of molecular systems that have been similarly characterized in previous studies. A summary of the NMR parameters is presented in Table 4.1.

Table 4.1. Experimental and theoretical ^{27}Al and ^{71}Ga EFG and CS tensor parameters.[a]

	C_Q[b] (MHz)	η_Q[c]	δ_{iso}[d] (ppm)	Ω[e] (ppm)	κ[f]	α[g] (°)	β (°)	γ (°)
Al(guan)$_3$	**3.3(2)**	**0.00(2)**	**15.7(1)**	**19(7)**	**-0.6 (1)**	**50(5)**	**90(2)**	**170(10)**
RHF / 631G**	3.8	0.01	-1.0	15	-0.88	114	88	3
RHF / 6-311G**	2.7	0.03	-9.8	15	-0.82	81	87	3
B3LYP / 6-31G**	2.9	0.03	46.5	12	-0.56	144	87	8
B3LYP / 6-311G**	2.4	0.04	60.1	14	-0.71	45	78	178
Ga(guan)$_3$	**8.6(2)**	**0.02(2)**	**17.5(1)**	**77(3)**	**-0.95 (10)**	**105(2)**	**90(2)**	**0(2)**
RHF / 6-31G**	-16.8	0.01		64	-0.63	28	83	187
RHF / 6-311G**	5.5	0.06		61	-0.91	92	90	178
B3LYP / 6-31G**	-20.7	0.01		69	-0.60	31	83	188
B3LYP / 6-311G**	4.1	0.09		59	-0.81	106	90	176
Al(guan)$_2$Cl	**7.5(2)**	**0.10(2)**	**58.5(1)**	**85(10)**	**-0.75(10)**	**42(10)**	**73(10)**	**139(10)**
RHF / 6-31G**	-6.8	0.24	36.9	56	-0.94	179	78	49
RHF / 6-311G**	-7.2	0.10	34.4	72	-0.88	144	84	42
B3LYP / 6-31G**	-5.8	0.10	90.7	63	-0.82	48	88	137
B3LYP / 6-311G**	-6.7	0.14	110.9	88	-0.69	64	88	144
Al(guan)$_2$NMe$_2$	**14.3(5)**	**0.45(6)**	**75(10)**	**190(30)**	**0.25(15)**	**40(15)**	**0(3)**	**300(15)**
RHF / 6-31G**	-9.9	0.65	37.1	80	-0.03	32	1	284
RHF / 6-311G**	-11.3	0.52	35.7	103	-0.07	49	2	276
B3LYP / 6-31G**	-8.9	0.50	92.0	84	-0.06	39	2	284
B3LYP / 6-311G**	-10.1	0.50	109.4	111	-0.08	60	3	274

[a] Experimental values are given in boldface. Values in parentheses denote the uncertainty in the last digit. The principal components of the chemical shift tensor are defined as $\delta_{11} \geq \delta_{22} \geq \delta_{33}$, where δ_{11} and δ_{33} are oriented along the directions of lowest and highest shielding, respectively. The principal components of the EFG shielding tensor are defined as $|V_{11}| \leq |V_{22}| \leq |V_{33}|$

[b] $C_Q = (eQV_{33}/h)$ where $Q(^{27}Al) = 14.660$ fm^2, $Q(^{71}Ga) = 10.700$ fm^2, $e = 1.602176487 \times 10^{-19}$ C, $h = 6.62606896 \times 10^{-34}$ Js.

[c] $\eta_Q = (V_{11} - V_{22}) / V_{33}$

[d] $\delta_{iso} = (\delta_{11} + \delta_{22} + \delta_{33})/3$. Values are with respect to $Al(NO_3)_3 \cdot 9H_2O$ ($\delta_{iso} = 0.0$ ppm) or $Ga(NO_3)_3 \cdot xH_2O$ ($\delta_{iso} = 0.0$ ppm). Theoretical values are with respect to the aluminum hexahydrate ion and calculated using $\delta_{iso} = \sigma_{ref} - \sigma_{iso}$.

[e] $\Omega = (\delta_{11} - \delta_{33})$. Based upon simulations of static spectra.

[f] $\kappa = 3(\delta_{22} - \delta_{iso})/\Omega$, $-1.0 \leq \kappa \leq 1.0$. Based upon simulations of static spectra.

[g] The convention employed for Euler angle determination is summarized elsewhere.[26]

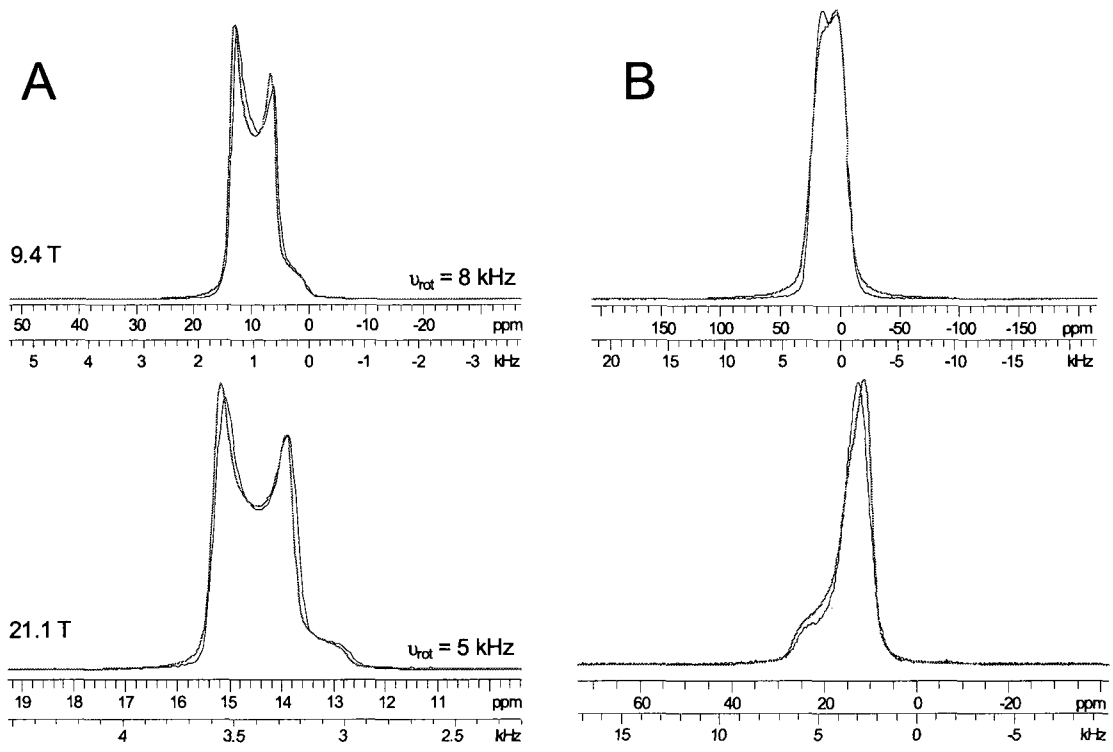

Figure 4.1: (A) ^{27}Al MAS and (B) ^{27}Al static SSNMR spectra of Al(guan)$_3$ acquired at 9.4 T (top) and 21.1 T (bottom), with analytical simulations.

The ^{27}Al MAS and static NMR spectra of Al(guan)$_3$ acquired at 9.4 T and 21.1 T are shown in Figure 4.1. The aluminum centre is in a six-coordinate environment where the three bidentate ligands give rise to a threefold rotational axis. All four spectra indicate that a single Al site is present. Simulations of the MAS NMR spectra acquired at both fields yield C_Q = 3.3 MHz and η_Q = 0.0. The small C_Q is typical of aluminum complexes with a relatively undistorted six-coordinate environment, and reflects the high degree of spherical symmetry in the electronic ground state of the molecule. The η_Q indicates that V_{33} is the unique component of the axially symmetric EFG tensor (i.e., V_{11} = V_{22}). Analysis of the CS tensor parameters yield Ω = 19 ppm and κ = -0.6, which indicates that δ_{11} is the distinct component of the CS tensor. Principal components of the

EFG and CS tensors can point any direction with respect to the molecular frame; however, their directions will be governed by local symmetry and structure. In cases of symmetry higher than C_1, or even in instances of high "pseudo-symmetry", the orientations of the principal components are constrained in or directed by symmetry elements. Consequently, it is likely that one of the unique/distinct principal components of both tensors is aligned along or near the threefold rotational axis. The Euler angles are consistent with these predictions; in particular, the Euler angle $\beta = 90°$ indicates the proximity of the V_{33} and δ_{11} components.

Previous studies have also examined six-coordinate aluminum centres via ^{27}Al SSNMR, including $Al(acac)_3$, $Al(trop)_3$ and $Al(TMHD)_3$,[13] where acac = acetylacetonate, trop = tropolonato, and TMHD = 2,2,6,6-tetramethyl-3,5-heptanedione (see Table 4.2). Though the aluminum sites in each of these compounds are coordinated by six oxygen atoms (rather than six nitrogens, as is the case here), the EFG tensor parameters of these systems and $Al(guan)_3$ are similar, suggesting that the coordination number may be of greater importance to the magnitude of the C_Q than the nature of the coordinating ligand. The C_Q of $Al(guan)_3$ falls between those of $Al(acac)_3$, $Al(TMHD)_3$ and $Al(trop)_3$ (C_Q = 3.03, 3.23 and 4.43 MHz, respectively), indicating that the aluminum centre has a similar local environment to these species. The crystal structures of $Al(acac)_3$ and $Al(trop)_3$ are known, and possess distorted octahedral environments; $Al(TMHD)_3$, whose structure is unknown, is undoubtedly in this category as well. Since $Al(guan)_3$ possesses a C_3 rotational axis, the η_Q is equal to zero. The values of η_Q for $Al(acac)_3$, $Al(TMHD)_3$ and $Al(trop)_3$ are all close to (but not exactly) zero, since they possess pseudo-threefold

rotational axes; based on these symmetries, the V_{33} in each case is predicted to be oriented along or near these axes.

Table 4.2. ^{27}Al EFG Parameters of previously reported compounds

Compound	C_Q (MHz)	η_Q	Coord.[c]	ref.
$Al(acac)_3$	3.03	0.15	6	13
$Al(trop)_3$	4.43	0.08	6	13
$Al(TMHD)_3$	3.23	0.10	6	13
$[Me_2\text{-}Al(\mu\text{-}OTHF)]_2$	19.9	0.98	5	16
$[Et_2\text{-}Al(\mu\text{-}OTHF)]_2$	19.6	0.97	5	16
AlNcCl[a]	5.4 - 9.8	0.10 - 0.50	5	17
$AlPc(SPh)_4Cl$[a]	5.4 - 10.0	0.10 - 0.50	5	17
AlPcCl[a]	5.4 - 9.8	0.10 - 0.50	5	17
$Al(CH_3)(7\text{-azain})_2(7\text{-azain-H})$	13.75	0.44	4	14
$Al(7\text{-azain})_3(7\text{-azain-H})$	3.65	1.0	4	14
$Al(7\text{-az})(7\text{-azH})(OCH(CF_3)_2)_2$	1.30	1.0	4	14
$AlMes_3$	48.2	0.00	3	16
$Al(NTMS_2)_3$	36.3	0.00	3	16
$AlMe_3$[b]	48.25	0.0	3	16
$AlCl_3$[b]	28.29	0.0	3	16

[a] Multiple aluminum sites were reported, hence a range of EFG tensor parameters are reported.
[b] Based on theoretical calculations.
[c] Denotes the aluminum coordination number.

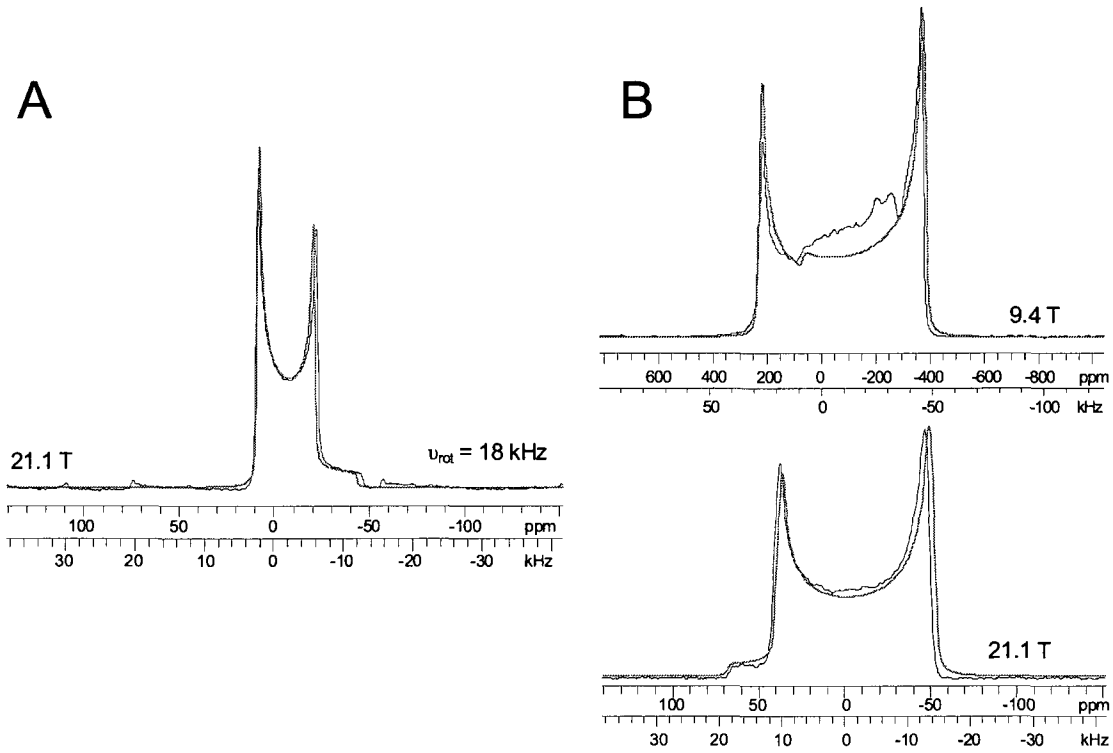

Figure 4.2: (A) ^{71}Ga MAS SSNMR spectrum of $Ga(guan)_3$ acquired at 21.1 T. (B) ^{71}Ga static SSNMR spectra of $Ga(guan)_3$ acquired at 9.4 T (top) and 21.1 T (bottom), with analytical simulations.

Figure 4.2 shows the static ^{71}Ga SSNMR spectra of $Ga(guan)_3$ acquired at 9.4 T and 21.1 T, and the ^{71}Ga 18 kHz MAS SSNMR spectrum acquired at 21.1 T. As with $Al(guan)_3$, the metal centre of $Ga(guan)_3$ is in a six-coordinate environment and has C_3 symmetry. The three ^{71}Ga SSNMR spectra indicate that a single Ga site is present. At first sight, the spectrum acquired at 9.4 T using a 90-180 echo sequence appears to indicate that an impurity may be present, due to the distortion or "bump" in the centre of the CT pattern at *ca.* -227 ppm. However, no distortions are observed in either the MAS or static powder patterns acquired using a 90-90 echo sequence at 21.1 T (we note that the 9.4 T spectrum was obtained first), so we discount this as a possibility. It is possible

that the "bump" in the 9.4 T spectrum is an artefact arising from non-uniform or incomplete excitation of the static pattern (possibly resulting from an imperfect refocusing π-pulse), or non-uniform nutation of the magnetization corresponding to crystallites with different orientations.[31]

The static ^{71}Ga powder pattern of Ga(guan)$_3$ is clearly much broader (*ca.* 80 kHz broad at 9.4 T, and *ca.* 34 kHz broad at 21.1 T) than the ^{27}Al SSNMR spectrum of its aluminum counterpart (*ca.* 5 kHz broad at 9.4 T, and *ca.* 6 kHz broad at 21.1T). This is due to the higher C_Q (8.5 MHz) of ^{71}Ga, which results from the much larger V_{33} value in the Ga compound (V_{33} = -0.342) than in the Al compound (V_{33} = -0.095). The V_{33} is smaller in the latter since the Al centre is in an environment of higher spherical symmetry: all six Al-N bonds are 2.024 Å, whereas the gallium species has three Ga-N bonds which are 2.084 Å, and three which are 2.096 Å. The ^{71}Ga pattern is also much broader because of its spin (I = 3/2); the CT patterns of spin-3/2 nuclides are considerably broader than those of spin-5/2 nuclei, as the breadth of a second-order quadrupolar powder pattern is given by:[8]

$$A = \frac{C_Q^2}{\nu_0} \cdot C_I \,, \quad \text{where } \nu_z = \frac{\gamma B_0}{2\pi}$$

where C_I is a scaling factor, which is 3/64 for spin-3/2 nuclei and 9/800 for spin-5/2 nuclei. As in the case of the Al(guan)$_3$, the value of η_Q for Ga(guan)$_3$, η_Q = 0.02, indicates that the EFG tensor is of high axial symmetry, and that V_{33} is the unique component. The gallium CSA in Ga(guan)$_3$ is significantly larger than that of the Al

species (Ω = 77 and 19 ppm, respectively). Moving down a group of the periodic table, the valence orbitals of the nuclei become larger and more polarizable. Since the chemical shift is dependent upon the circulation of electrons within the ground state molecular orbitals (MO's), and symmetry-allowed magnetically induced mixing of occupied and virtual MO's which are close in energy, it is generally observed that the chemical shift range (and hence, the magnitude of the CSA) of a particular nucleus increases as one moves from the top of a group to the bottom.[32] Consequently, the observation of the larger gallium CSA is unsurprising, given the structural similarity of these systems. The skew (κ = -0.95) indicates a highly axially symmetric gallium CS tensor; this, combined with the Euler angles, strongly suggest co-alignment of the V_{33} and δ_{11} components.

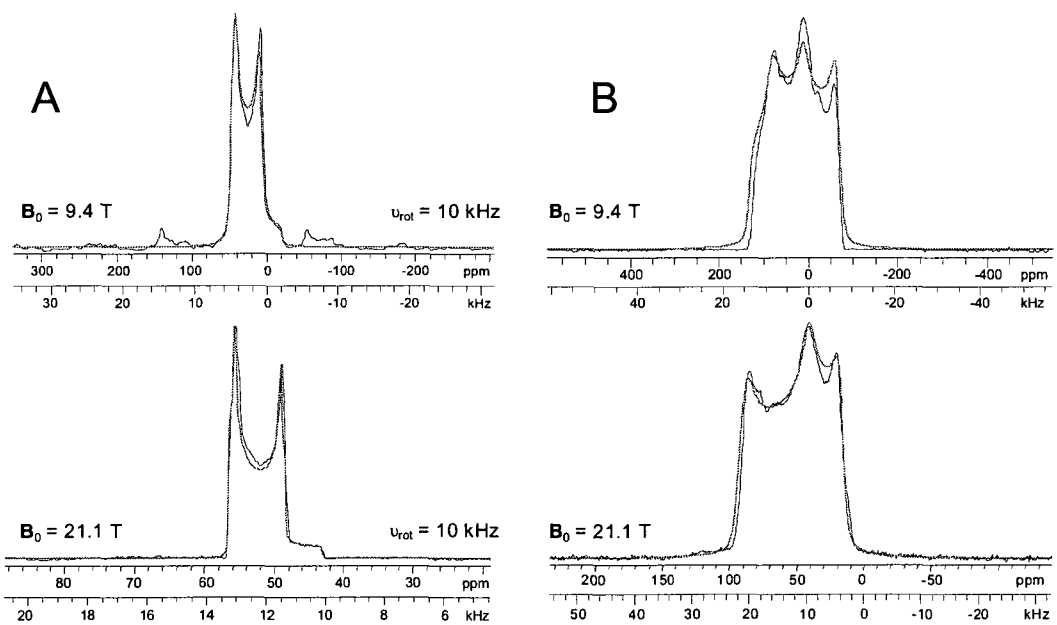

Figure 4.3: (A) ^{27}Al MAS and (B) ^{27}Al static SSNMR spectra of Al(guan)$_2$Cl acquired at 9.4 T (top) and 21.1 T (bottom), with analytical simulations.

Al(guan)$_2$Cl has a single, five-coordinate aluminum site, and its MAS and static

^{27}Al NMR spectra acquired at 21.1 T and 9.4 T are shown in Figure 4.3. Again, the spectra might seem to indicate that an impurity is present, as there is a slight "bump" on the low-frequency side of the high-frequency discontinuity of the MAS spectrum acquired at 21.1 T, and a noticeable "peak" at *ca.* -35 ppm in the static spectrum acquired at 9.4 T. Simulations of the MAS NMR powder patterns yield a C_Q of 7.5 MHz, which is greater than that of the six-coordinate Al(guan)$_3$, but similar to values reported for a series of aluminum dyes with an AlN_4Cl environment.[17] The $\eta_Q = 0.1$, which indicates a high degree of axial symmetry for the EFG tensor; however, V_{11} and V_{22} are slightly different from one another. Simulations of the static ^{27}Al SSNMR spectra yield $\Omega = 85$ ppm and $\kappa = -0.75$. The span is significantly larger than that of Al(guan)$_3$, but the skew is similar. The large C_Q in Al(guan)$_2$Cl with respect to that in Al(guan)$_3$ largely stems from the non-spherical environment in the former. The Al(guan)$_2$Cl has a pseudo two-fold rotational axis containing the lone Al-Cl bond, along which V_{33} is likely directed. The non-zero η_Q value is consistent with the two-fold rotational axis as well. The $\kappa = -0.75$ identifies δ_{11} as the distinct component of the CS tensor, which might suggest that it is oriented along or near the two-fold rotational axis; however, the Euler angles indicate otherwise, placing V_{33} and δ_{22} in close proximity. This will be discussed further in the computational section below.

Figure 4.4 depicts the ^{27}Al NMR spectrum of Al(guan)$_2$NMe$_2$, another five-coordinate aluminum species, acquired at 9.4 T (unfortunately, no spectra could be acquired at 21.1 T due to decomposition of the sample in transit from Windsor to Ottawa). The molecular structure is similar to that of Al(guan)$_2$Cl, with a pseudo-twofold

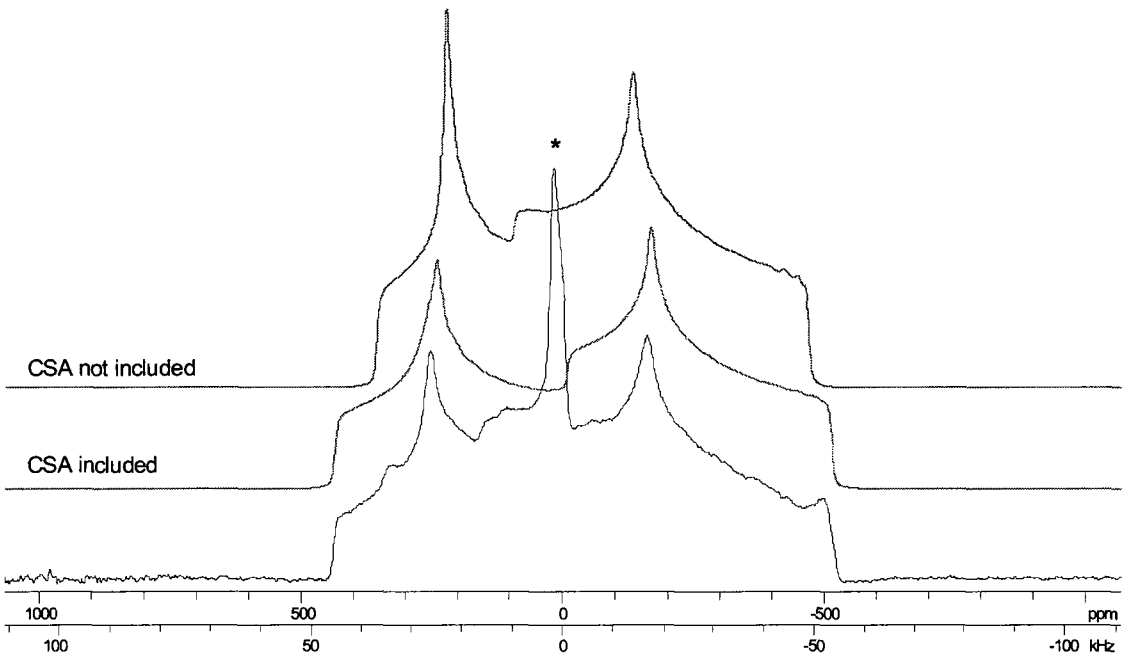

Figure 4.4: Bottom trace: ^{27}Al static SSNMR spectrum of Al(guan)$_2$NMe$_2$ acquired at 9.4 T. Middle trace: Analytical simulation including CSA. Top Trace: Analytical simulation without CSA included. Note: * denotes impurity.

rotational axis directed along the Al-NMe$_2$ bond. A notable feature of the static ^{27}Al SSNMR spectrum is the sharp, intense peak at *ca.* 0 ppm, which indicates the presence of an impurity in this case. Also notable is the breadth of the powder pattern, *ca.* 100 kHz, which is significantly greater than any of the previously discussed aluminum compounds. Analytical simulation of the spectrum yields C_Q = 14.3 MHz and η_Q = 0.45; however, due to the breadth of the static spectrum, an MAS experiment could not be employed to refine these EFG tensor parameters, since there is considerable overlap between the isotropic pattern and the spinning sidebands (data not shown). The large quadrupolar coupling constant indicates that the ground state electronic environment at the aluminum site is of very reduced spherical symmetry compared to that of Al(guan)$_2$Cl, and the value of η_Q indicates that all three tensor parameters are distinct from one another. CS tensor

parameters of Ω = 190 ppm and κ = 0.25 were obtained from simulation of the 9.4 T spectrum; the lack of static spectra at two fields casts some doubt on the size of this span, since it would be significantly larger than the largest known ^{27}Al span measured by solid-state NMR to date, Ω = 120 ppm, observed for a five-coordinate AlNcCl species.[17] Coupled with the absence of ultra-high field data, the impurity peak renders increasingly accurate determination of CS tensor parameters difficult; nonetheless, a relatively accurate measurement of C_Q has been made, since the pattern is dominated by the quadrupolar interaction (Figure 4.4).

It is clear from this study of molecular Al-species and the work of others (on both molecular and periodic solids) that six-coordinate (and four-coordinate) metal environments must have smaller C_Q values than five-coordinate environments, owing largely to the high spherical symmetry of the former. But what of comparing the variety of five- and three- coordinate environments with varying symmetries? Previously, our group acquired ultra-wideline (UW) ^{27}Al SSNMR spectra of three- and five-coordinate aluminum compounds.[16] The five-coordinate species, $[Me_2\text{-}Al(\mu\text{-}OTHF)]_2$ and $[Et_2\text{-}Al(\mu\text{-}OTHF)]_2$, have very large quadrupolar coupling constants of 19.9 MHz and 19.6 MHz, respectively (Table 4.2), dwarfing those of $Al(guan)_2Cl$ and $Al(guan)_2NMe_2$. The Al environments in these systems feature coordination of the Al by three O atoms (in a plane) and two C atoms (above and below the plane, at ca. 120° from the outer O atoms).[16] On the other hand, Mroué et al. have reported values of C_Q ranging between 5.4 and 10 MHz for five-coordinate Al centres in phthalocyanine dyes (Table 4.2), where the Al atoms are coordinated equatorially by four N atoms and axially by a single Cl

atom.[17] Of these varying structural motifs, it would seem that the dyes have the least spherical symmetry about the Al atoms; yet, it is clearly the nature of the surrounding ligands and their bonding to the Al centre that determines the characteristics of the ^{27}Al EFG tensors. Therefore, one must be careful in making generalizations about decreasing geometrical spherical symmetry and corresponding increases in C_Q for systems having the same coordination number, but dissimilar atoms (and arrangements of atoms) in the first coordination sphere.

In comparing two systems of superficially similar geometry like $Al(guan)_2NMe_2$ and $Al(guan)_2Cl$, it is possible to make some generalizations about the spherical symmetry of the ground electronic state at the Al site. For instance, in our group's investigation of three-coordinate Al environments, it was observed that two compounds with similar planar threefold geometries in the first coordination sphere, $AlMes_3$ and $Al(NTMS_2)_3$ (Mes = mesityl, NTMS = bis(trimethylsilyl)amino), that the values of C_Q are very different, 48.2 and 36.3 MHz, respectively (Table 4.2).[16] Similarly, C_Q values of 48.75 and 28.29 MHz have been calculated for trigonal planar $AlMe_3$ and $AlCl_3$ molecules, respectively, in the gas phase.[33,34] Detailed RHF and B3LYP calculations,[16] as well as a recently published NLMO analysis of the EFG tensor contributions,[35] show that a complex interplay of contributions to the EFG tensor from σ-bonding, π-bonding (in the case of Cl and N atoms) and Al core electrons gives rise to different magnitudes of V_{33} along the threefold rotational axes of these molecules. It was found that the V_{33} decreases as the bond length increases, and as there is back donation from the π-orbitals of the ligand into the empty $3p$ AO of the aluminum atom. In comparing $Al(guan)_2NMe_2$ and

$Al(guan)_2Cl$, something similar is clearly at work, with a decrease in C_Q for the latter compound, where the longest covalent bond and highest degree of back-bonding. A detailed theoretical treatment of these systems is currently underway.

Further, the presence of Al-C bonds is seen to result in significant increases in the $C_Q(^{27}Al)$ with respect to systems with just Al-O, Al-N and/or Al-Cl bonds.[21,22] For instance, one study, which reported ^{27}Al NMR data for distorted tetrahedral aluminum azaindole species, found that C_Q = 13.75 MHz for $Al(CH_3)(7\text{-azain})_2(7\text{-azain-H})$. Given that the local geometry appears to be spherically symmetric, this C_Q is quite large, especially when compared to similar complexes with AlN_4 and AlN_4O_2 environments, which exhibited C_Q's of 3.65 MHz and 1.30 MHz respectively.[14]

Hence, it is clearly not simple geometric spherical symmetry that influences the character of the EFG tensor; rather, it is the spherical symmetry of the electronic ground state, which is depend upon the nature of the metal, surrounding ligands and modes of bonding.

4.3.2 Ab initio Calculations of Nuclear Shielding and Electric Field Gradient Tensor Parameters

Ab initio calculations aid in correlating the NMR parameters observed experimentally with molecular structure. To this end, the Gaussian 03 program suite was employed to investigate the origins of the NMR interaction tensors observed in the guanidinate complexes. Select methods and basis sets were chosen based on previous studies of aluminum-containing materials by our research group.[16]

The theoretically predicted ^{27}Al NS and EFG tensor parameters generally agree

well with those obtained experimentally (Table 4.1). Of all the method/basis set combinations, RHF/6-311G** yielded the values that most closely match those observed experimentally. The B3LYP method is the best predictor of η_Q, with both basis sets providing values that match reasonably well with experiment. The isotropic shifts are consistently underestimated by RHF and overestimated by B3LYP, and the span is generally best predicted by B3LYP/6-311G**. The skew values generally match very well with experimental data, with the 6-311G** basis set providing the best results. The theoretically predicted ^{71}Ga NS and EFG tensor parameters of Ga(guan)$_3$ are generally not as accurate as those of the aluminum compounds, though still provide a reasonable estimate of what to expect experimentally.

In surveying the summary of the calculations presented in Table 4.1, there are some general features that must be discussed. Regardless of the method/basis set employed, the theoretically predicted EFG and NS tensor parameters of Al(guan)$_3$ and Al(guan)$_2$Cl agree well with those obtained experimentally. Though the sign of the C_Q cannot be determined experimentally, the calculations predict a positive C_Q for the former, but a negative value for the latter. The positive V_{33} in Al(guan)$_3$ is consistent with its orientation into a region of low electron density (i.e., along the threefold rotational axis), and the negative V_{33} in Al(guan)$_2$Cl is consistent with its orientation along the Al-Cl bond into a region of high electron density (see also the discussion of NS tensor orientations below).[35] In the case of Ga(guan)$_3$, V_{33} is aligned in a similar manner to that of Al(guan)$_3$, and hence, a positive C_Q is expected. Of the theoretically predicted C_Q's, only those carried out with the 6-311G** basis yet yield a C_Q with a positive sign.

This result, combined with the generally poor correlation of predicted and experimental parameters, indicates that the 6-31G** basis set is unsuitable for use in this instance. Calculations with larger all-electron basis sets on Ga are currently underway. Finally, the tensor parameters predicted for $Al(guan)_2NMe_2$, are not in very good agreement with experiment. The EFG tensor parameters are calculated reasonably well (notably, the values of η_Q), but the spans are consistently predicted to be about half the magnitude of the experimentally measured values. Given the reliability of calculated NMR interaction tensor parameters for the first three rows of the periodic table, these results cast further doubt upon the veracity of the experimentally determined parameters. This reiterates the need for reacquisition of experimental data at 9.4 T, and acquisition of new spectra at 21.1 T, for a freshly synthesized batch of $Al(guan)_2NMe_2$.

4.3.3 Nuclear Shielding (NS) and Electric Field Gradient (EFG) Tensor Orientations

Prediction of the NS and EFG tensor orientations within the molecular frame via first principles calculations aids in connecting the molecular geometry with the SSNMR powder pattern and related parameters. In an effort to gain insight into the origins of the NMR interactions responsible for the characteristic appearance of each powder pattern acquired in this work, these tensor orientations have been calculated and examined (Figure 4.5).

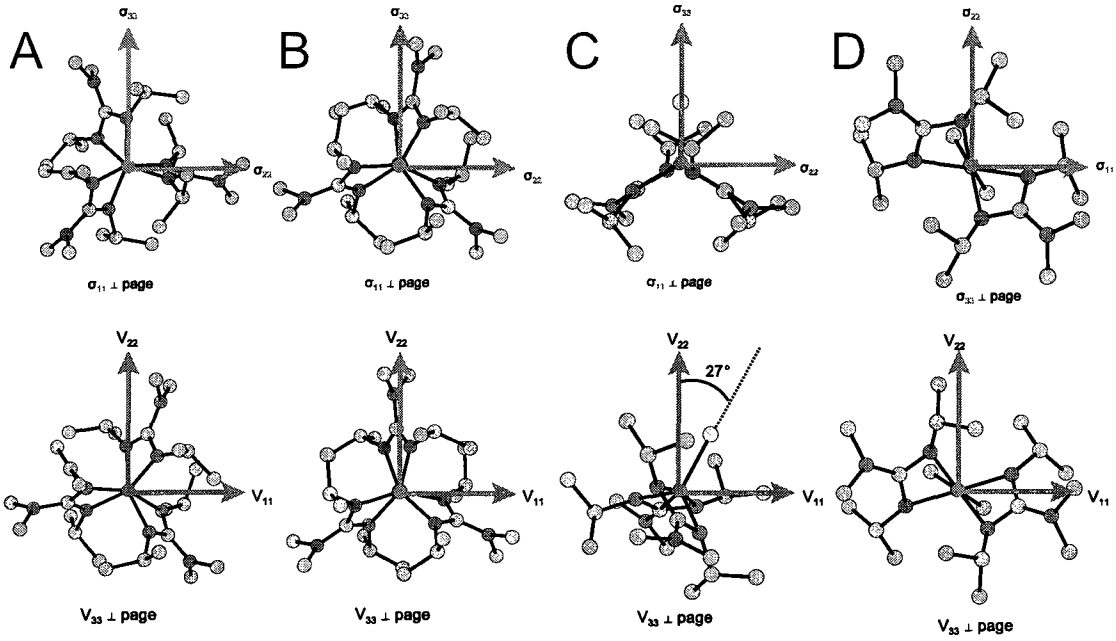

Figure 4.5. NS (top) and EFG (bottom) tensor orientations of (A) $Al(guan)_3$, (B) $Ga(guan)_3$, (C) $Al(guan)_2Cl$ and (D) $Al(guan)_2NMe_2$.

For $Al(guan)_3$, both the ^{27}Al NS and EFG tensors are oriented such that the unique components (σ_{11} and V_{33}, respectively) are aligned along a threefold rotation axis, as predicted from our experimental results. Similarly, $Ga(guan)_3$, which has a similar coordination geometry to $Al(guan)_3$, has σ_{11} and V_{33} (the unique components of its NS and EFG tensors) directed along its threefold rotation axis. The precise orientations of V_{11} and V_{22} are not of great importance, since $\eta_Q = 0$ and the EFG tensor is axially symmetric about the threefold axis. The distinct components of the NS and EFG tensors of $Al(guan)_2Cl$ are aligned in different directions: σ_{33} is aligned in the direction of the Cl ligand, as predicted, which is along the pseudo two-fold rotation axis of the molecule. V_{33} is aligned perpendicular to the Al-Cl bond, with V_{22} oriented at an angle of ca. 27° from the Al-Cl bond, which was unexpected; it was believed that V_{33} would be aligned

along the Al-Cl bond. For $Al(guan)_2NMe_2$, σ_{33} is the unique component of the NS tensor, and as predicted, is aligned along the Al-NMe_2 bond in a similar fashion to that in $Al(guan)_2Cl$. Interestingly, V_{33}, is also aligned along this direction, which is distinct from the case for $Al(guan)_2Cl$; clearly, the nature of the Al-NMe_2 and Al-Cl bonding in these complexes is very different. We are currently conducting an NLMO analysis of the molecular orbitals that contribute to the EFG tensors, so further discussion of this is beyond the scope of this study.

4.4 Conclusions

^{27}Al SSNMR spectroscopy has been successfully applied to determine the CS and EFG tensor parameters of $Al(guan)_3$, $Al(guan)_2Cl$, and $Al(guan)_2NMe_2$ (though further work is needed on this latter complex). The use of multiple field strengths in spectral acquisition, especially the ultra-high 900 MHz field, aids in significantly improving the accuracy of the experimentally determined EFG and CS tensor parameters. Though C_Q tends to increase with decreasing coordination number, we note that the nature of the ligands and their bonding in the first coordination sphere has a dramatic effect on the magnitude of the C_Q, as evidenced by comparison of $Al(guan)_2Cl$ and $Al(guan)_2NMe_2$. Hence, unless the ligands are very similar between metal centres, generalized statements relating coordination number to C_Q should be avoided. η_Q varies significantly mong the different systems, and is a powerful indicator of different symmetry elements (i.e., $\eta_Q = 0$ indicates a threefold rotational axis, and intermediate values of η_Q indicate the lack of rotational or pseudo-rotational axes). Though similar in structure to $Al(guan)_3$, slight

differences in bond lengths and atomic positions give rise to a much larger V_{33} in $Ga(guan)_3$, resulting in a larger C_Q than that of $Al(guan)_3$.

The span tends to increase with decreasing coordination number; however, before a definitive conclusion can be drawn, the ^{27}Al SSNMR spectrum of $Al(guan)_2NMe_2$ must be reacquired at multiple field strengths; the experimentally determined span of 190 ppm represents the largest reported from a ^{27}Al NMR experiment, casting doubt on our simulated parameters. $Ga(guan)_3$ has a much larger span than that of $Al(guan)_3$, owing to its larger, more polarizable orbitals and associated magnetic shielding effects.

Aside from the isotropic chemical shifts, the ^{27}Al EFG and CS tensor parameters are predicted with reasonable accuracy by *ab initio* calculations. For $Al(guan)_2NMe_2$, the prediction of a span consistent with those measured in analogous Al systems leads us to believe that our experimental data requires reacquisition and reexamination. Theoretically predicted ^{71}Ga tensor parameters are less successful, especially those calculated with the 6-31G** basis set, indicating that the use of larger basis sets is required.

This preliminary account demonstrates the utility of SSNMR of half-integer quadrupolar metal nuclides for investigating the relationships between structure, symmetry and anisotropic NMR parameters, especially for distinguishing between structural environments which seem superficially analogous. Future work in this area will include further study of other compounds in the main group guanidinate series, such as the four-coordinate $Al(guan)(NMe_2)_2$ and analogous gallium species.[1] Extending the current study to include transition metal guanidinates, we wish to conduct an

investigation of copper(I) guanidinate dimers,[36] which have copper sites in nearly linear, two-coordinate environments. We will apply the specialized acquisition techniques and hardware utilized in our first two exploratory papers describing ^{65}Cu ultra-wideline NMR of Cu(I) species in environments of low spherical symmetry.[37,38]

Bibliography

(1) Kenney, A. P.; Yap, G. P. A.; Richeson, D. S.; Barry, S. T. *Inorg. Chem.* 2005, 44, 2926-2933.

(2) Brazeau, A. L.; Wang, Z. H.; Rowley, C. N.; Barry, S. T. *Inorg. Chem.* 2006, 45, 2276-2281.

(3) Brazeau, A. L.; DiLabio, G. A.; Kreisel, K. A.; Monillas, W.; Yap, G. P. A.; Barry, S. T. *Dalton Trans.* 2007, 3297-3304.

(4) Dagorne, S.; Guzei, I. A.; Coles, M. P.; Jordan, R. F. *J. Am. Chem. Soc.* 2000, 122, 274-289.

(5) Duchateau, R.; Meetsma, A.; Teuben, J. H. *Chem. Commun.* 1996, 223-224.

(6) Barker, J.; Blacker, N. C.; Phillips, P. R.; Alcock, N. W.; Errington, W.; Wallbridge, M. G. H. *J. Chem. Soc.-Dalton Trans.* 1996, 431-437.

(7) MacKenzie, K. J. D.; Smith, M. E. In *Multinuclear Solid-state NMR of Inorganic Materials*; Pergamon: New York, 2002; Vol. 6, pp 271-330.

(8) Kentgens, A. P. M. *Geoderma* 1997, 80, 271-306.

(9) Sato, R. K.; McMillan, P. F.; Dennison, P.; Dupree, R. *J. Phys. Chem.* 1991, 95, 4483-4489.

(10) Kinsey, R. A.; Kirkpatrick, R. J.; Hower, J.; Smith, K. A.; Oldfield, E. *Am. Miner.* 1985, 70, 537-548.

(11) Timken, H. K. C.; Oldfield, E. *J. Am. Chem. Soc.* 1987, 109, 7669-7673.

(12) Fyfe, C. A.; WongMoon, K. C.; Huang, Y. *Zeolites* 1996, 16, 50-55.

(13) Schurko, R. W.; Wasylishen, R. E.; Foerster, H. *J. Phys. Chem. A* 1998, 102, 9750-

9760.

(14) Ashenhurst, J.; Wu, G.; Wang, S. N. *J. Am. Chem. Soc.* 2000, 122, 2541-2547.

(15) Schurko, R. W.; Hung, I.; Macdonald, C. L. B.; Cowley, A. H. *J. Am. Chem. Soc.* 2002, 124, 13204-13214.

(16) Tang, J. A.; Masuda, J. D.; Boyle, T. J.; Schurko, R. W. *ChemPhysChem* 2006, 7, 117-130.

(17) Mroue, K. H.; Emwas, A. H. M.; Power, W. P. *Can. J. Chem.-Rev. Can. Chim.* 2010, 88, 111-123.

(18) Harris, R. K.; Becker, E. D.; De Menezes, S. M. C.; Goodfellow, R.; Granger, P. *Pure and Applied Chemistry* 2001, 73, 1795-1818.

(19) MacKenzie, K. J. D.; Smith, M. E. In *Multinuclear Solid-state NMR of Inorganic Materials*; Pergamon: New York, 2002; Vol. 6, pp 653-657.

(20) Massiot, D.; Farnan, I.; Gautier, N.; Trumeau, D.; Trokiner, A.; Coutures, J. P. *Solid State Nucl. Magn. Reson.* 1995, 4, 241-248.

(21) Bayense, C. R.; Kentgens, A. P. M.; Dehaan, J. W.; Vandeven, L. J. M.; Vanhooff, J. H. C. *J. Phys. Chem.* 1992, 96, 775-782.

(22) Merrouche, A.; Patarin, J.; Kessler, H.; Soulard, M.; Delmotte, L.; Guth, J. L.; Joly, J. F. *Zeolites* 1992, 12, 226-232.

(23) O'Dell, L. A.; Schurko, R. W. *Chem. Phys. Lett.* 2008, 464, 97-102.

(24) Bennett, A. E.; Rienstra, C. M.; Auger, M.; Lakshmi, K. V.; Griffin, R. G. *J. Chem. Phys.* 1995, 103, 6951-6958.

(25) Eichele, K.; Wasylishen, R. E., WSolids: Solid-State NMR Spectrum Simulation,

2001.

(26) Adiga, S.; Aebi, D.; Bryce, D. L. *Can. J. Chem.-Rev. Can. Chim.* 2007, 85, 496-505.

(27) Frisch, M. J.; Trucks, G. W.; Schlegel, H. B.; Scuseria, G. E.; Robb, M. A.; Cheeseman, J. R.; Montgomery, J., J. A.; Vreven, T.; Kudin, K. N.; Burant, J. C.; Millam, J. M.; Iyengar, S. S.; Tomasi, J.; Barone, V.; Mennucci, B.; Cossi, M.; Scalmani, G.; Rega, N.; Petersson, G. A.; Nakatsuji, H.; Hada, M.; Ehara, M.; Toyota, K.; Fukuda, R.; Hasegawa, J.; Ishida, M.; Nakajima, T.; Honda, Y.; Kitao, O.; Nakai, H.; Klene, M.; Li, X.; Knox, J. E.; Hratchian, H. P.; Cross, J. B.; Bakken, V.; Adamo, C.; Jaramillo, J.; Gomperts, R.; Stratmann, R. E.; Yazyev, O.; Austin, A. J.; Cammi, R.; Pomelli, C.; Ochterski, J. W.; Ayala, P. Y.; Morokuma, K.; Voth, G. A.; Salvador, P.; Dannenberg, J. J.; Zakrzewski, V. G.; Dapprich, S.; Daniels, A. D.; Strain, M. C.; Farkas, O.; Malick, D. K.; Rabuck, A. D.; Raghavachari, K.; Foresman, J. B.; Ortiz, J. V.; Cui, Q.; Baboul, A. G.; Clifford, S.; Cioslowski, J.; Stefanov, B. B.; Liu, G.; Liashenko, A.; Piskorz, P.; Komaromi, I.; Martin, R. L.; Fox, D. J.; Keith, T.; Al-Laham, M. A.; Peng, C. Y.; Nanayakkara, A.; Challacombe, M.; Gill, P. M. W.; Johnson, B.; Chen, W.; Wong, M. W.; Gonzalez, C.; Pople, J. A. G., Inc., Wallingford CT, 2004. *Gaussian, Inc., Wallingford CT, 2004.*

(28) Lipton, A. S.; Wright, T. A.; Bowman, M. K.; Reger, D. L.; Ellis, P. D. *J. Am. Chem. Soc.* 2002, 124, 5850-5860.

(29) Power, W. P.; Wasylishen, R. E.; Mooibroek, S.; Pettitt, B. A.; Danchura, W. *J. Phys. Chem.* 1990, 94, 591-598.

(30) Cheng, J. T.; Edwards, J. C.; Ellis, P. D. *J. Phys. Chem.* 1990, 94, 553-561.

(31) Samoson, A.; Lippmaa, E. *Phys. Rev. B* 1983, 28, 6567-6570.

(32) Jameson, C. J.; Mason, J. In *Multinuclear NMR*; Mason, J., Ed.; Plenum Press: New York, 1987.

(33) Dewar, M. J. S.; Patterso.Db; Simpson, W. I. *J. Am. Chem. Soc.* 1971, 93, 1030-&.

(34) Dewar, M. J. S.; Patterso.Db; Simpson, W. I. *J. Chem. Soc.-Dalton Trans.* 1973, 2381-2390.

(35) Autschbach, J.; Zheng, S.; Schurko, R. W. *Conc. Magn. Reson* 2010, In Press.

(36) Coyle, J. P.; Monillas, W. H.; Yap, G. P. A.; Barry, S. T. *Inorg. Chem.* 2008, 47, 683-689.

(37) Tang, J. A.; Ellis, B. D.; Warren, T. H.; Hanna, J. V.; Macdonald, C. L. B.; Schurko, R. W. *J. Am. Chem. Soc.* 2007, 129, 13049-13065.

(38) Lucier, B. E. G.; Tang, J. A.; Schurko, R. W.; Bowmaker, G. A.; Healy, P. C.; Hanna, J. V. *J. Phys. Chem. C* 2010, In Press, DOI: 10.1021/jp907477m.

Chapter 5

General Conclusions and Future Work

The WURST-CPMG pulse sequence was found to be effective for acquiring UW SSNMR spectra of a wide variety of nuclei, offering increased excitation bandwidths, and often reducing experimental times in comparison to conventional experiments. Pulses generated with optimal control theory also prove effective, though further investigation into their use is required. The next step is a detailed investigation of the effectiveness of pulses generated with OCT at acquiring UW spectra of a broad array of nuclei. Owing to their effectiveness at low rf pulse strengths, the acquisition of SSNMR spectra of low-γ nuclei (*e.g.*, $^{107/109}$Ag, ^{15}N, ^{57}Fe, etc.) is of particular interest. Development of a CPMG-type train of these pulses would also be an interesting endeavour, though certainly not a trivial one. It would also be of great interest to utilize optimal control theory in the context of a double-resonance cross-polarization experiment, in order to obtain simultaneous signal enhancement and broad banded excitation from CP and shaped pulses, respectively.

In Chapter 3, ^{207}Pb UW SSNMR was found to be a sensitive probe of local lead environments in a series of Pb(II) thiolates, with subtle differences in the lead coordination sphere resulting in significantly different CS tensor parameters. Further experimentation includes determination of the origin of the resonances observed in the ^{31}P SSNMR spectrum of $[(2,6\text{-}Me_2C_6H_3S)_2Pb]_3(dmpe)$, as well as the study of similar Pb (II) thiolates with ^{207}Pb SSNMR to allow for the eventual characterization of materials

derived from related complexes. It would also be of great interest to utilize the experimental techniques and lead CS tensor data to investigate structural motifs such as these in a variety of different Pb complexes and Pb-containing materials.

Chapter 4 reports the study of a series of guanidinate complexes with ^{27}Al and ^{71}Ga SSNMR. It was found that ^{27}Al and ^{71}Ga SSNMR could be readily employed to distinguish between the various guanidinate species, with small differences in coordination environments being reflected by large changes in quadrupolar parameters. Since the NMR tensor parameters vary widely between the guanidinate complexes, more of these molecules must be studied to fully explore the trends associated with changing the metal centre coordination environment. Particularly, examination of four coordinate aluminum guanidinate species would complete a series of four-, five-, and six-coordinate guanidinates, allowing for broader conclusions to be drawn. A similar investigation of a complete series of gallium and copper guanidinates with ^{71}Ga and $^{63/65}$Cu SSNMR, respectively, is also forthcoming.

It has been demonstrated herein that SSNMR is an extremely sensitive probe of local nuclear environments, as small variations in the coordination environment are reflected in changing EFG and CS tensor parameters. Furthermore, the WURST-CPMG pulse sequence, the CP/CPMG pulse sequence and pulses generated with OCT have all been shown to be effective methods for acquiring UW SSNMR spectra. It is hoped that this work inspires further research in the area of UW SSNMR, leading to further advancements in acquisition techniques and the study of a broader array of materials.

Appendix A

Supporting Information - New Methods for the Acquisition of Static CSA Patterns from Spin-1/2 Nuclides

A.1. Supporting Experimental Information

A.1.1. Experimental Parameters for SSNMR Experiments

Table A1. Experimental parameters for WURST-CPMG NMR experiments

	SnO	$Pb(OAc)_2$	$Hg(OAc)_2$	K_2PtCl_4
Number of transients per subspectrum	80	248	72	40
Number of subspectra	1	1	1	5
Experimental time (minutes)	2.7	28.9	1740	133.35
WURST sweep range (kHz)	2000	2000	2000	2000
Recycle delay (s)	2	7	1450	40
Number of Meiboom-Gill Loops	64	75	80	250
Acquisition points per echo	200	200	200	200
Spikelet Separation (kHz)	2.5	2	2.5	10
WURST pulse length (μs)	50	50	50	50
Proton decoupling power (kHz)	N/A	0.25	0.3	N/A
WURST pulse power (kHz)	30	47	28	67
Spectral width	500	400	500	2000

Table A2. Experimental parameters for ^{119}Sn CPMG NMR spectrum of SnO.

	SnO
Number of transients per subspectrum	80
Number of subspectra	10
Transmitter offset per piece (kHz)	45
Recycle delay (s)	2
Total experimental time (minutes)	26.7
Number of Meiboom-Gill Loops	64
Acquisition points per echo	200
Spikelet Separation (kHz)	2.5
pw90 (μs)	3.33
90° pulse power (kHz)	75
Spectral width (kHz)	500

Table A3. Experimental parameters for the ^{207}Pb CP/CPMG NMR spectrum of $Pb(OAc)_2 \cdot 3H_2O$

	$Pb(OAc)_2 \cdot 3H_2O$
Number of Subspectra	9
Scans per subspectrum	192
Trans. Offset per piece (kHz)	20
Recycle delay (s)	4
Number of Meiboom-Gill Loops	80
Acquisition points per echo	200
Spikelet Separation (kHz)	2
90° ^{1}H pulse power (kHz)	142
Decoupling power (kHz)	57
Hartmann-Hahn match (kHz)	48
Contact time (ms)	3
Spectral width	400

A.1.2. Experimental Parameters for SSNMR Experiments using pulses generated with optimal control theory.

Table A4. Experimental details for ^{119}Sn NMR spectra acquired with pulses generated using OCT

	15 kHz	50 kHz	150 kHz
Number of transients per spectrum	800	800	800
Recycle delay (s)	2	2	2
Total experimental time (minutes)	26.7	26.7	26.7
pw90 (μs)	50	50	50
Max. pulse power achieved (kHz)	15	50	115
Spectral width (kHz)	400	400	400
Dwell (μs)	2.5	2.5	2.5

A.1.3. Supplementary SSNMR Spectra

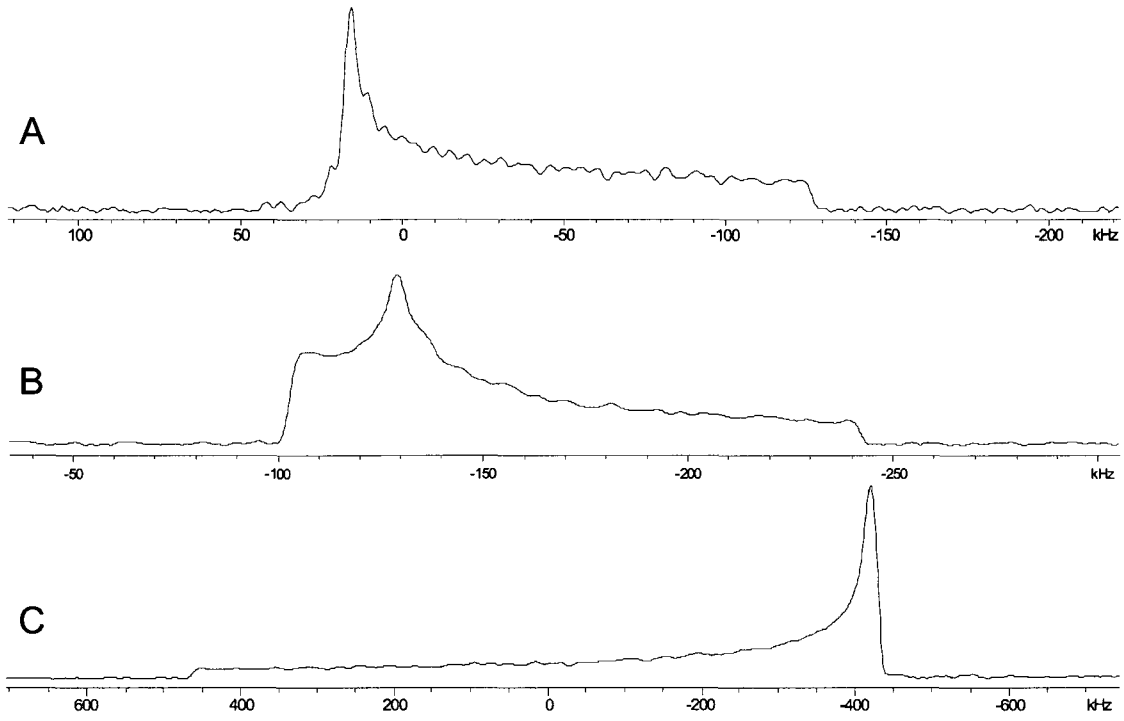

Figure A1. Echo spectra produced from Fourier transformation of the time-domain sum of the spin-echoes of WURST-CPMG experiments. Shown are (A) the ^{119}Sn NMR spectrum of SnO , (B) the ^{207}Pb NMR spectrum of $Pb(OAc)_2$ and (C) the ^{195}Pt NMR spectrum of K_2PtCl_4.

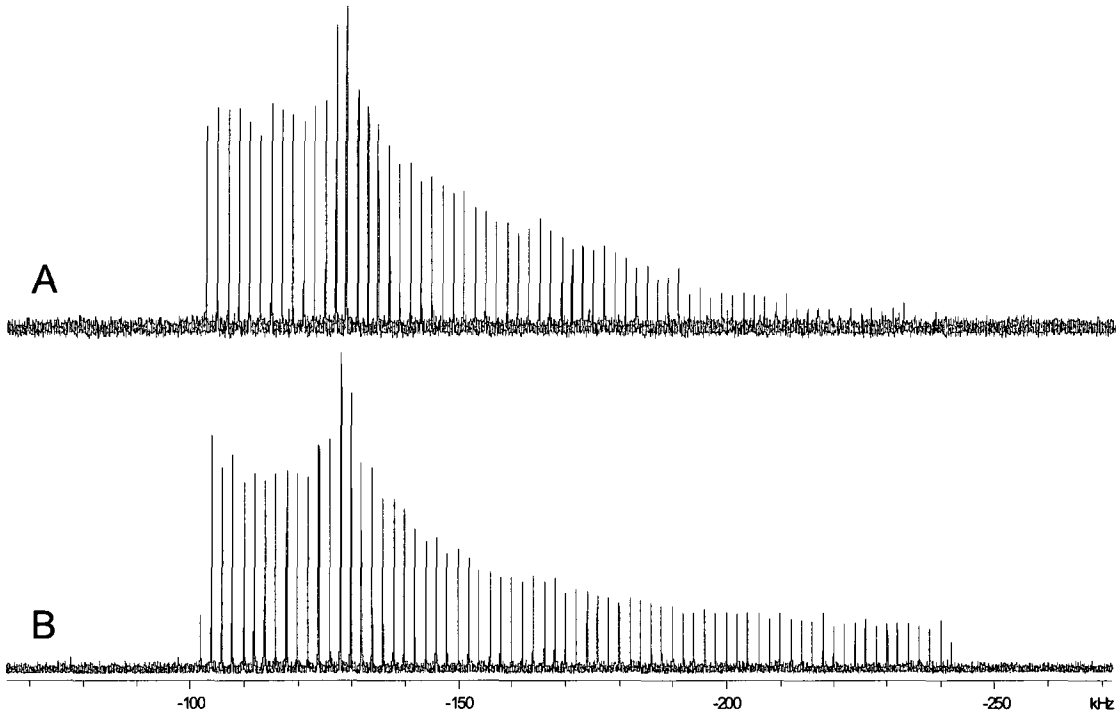

Figure A2. (A) ^{207}Pb CP/CPMG NMR spectrum of $Pb(OAc)_2 \cdot 3H_2O$ prior to recrystallization of the sample. Shown is the co-addition of 9 sub-spectra, each of which consist of 64 averaged transients. (B) ^{207}Pb WURST-CPMG NMR spectrum of $Pb(OAc)_2 \cdot 3H_2O$ prior to recrystallization of the sample. The spectrum consists of 198 averaged transients and was acquired in a single experiment. The large "lump" at the high-frequency end of the spectra is not present after recrystallization, indicating that the sample used initially was partially dehydrated.

A.1.4. Explanation for the estimated time required to acquire the ^{195}Pt CPMG SSNMR spectrum of K_2PtCl_4

When discussing the WURST-CPMG ^{195}Pt NMR spectrum of K_2PtCl_4, we estimated that it would take at least 9 hours to acquire the same spectrum with CPMG. This estimation was formulated by examining previous ^{195}Pt SSNMR studies carried out by our group,[1] in which the CP/CPMG experiment was employed. Spectra ca. 500 kHz broad required 13-18 sub-spectra; hence, many more sub-spectra would be required to acquire the spectrum of K_2PtCl_4 which is ca. 910 kHz broad. Though CPMG may have a greater excitation bandwidth than CP/CPMG, we assume at least 20 sub-spectra would be required, which would take ca. 9 hours if each sub-spectrum took 27 minutes to acquire, as they did for WURST-CPMG. In fact, this is likely a conservative estimate, as 16 sub-spectra were required to obtain the 160 kHz broad pattern of SnO, as mentioned previously in this report..

Bibliography

(1) Tang, J. A.; Kogut, E.; Norton, D.; Lough, A. J.; McGarvey, B. R.; Fekl, U.; Schurko, R. W. *J. Phys. Chem. B* 2009, *113*, 3298.

Appendix B

Supporting Information - ^{207}Pb SSNMR Investigations of Pb(II) Thiolates

B.1. Supporting Experimental information

B.1.1. Experimental Parameters for ^{207}Pb SSNMR Experiments

Table B1. CP/CPMG experimental parameters

	1	2	3	4
Number of subspectra	20	23	19	22
Scans per subspectrum	128	120	192	120
Trans. Offset per piece (kHz)	20	24	20	24
Recycle delay	45	30	20	30
Number of Meiboom-Gill Loops	204	163	101	163
Real points per loop	40	50	80	50
Dwell (μs)	2.5	2.5	2.5	2.5
Spikelet Separation (kHz)	10	8	5	8
Acq. Length	8192	8192	8192	8192
pw90 (μs)	1.8	1.98	1.8	1.98
pw180 (μs)	3.6	3.5	3.6	3.5
Ring-down Delays ($\tau_1 = \tau_2 = \tau_3 = \tau_4$)	40	40	40	40
Contact time (s)	0.021	0.015	0.011	0.014
aH dec	0.25	0.25	0.25	0.25
aH cp	0.35	0.35	0.35	0.35
aH	0.6	0.6	0.6	0.6
aX cp	0.25	0.18	0.25	0.18
aX	0.6	0.6	0.6	0.6
Spectral width (kHz)	400	400	400	400

Table B2. WURST-QCPMG experimental parameters.

	1	2	3	4
Number of transients	759	808	1664	2400
Experimental time (hours)	19	20.2	41.6	60
Offset (kHz)	1000	1000	1000	1000
Recycle delay (s)	90	90	90	90
Number of Meiboom-Gill Loops	200	200	100	100
Real points per loop	100	100	200	200
Spectral window of subspectra (kHz)	1000	1000	1000	1000
Dwell (μs)	1	1	1	1
Spikelet Separation (kHz)	10	10	10	5
Acq. Time (s)	0.02	0.02	0.02	0.02
pw90 (μs)	50	50	50	50
aH dec	0.15	0.15	0.15	0.15
aX	0.2	0.2	0.2	0.2
Sweep width (kHz)	1000	1000	1000	1000

B.1.2. DFT calculations of ^{31}P Shielding Parameters for Compound 4

Table B3. Calculated ^{31}P NS tensor components for the phosphorous nuclei in **4**.

	σ_{11}	σ_{22}	σ_{33}	σ_{iso}
site 1	158.42	309.73	389.52	285.89
site 2	166.47	307.42	397.32	290.40

ADF predicts that there will be a ca. 4.51 ppm difference between the chemical shifts of the two phosphorous nuclei ($\Delta\sigma_{iso} = \Delta\delta_{iso}$).

B.1.3. Supplementary SSNMR Spectra

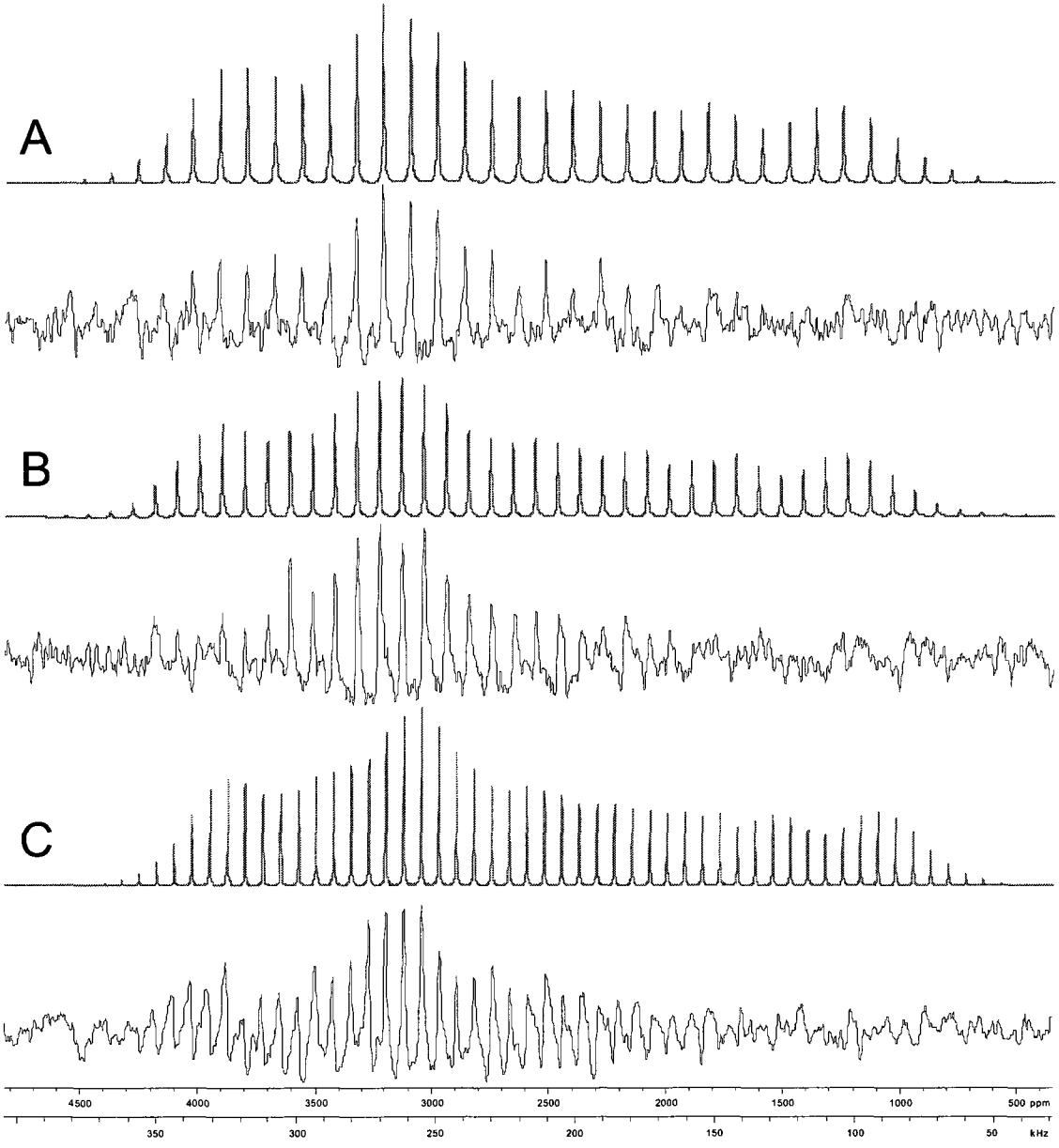

Figure B1. SIMPSON simulations (top traces) and experimental ^{207}Pb CP/MAS spectra (bottom traces) of **1** at spinning speeds of (A) 9.7 kHz, (B) 8.0 kHz and (C) 6.3 kHz.

B.1.4. Powder X-Ray Diffraction of Compound 4

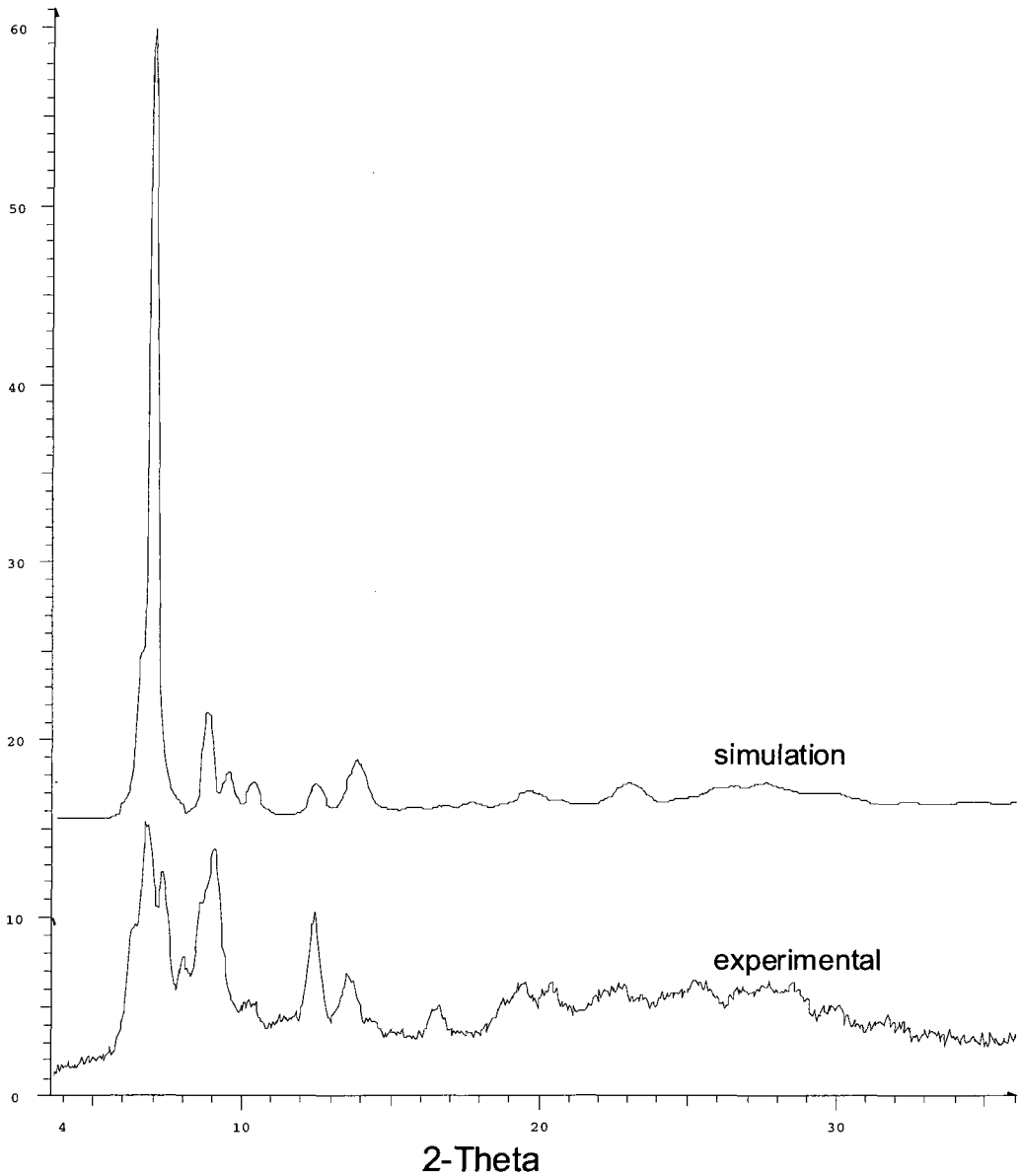

Figure B2. Powder X-ray diffraction pattern of **4.**

Appendix C

Supporting Information - Solid-state NMR Investigations of Metal Guanidinates

C1. Supporting Experimental Information

C1.1. Selected SSNMR Experimental Parameters

Table C1. 9.4 T ^{27}Al and ^{71}Ga static experimental parameters

	$Al(guan)_3$	$Al(guan)_2NMe_2$	$Al(guan)_2Cl$	$Ga(guan)_3$
Number of Scans	14416	23424	1456	43600
Recycle delay (s)	4	2	4	0.1
Dwell (μs)	10	2.5	5	1
Acq. Length	1024	2048	1024	2048
90° pulse power (kHz)	3.77	47.2	10.8	33.6
Spectral Window (kHz)	100	400	200	1000

Table C2. 9.4 T ^{27}Al MAS NMR experimental parameters

	$Al(guan)_3$	$Al(guan)_2Cl$
Number of Scans	1328	80
Recycle delay (s)	4	4
Dwell (μs)	5	2
Acq. Length	4096	4096
90° pulse power (kHz)	6.12	20
Spectral Window (kHz)	200	500

Vita Auctoris

Alan W. MacGregor was born in New Glasgow, Nova Scotia, Canada. He Graduated from East Pictou Rural High School in June of 2003, and St. Francis Xavier University in May of 2007 with a B.Sc.(Honours) in Chemistry. After completion of his Master's Degree requirements in April of 2010, he will undertake a position in the research department of Imperial Oil.